

EXPERIMENTAL INVESTIGATION OF THE TEMPERATURE EFFECTS ON THE  
BEHAVIOR OF ADHESIVELY-BONDED DISSIMILAR MATERIALS

A Thesis  
Submitted to the Graduate Faculty  
of the  
North Dakota State University  
of Agriculture and Applied Science

By

Britt Alan Helten

In Partial Fulfillment of the Requirements  
for the Degree of  
MASTER OF SCIENCE

Major Department:  
Mechanical Engineering

March 2017

Fargo, North Dakota

North Dakota State University  
Graduate School

---

**Title**

Experimental Investigation of the Temperature Effects on the Behavior of  
Adhesively-Bonded Dissimilar Materials

---

**By**

Britt Alan Helten

---

The Supervisory Committee certifies that this *disquisition* complies with North Dakota  
State University's regulations and meets the accepted standards for the degree of

**MASTER OF SCIENCE**

SUPERVISORY COMMITTEE:

Dr. Chad Ulven

---

Chair

Dr. Xiangfa Wu

---

Dr. Dean Webster

---

Approved:

4/7/17

---

Date

Dr. Alan R. Kallmeyer

---

Department Chair

## **ABSTRACT**

The effects of temperature on the fatigue and low velocity impact (LVI) behaviors of adhesively-bonded single-lap joints (SLJs) composed of a pultruded E-glass/polyurethane composite bonded to 5052 aluminum and A36 steel were investigated. The fatigue behavior was studied via the evaluation of the F-N and stiffness degradation diagrams at load levels between 50% and 80% of the ultimate static load and temperatures between 0°C and 75°C. Fatigue life was found to decrease with increasing temperature and was independent of adherend material. Adherend material and load level did not have a significant effect on the stiffness degradation behavior. The LVI behavior was studied at temperatures between -20°C and 120°C at an impact velocity of 1 m/s with a drop mass of 7.19 kg. The joint performance was evaluated at initial failure and overall response. The LVI responses exhibited material dependencies at temperatures below  $T_g$  and temperature dependencies near and above  $T_g$ .

## **ACKNOWLEDGEMENTS**

I would like to thank AGCO Corporation for providing the funding for this research to be conducted, Tecton Products, LLC for providing the pultruded E-glass/polyurethane composite, and Novum Glass, LLC for providing the glass spacing beads.

I would like to thank my advisor, Dr. Chad Ulven, for providing the resources necessary to conduct this research and guidance in its development as well as in analyzing the impact data. I would also like to thank my committee members, Dr. Xiangfa Wu and Dr. Dean Webster, and the chair of the Mechanical Engineering department Dr. Kallmeyer for their guidance and advice throughout this research.

# TABLE OF CONTENTS

ABSTRACT.....	iii
ACKNOWLEDGEMENTS.....	iv
LIST OF TABLES.....	vii
LIST OF FIGURES.....	viii
LIST OF APPENDIX TABLES.....	xii
LIST OF APPENDIX FIGURES.....	xiii
CHAPTER 1. INTRODUCTION.....	1
CHAPTER 2. LITERATURE REVIEW.....	3
2.1. Adhesion and Adhesives.....	3
2.2. Fatigue of Adhesively-Bonded Joints.....	5
2.2.1. Specimen Preparation & Test Parameters.....	7
2.2.2. Temperature Effects.....	10
2.2.3. Dissimilar Adherends.....	12
2.2.4. Stiffness Degradation.....	14
2.3. Impact Response of Adhesively-Bonded Joints.....	15
CHAPTER 3. OBJECTIVES.....	19
3.1. Experimental Objectives.....	19
3.2. Analytical Objective.....	19
CHAPTER 4. MATERIALS AND METHODS.....	20
4.1. Materials.....	20
4.1.1. Adherends.....	20
4.1.2. Adhesive.....	20
4.1.3. Spacing Beads.....	21

4.2. Experimental Methods .....	22
4.2.1. Adhesive Characterization.....	22
4.2.2. Temperature Effects on the Monotonic and Fatigue Behaviors of Adhesively-Bonded Dissimilar Material SLJs .....	26
4.2.3. Temperature Effects on the Low Velocity Transverse Impact Behavior of Adhesively-Bonded Dissimilar Material SLJs.....	36
CHAPTER 5. RESULTS AND DISCUSSION.....	43
5.1. Adhesive Characterization .....	43
5.1.1. Decomposition.....	43
5.1.2. Temperature Effects on Adhesive Stiffness .....	44
5.1.3. Bond Line Thickness.....	45
5.2. Temperature Effects on the Monotonic and Fatigue Behaviors of Adhesively-Bonded Dissimilar Material SLJs .....	48
5.2.1. Monotonic Tension.....	48
5.2.2. Tension-Tension Fatigue .....	54
5.3. Temperature Effects on the Low Velocity Transverse Impact Behavior of Adhesively-Bonded Dissimilar Material SLJs .....	68
5.4. Sources of Error .....	85
CHAPTER 6. CONCLUSIONS AND RECOMMENDATIONS .....	88
6.1. Conclusions .....	88
6.2. Recommendations for Future Work.....	93
REFERENCES .....	96
APPENDIX A. MATERIAL PROPERTIES AND INFORMATION .....	102
APPENDIX B. TECHNICAL DRAWINGS.....	104
APPENDIX C. EXPERIMENTAL DATA .....	106

## LIST OF TABLES

<u>Table</u>	<u>Page</u>
2.1: Summary of literature utilizing polyurethane adhesives in joint fabrication.....	4
2.2: Literature summary of joint specimen preparation parameters .....	7
2.3: Literature summary of experimental fatigue test parameters .....	10
2.4: Literature summary of the temperature effects on ABJs .....	12
2.5: Literature summary of dissimilar adherend materials in ABJs .....	13
2.6: Literature summary of joint stiffness degradation.....	14
2.7: Literature summary of the impact response of ABJs.....	18
4.1: Experimental fatigue test program.....	33
4.2: Experimental LVI test program .....	40
5.1: Fatigue loading parameters.....	55

# LIST OF FIGURES

<u>Figure</u>	<u>Page</u>
2.1: Joint modes of failure: (a) interfacial, (b) cohesive, and (c) adherend .....	3
2.2: Schematic of constant amplitude sinusoidal loading fatigue parameters .....	6
4.1: (a) Pultruded E-glass/polyurethane composite, (b) 5052 aluminum, (c) A36 Steel .....	20
4.2: DP620NS adhesive manufactured by 3M.....	21
4.3: Diagram of the mechanical support provided via the incorporation of spacing beads.....	21
4.4: (a) Pre- and (b) post-acetone vapor treatment of the DMA sample mold .....	23
4.5: DMA sample manufacturing setup .....	24
4.6: Zeiss microscope and JENOPTIK camera used to measure bond line thicknesses.....	25
4.7: Geometry and dimensions of fatigue SLJ specimens (all dimensions in mm).....	27
4.8: Diagram of abrasion path (a) initial horizontal motion and (b) final elliptical motion .....	28
4.9: Representative upper (nearest the jig clamp) fillets.....	29
4.10: Representative lower (nearest the jig base) fillets .....	29
4.11: Joint assembly jig.....	30
4.12: Monotonic and fatigue experimental test setup .....	31
4.13: SLJ fatigue test fixture (all dimensions in mm).....	31
4.14: Fixture diagram for monotonic and fatigue specimens .....	32
4.15: Geometry and dimensions of impact SLJ specimens (all dimensions in mm).....	36
4.16: LVI testing apparatus setup .....	37
4.17: Pneumatic clamping mechanism used to secure impact specimens .....	38
4.18: Diagram of transverse SLJ impact.....	38
4.19: Schematic of LVI specimen and clamping jig.....	39
4.20: Identification of the reduced LVI data.....	42
5.1: (a) TGA and (b) DTGA curves.....	43



5.2: Linear fit of the degradation results .....	44
5.3: Storage modulus and tan delta vs temperature of a representative two-part polyurethane adhesive specimen .....	45
5.4: Comparison of bond line thickness between SLJ adherends .....	46
5.5: Microscopy image of a composite SLJ bond line .....	46
5.6: Microscopy image of a aluminum SLJ bond line .....	47
5.7: Microscopy image of a steel SLJ bond line .....	47
5.8: Representative monotonic load vs displacement of steel SLJs.....	48
5.9: Representative monotonic load vs displacement of aluminum SLJs.....	49
5.10: Ultimate load versus temperature of steel and aluminum SLJs.....	50
5.11: Failure displacement versus temperature of steel and aluminum SLJs .....	50
5.12: Stiffness versus temperature of steel and aluminum SLJs.....	51
5.13: Demonstration of the effect of stiffness imbalance on SLJ stress distribution and deformation when loaded in tension. (a) Undeformed SLJ, (b) SLJ with adherends of equivalent stiffness, (c) SLJ with adherend 1 having a greater stiffness than adherend 2 ..	52
5.14: Representative monotonic fracture surfaces of steel SLJs at (a) 0°C, (b) 25°C, (c) 50°C, and (d) 75°C.....	53
5.15: Representative monotonic fracture surfaces of aluminum SLJs at (a) 0°C, (b) 25°C, (c) 50°C, and (d) 75°C .....	54
5.16: F-N diagram for steel SLJs at each test temperatures.....	56
5.17: F-N diagram for aluminum SLJs at each test temperatures.....	56
5.18: Representative hysteretic fatigue loading loops at quarterly normalized cycles used in the determination of stiffness.....	58
5.19: Stiffness vs normalized number of cycles of steel and aluminum SLJs at 0°C.....	59
5.20: Normalized stiffness vs normalized number of cycles of steel and aluminum SLJs at 0°C .....	59
5.21 Stiffness vs normalized number of cycles of steel and aluminum SLJs at 25°C.....	60
5.22: Normalized stiffness vs normalized number of cycles of steel and aluminum SLJs at 25°C .....	60

5.23: Stiffness vs normalized number of cycles of steel and aluminum SLJs at 50°C.....	61
5.24: Normalized stiffness vs normalized number of cycles of steel and aluminum SLJs at 50°C .....	61
5.25: Stiffness vs normalized number of cycles of steel and aluminum SLJs at 75°C.....	62
5.26: Normalized stiffness vs normalized number of cycles of steel and aluminum SLJs at 75°C .....	62
5.27: Stiffness vs normalized number of cycles of steel SLJs.....	63
5.28: Normalized stiffness vs normalized number of cycles of steel SLJs.....	64
5.29: Stiffness vs normalized number of cycles of aluminum SLJs .....	64
5.30: Normalized stiffness vs normalized number of cycles of aluminum SLJs.....	65
5.31: Representative fatigue fracture surfaces of steel SLJs at (a) 0°C and LL=0.50, (b) 0°C and LL=0.65, (c) 0°C and LL=0.80, (d) 25°C and LL=0.50, (e) 25°C and LL=0.65, (f) 25°C and LL=0.80, (g) 50°C and LL=0.50, (h) 50°C and LL=0.65, (i) 50°C and LL=0.80, (j) 75°C and LL=0.50, (k) 75°C and LL=0.65, and (l) 75°C and LL=0.80.....	66
5.32: Representative fatigue fracture surfaces of aluminum SLJs at (a) 0°C and LL=0.65, (b) 0°C and LL=0.80, (c) 25°C and LL=0.50, (d) 25°C and LL=0.65, (e) 25°C and LL=0.80, (f) 50°C and LL=0.50, (g) 50°C and LL=0.65, (h) 50°C and LL=0.80, (i) 75°C and LL=0.50, (j) 75°C and LL=0.65, and (k) 75°C and LL=0.80.....	67
5.33: Initial impact velocity for all LVI samples .....	68
5.34: Maximum energy vs temperature of all SLJ samples.....	69
5.35: Representative impact force-energy-time response curves of steel SLJs at each test temperature .....	70
5.36: Representative impact force-energy-time response curves of aluminum SLJs at each test temperature.....	70
5.37: Representative impact force-energy-time response curves of composite SLJs at each test temperature.....	71
5.38: Impact force vs deflection of representative steel SLJs at each test temperature .....	71
5.39: Impact force vs deflection of representative aluminum SLJs at each test temperature .....	72
5.40: Impact force vs deflection of representative composite SLJs at each test temperature.....	72
5.41: Initial stiffness vs temperature for all SLJ adherend materials.....	73

5.42: Initial failure load vs temperature for all SLJ adherend materials.....	74
5.43: Initial failure energy vs temperature for all SLJ adherend materials.....	74
5.44: Resulting crack formation in a composite SLJ at 80°C under LVI loading .....	75
5.45: 2D crack propagation diagram of a typical composite SLJ.....	75
5.46: 2D crack propagation diagram of a typical metal SLJ.....	75
5.47: Impact force vs deflection for aluminum SLJs in which the impact surface was varied between the composite and aluminum adherend .....	76
5.48: Impact force vs deflection for steel SLJs in which the impact surface was varied between the composite and steel adherend.....	77
5.49: Image of a representative fillet crack in a composite SLJ .....	78
5.50: Secondary stiffness vs temperature for all SLJ adherend materials .....	79
5.51: Maximum impact force vs temperature for all SLJ adherend samples.....	80
5.52: Energy absorbed vs temperature of all SLJ adherend samples.....	81
5.53: Representative LVI fracture surfaces of steel SLJs at (a) -20°C, (b) 0°C, (c) 25°C, (d) 40°C, (e) 80°C, and (f) 120°C .....	83
5.54: Representative LVI fracture surfaces of aluminum SLJs at (a) -20°C, (b) 0°C, (c) 25°C, (d) 40°C, (e) 80°C, and (f) 120°C.....	84
5.55: Representative LVI fracture surfaces of composite SLJs at (a) -20°C, (b) 0°C, (c) 25°C, (d) 40°C, (e) 80°C, and (f) 120°C.....	85

## LIST OF APPENDIX TABLES

<u>Table</u>	<u>Page</u>
A1: Mechanical, physical, and thermal adherend properties.....	102
A2: Adherend thickness measurement summary.....	102
C1: Fatigue specimen spacing bead concentration summary.....	106
C2: LVI specimen spacing bead concentration summary .....	107
C3: Bond line thickness summary .....	107
C4: Bond line thickness t test summary .....	107
C5: Thermal degradation heating rate and temperature results .....	108
C6: Summary of DMA $T_g$ results.....	108
C7: Summary of monotonic results .....	108
C8: Summary of steel SLJ fatigue results .....	109
C9: Summary of aluminum SLJ fatigue results.....	110
C10: Summary of composite SLJ LVI results.....	111
C11: Summary of aluminum SLJ LVI results .....	112
C12: Summary of steel SLJ LVI results.....	113

## LIST OF APPENDIX FIGURES

<u>Figure</u>	<u>Page</u>
A1: Spacing bead certificate of analysis provided by Novum Glass, LLC .....	103
B1: Technical drawing of the sample manufacturing jig components: (a) base and (b) clamp, dimensions in mm .....	104
B2: Technical drawing of the LVI jig components: (a) lower and (b) upper, dimensions in mm .....	105

# CHAPTER 1. INTRODUCTION

The efficiency and confidence in the design of load bearing structures becomes increasingly complicated when predictions of the behavior of such structures under various loading and environmental conditions are to be accurately made. The methods used for such predictions are ever-changing as new techniques, designs, and models are developed which require extensive experimental validation. These complications are especially pertinent in the realm of joints which are complex systems that can include multiple materials, a varying number of interfaces, and complex shapes. Adhesively-bonded joints (ABJs) offer many advantages in comparison to traditionally used joining methods, such as welding, brazing, and mechanical fastening, which include improved corrosion resistance, lower stress concentration, better fatigue properties, proficiency in the bonding of dissimilar materials, and expanded flexibility for designers [1, 2].

Composite materials have become widely used to reduce weight and maximize the efficiency of structures and products. This is due to their high strength to weight ratios and directionally tailorable properties. Introducing these materials into ABJs allows designers, engineers, and scientists to customize and optimize not only the structure but the material with which the structure is made as well. This degree of tailorability of a structure and the materials with which it is made allows for increased efficiency via the control of the load transfer and stress distributions within the joints and structure itself.

When designing a structure one must have knowledge of the environmental and loading conditions to which said structure is to be subjected. These conditions can include, but are not limited to, static loading, fatigue loading, impact loading, and temperature variations; all of which should be considered during the design process. This becomes increasingly difficult when multiple materials and interfaces critical to the integrity of the structure are involved. Implementation of

these materials and joints in load bearing applications on a widespread industrial scale requires design confidence which stems from the predictability of failure and understanding of the mechanisms which govern failure.

The research on the temperature effects on the fatigue and impact behaviors of adhesively-bonded dissimilar materials has been conducted to address some areas in which there is a lack of confidence in ABJs and is detailed in the remaining 5 chapters. The second chapter provides a literature review which summarizes some of the major works in the relevant fields which makes up a portion of the basis of knowledge which has allowed for advancements, developments, and innovations within the field of ABJs. The third chapter provides context for and states the research objectives which guided this work. The objectives included the evaluation of the temperature effects on the mechanical properties of a commercially available two-part polyurethane adhesive, evaluation of the applicability of a previously proposed sigmoid model to dissimilar material single-lap joints (SLJs) bonded with polyurethane adhesive, and evaluation the temperature effects on the fatigue and impact behaviors of dissimilar material SLJs. The fourth chapter details the methodology with which the stated objectives were achieved in regards to the materials of interest, specimen geometry and manufacture, apparatuses and fixturing, design of experiments, experimental procedure, and data reduction processes. The fifth chapter details the obtained results and discusses the behavioral mechanisms which are supported by literature as well as hypothesize as to potential mechanisms which are not currently supported by literature and require further testing and validation. The sixth chapter summarizes the research which has been conducted and its implications. It also details some thoughts regarding future research to be conducted in order to expand the basis of knowledge and understanding within the field of ABJs.

## CHAPTER 2. LITERATURE REVIEW

### 2.1. Adhesion and Adhesives

As is common with scientific developments, the concepts for adhesives were initiated through the observation of those used in nature to form bird nests and spider webs [3]. Adhesive technologies have progressed through the centuries, beginning with those taken directly from nature such as beeswax, tar, rubber, and rosin to name a few [3]. Most of the adhesives used today are synthetic resins and hardeners which allow for tailorability to specific application and adherend materials.

ABJs can exhibit three different modes of failure, or a combination thereof, which include interfacial, cohesive, and adherend and are shown in Figure 2.1.

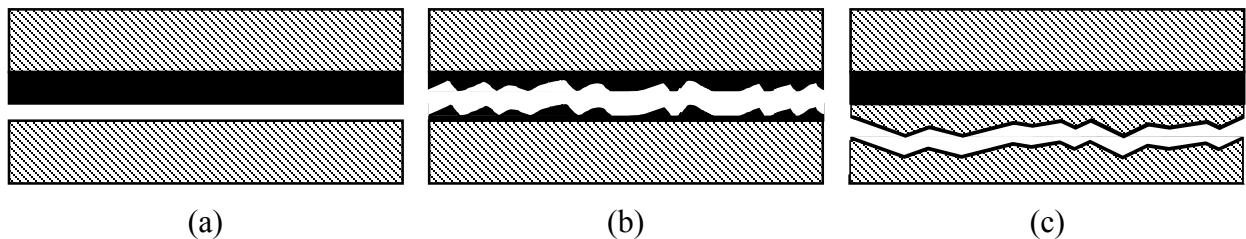


Figure 2.1: Joint modes of failure: (a) interfacial, (b) cohesive, and (c) adherend

Adherend failure is desired as it maximizes the load carrying capacity of the structure; whereas interfacial failure is an indication of weak bonding.

Epoxy adhesives are commonly used today due to their highly tailorable properties, degree of development, and wettability with many composites (epoxy matrix composites are highly ubiquitous [4]) and this ubiquity is reflected in literature where they are used in the manufacture of joints. Published studies which use polyurethane adhesives to create joints are less common, however. Vallée et al. [5] investigated the influence of adhesive thickness and overlap length on double lap joints (DLJs) composed of pultruded glass fiber-reinforced polymer (GFRP) composite



adherends bonded with a two-component polyurethane adhesive (S-Force 7851, Sika AG, Baar, Switzerland). The optimum bond line thickness was determined to be 1 mm and observed increased strength with longer overlap length. Vallée et al. [6] studied the influence of rounded fillets on the strength of DLJs and observed negligible strength increases . The DLJs were constructed of the same materials as in [5]. Neto et al. [7] fabricated SLJs using unidirectional carbon fiber/epoxy composite adherends bonded with a two-part polyurethane adhesive (SikaForce 7888, Sika AG, Baar, Switzerland) and a two-part epoxy adhesive (Araldite AV138, Huntsman Corporation, The Woodlands, TX). It was found that the polyurethane adhesive exhibited increasing failure loads with increasing overlap lengths. The mode of failure was cohesive. The joints bonded with epoxy reached a plateau of failure load where failure was interlaminar within the composite adherends. The polyurethane adhesive yielded higher failure loads than that those of the epoxy. Na et al. [8] fabricated butt joints (BJs) and SLJs composed of 6005A aluminum adherends and a single component polyurethane adhesive (Sikaflex-265, Sika AG, Baar, Switzerland). They observed decreasing joint strength with increasing temperature. A summary these studies is presented in Table 2.1.

Table 2.1: Summary of literature utilizing polyurethane adhesives in joint fabrication

<b>Adherend(s)</b>	<b>Adhesive(s)</b>	<b>Joint Type</b>	<b>Source</b>
E-glass/Polyester	Polyurethane	DLJ	[5]
GFRP, Timber	Epoxy, Polyurethane, Acrylic	DLJ	[6]
CFRP	Epoxy, Polyurethane	SLJ	[7]
6005A Aluminum	Polyurethane	BJ, SLJ	[8]

## 2.2. Fatigue of Adhesively-Bonded Joints

The desired lifespan of a given product is an important parameter for consideration throughout the design process. A widely used method to study the fatigue behavior of a material or structure which is subjected to repetitive or cyclic loading scenarios throughout its lifetime is to subject such a material or structure to a simulated cyclic loading program in a laboratory via a universal testing machine. The geometry of the joint which is studied is often simplified in order to minimize the complexity, thereby allowing for a better understanding of joint behavior.

The experimental evaluation of the fatigue performance of adhesively-bonded joints has been increasingly studied as the use of such joints has increased due to efficiency demands in a multitude of industrial sectors including automotive, aerospace, agriculture, and infrastructure [9]. There has been an attempt to move toward the standardization of methods by which engineers, scientists, and designers can examine and design new materials and structures. Currently few standards exist which explicitly include joints composed of composite adherends, not to mention those composed of dissimilar materials, and most experimentation has been performed referencing standards for fiber-reinforced polymers (FRP) and metal-metal joints [9]. Previous work in this area have referenced testing standards, such as ASTM D3166 [10], to develop experimental procedures which subject specimens to a cyclic load, typically of a sinusoidal waveform, where the maximum load,  $F_{\max}$ , and minimum load,  $F_{\min}$ , are the upper and lower limits of the sinusoidal wave form, respectively. The average load,  $F_{mean}$ , is the average load to which the sample is subjected. The period,  $T$ , is the time required for the completion of a single cycle and is usually stated in terms of frequency,  $f$ , which is inversely related to period as:

$$T = \frac{1}{f} \quad (2.1)$$

Another parameter typically used to define the sinusoidal waveform is the loading ratio,  $R$ , and is expressed as:

$$R = \frac{F_{\min}}{F_{\max}} \quad (2.2)$$

A schematic of these loading parameters have been shown in Figure 2.2 with notations preserved from Sarfaraz [11].

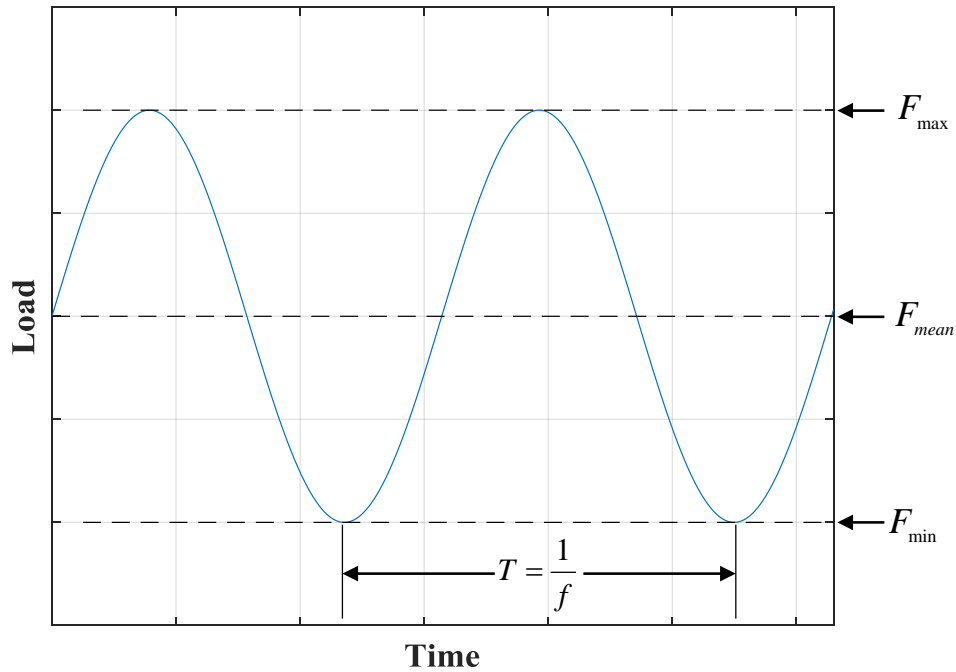


Figure 2.2: Schematic of constant amplitude sinusoidal loading fatigue parameters

The determination of these parameters is dependent on the practical application of the joints and are chosen to best simulate such an application with laboratory experiments; which is itself a complicated task. The loading to which a typical structure could be subjected is rarely completely known beforehand and therefore necessitates the consideration of a wide range of parameters. This is typically done by determining the maximum load as a percentage of the ultimate static load ( $F_{s,ult}$ ), hereafter referred to as load level ( $LL$ ), and specifying a frequency which would be

applicable to the situation of interest. The values of the minimum and mean cyclic loading can be determined by specifying a loading ratio value which, again, best simulates the practical application. Values of R between 0 and 1 result in tension-tension fatigue, values above 1 result in compression-compression fatigue, and values below 0 result in mixed tension-compression fatigue.

The remainder of this section has been dedicated to the available literature which includes specimen preparation and test parameters, temperature effects, dissimilar adherend materials, and stiffness degradation with regards to the cyclic fatigue behavior of ABJs.

### 2.2.1. Specimen Preparation & Test Parameters

A summary of the some of the available specimen preparation parameters in the literature is given in Table 2.2 with the relevant findings summarized in the applicable sections to follow.

Table 2.2: Literature summary of joint specimen preparation parameters

<b>Bonding Pressure (kPa)</b>	<b>Bond Line Thickness Control</b>	<b>Fillet</b>	<b>Source</b>
-	0.4 mm SS wire	Natural	[12]
500.00	-	Natural	[13]
100.00	1 wt% 150 $\mu$ m glass spheres	Square, Spew	[14]
-	-	0.3-0.5 mm	[15]
-	PVC Washers	2-10 mm radius	[6]
280.00	-	-	[16]

There has been much work done to further the understanding of the fatigue behavior of ABJs and, as previously stated, the test parameters to which samples are subjected can greatly affect the resulting behavior. Curley et al. [12] studied SLJs composed of mild steel adherends bonded with a single component rubber toughened epoxy adhesive (Araldite AV 119, Huntsman Corporation, The Woodlands, TX). Monotonic tensile testing was conducted at a rate of 0.5 mm/min and used the ultimate loads to determine the maximum fatigue loading. Fatigue testing

was conducted by applying a sinusoidal waveform at a frequency of 5 Hz. The sinusoidal wave was defined by a load ratio of 0.5 and varying load levels which ranged between 30 and 90%. Backface-strain measurements were used to monitor crack growth which they correlated with the strain energy release rate. The resulting F-N diagrams indicated a decreasing fatigue life with increasing load level and found evidence of the existence of a fatigue threshold at a load level of 30%. The mode of failure observed was initially determined to be interfacial but upon further investigation using scanning electron microscopy (SEM), a thin layer of adhesive was found still attached to the adherend, thereby indicating cohesive failure. Hadavinia et al. [13] studied SLJs composed of aluminum adherends (EN AW 2014A) bonded with a hot-curing rubber toughened epoxy (LOCTITE EA9628, Henkel AG, Germany). It was found that the fatigue lifetime was dominated by crack propagation as opposed to crack initiation. Quaresimin and Ricotta [14] studied SLJs composed of carbon fiber/epoxy composite adherends and a two-part epoxy adhesive (9323 B/A, 3M Company, St. Paul, MN). Joints were fabricated with overlap lengths of 20, 30, and 40 mm along with square (no fillet) and spew fillets. Glass spacing beads of 150  $\mu\text{m}$  diameter were added to the adhesive at 1 wt% and a pressure of 0.1 MPa was applied to the joints during manufacture to obtain consistent bond line thicknesses. Monotonic tensile testing was conducted at a rate of 2 mm/min. The used load controlled fatigue test parameters of the applied sinusoidal wave included a load ratio of 0.5 and frequencies ranging from 10 to 15 Hz. An increase in load carrying capacity and fatigue strength was observed in the samples which included a spew fillet in comparison to those without. The failure mode was observed to be interfacial between the adhesive and adherend. Crack initiation was observed through 20% to over 70% of some fatigue lives which was mainly dependent upon the overlap length and load level. Khoramishad et al. [16] studied SLJs composed of 2024-T3 aluminum adherends bonded with a toughened epoxy film adhesive

(FM 73 M OST, Cytec Industries, Woodland Park, NJ) and a single component rubber toughened epoxy adhesive (Araldite AV 119, Huntsman Corporation, The Woodlands, TX). The effect of the load ratio on the fatigue lives was evaluated and the results indicated that a decreasing load ratio resulted in a detrimental effect on fatigue life. Ferreira et al. [17] studied SLJs composed of E-glass/polypropylene composite adherends bonded with an ethyl cyanoacrylate adhesive (7452-Super Glue 4, Bostik, Paris, France). Samples were exposed to water immersion periods of 90 days at temperatures of 20, 40, and 70°C. Constant amplitude fatigue test parameters included a load ratio of 0.025 and frequency of 10 Hz. The testing was conducted at room temperature. To evaluate the effects of heat build-up/temperature rise throughout the duration of the fatigue testing, some specimens were monitored with a thermocouple at the edges of the bond line. The resulting temperature rise was in the range of 4°C to 6°C throughout the portion of fatigue life described as stable and rose to 10°C near failure. It was claimed that this rise in temperature had a negligible effect on fatigue life. Shenoy et al. [15] studied SLJs composed of 7075-T6 aluminum adherends bonded with a single part toughened epoxy adhesive (FM 73 M, Cytec Industries, Woodland Park, NJ). Monotonic testing was conducted at a rate of 6 mm/min. The fatigue test parameters used included a load ratio of 0.10 and a frequency of 5 Hz. Backface strain gauges were used to monitor crack propagation and indicated large damage acceleration towards the end of life. Reis et al. [18] studied SLJs composed of steel adherends bonded with a two-part epoxy adhesive (Araldite 420 A/B, Huntsman Corporation, The Woodlands, TX). A constant amplitude sinusoidal waveform was applied with a load ratio of 0.05 at frequencies of 2, 10, and 40 Hz. Temperature increase of the joint was monitored via a 1.50 mm hole which was machined near the joint edge on one of the adherends with a type K thermocouple. The temperature rise at frequencies of 2 and 10 Hz was observed to be small, i.e. less than 1.10°C, and reached a state of equilibrium with the heat removed

by convection and adherend heat absorption. The temperature rise at 40 Hz, however, was observed to exhibit 3 stages. The first of which was the initial increase of approximately 4.00% of the final temperature rise followed by a quasi-constant increase through approximately 40.0% of the fatigue life. The final stage was a significant increase until failure. These studies are in Table 2.3.

Table 2.3: Literature summary of experimental fatigue test parameters

<b>Monotonic (mm/min)</b>	<b>Frequency (Hz)</b>	<b>R</b>	<b>LL</b>	<b>Source</b>
0.50	5.00	0.50	0.30,0.90	[12]
-	10.00	0.025	-	[17]
1.00	5.00	0.50	0.4	[13]
2.00	10-15	0.05	-	[14]
6.00	5.00	0.10	0.40,0.50	[15]
-	-	0.10,0.50	0.50,0.75	[19]
-	2,10,40	0.05	-	[18]

### 2.2.2. Temperature Effects

Increasing the confidence in the use of ABJs in practical structural applications, in the automotive, aeronautic, agricultural, construction, etc. industrial sectors for example, requires knowledge of the behavioral changes of these joints within the temperature range to which they are expected to be exposed. Some of the work that has been done relating to the temperature effects on the fatigue behavior of ABJs has been done by Ashcroft et al. [20], Ashcroft et al. [21], and Ashcroft and Shaw [22] where DLJs, lap strap joints (LSJs), and double cantilever beams (DCBs) were studied, respectively. All joints were composed of carbon fiber-reinforced polymer (CFRP) composite adherends bonded with a proprietary adhesive which was diglycidyl ether of bisphenol A epoxy and was crosslinked with a primary amine curing agent. The adhesive was toughened based on a carboxyl terminated butadiene acrylonitrile rubber. All studies included temperatures

of -50, 22-25, and 90°C. The highest temperature was observed to yield the lowest ultimate static load and fatigue resistance. The influence of creep in the acceleration of failure at elevated temperatures was proposed. These results did not agree with the trends observed in the results of the LSJs, hence the authors warned about applying the trends of results from one joint type to another without complete understanding of the mechanisms. All studies saw shifts in the failure mode from adherend failure to either cohesive or adhesive failure at the elevated temperature. Zhang et al. [23] studied DLJs composed of pultruded GFRP adherends bonded with a two-part epoxy adhesive (SikaDur 330, Sika AG, Baar, Switzerland). Testing was performed at -35°C, 23°C, and 40°C at a frequency of 10 Hz and a load ratio of 0.10. There was no observable influence of temperature on the failure behavior of the DLJs, although exposing the joint to 90% humidity during the testing cause a change in failure mode from adherend failure to interfacial failure. The stiffness of the joint during the fatigue testing was determined as the secant modulus and was calculated as:

$$E(N) = \frac{F_{\max}(N) - F_{\min}(N)}{\Delta\delta_{\max}(N) - \Delta\delta_{\min}(N)} \quad (2.3)$$

where  $F_{\max}(N)$  and  $F_{\min}(N)$  are the maximum and minimum load in cycle  $N$ , respectively and  $\Delta\delta_{\max}(N)$  and  $\Delta\delta_{\min}(N)$  are the maximum and minimum displacement in cycle  $N$ , respectively. Fatigue lives at lower temperatures were longer than those at higher temperatures even though the ultimate static loads were lower. The overall stiffness degradation for all samples was in the approximate range of 6 to 7% and exhibited a linear trend throughout the majority of fatigue life. This linear trend was attributed to stable crack propagation after which point crack propagation becomes unstable and results in a rapid decrease in stiffness. Slight increases in stiffness degradation were observed at increased temperatures. Nguyen et al. [24] studied double-strap joints (DSJs) composed of steel (inner) and CFRP (outer) adherends bonded with a two-part epoxy



adhesive (Araldite 420, Huntsman Corporation, The Woodlands, TX). The study consisted of the modeling of the joint performance in the temperature range between 20°C and 60°C. The models consisted of adhesive stiffness degradation modeling and effective bond length of the joint as described initially by Hart-smith [25]. The ultimate static load and joint stiffness were found to significantly decrease at temperatures nearing and those above the  $T_g$  of the adhesive. A summary of these studies with the addition of some which were not heavily drawn upon in the development of the present research is provided in Table 2.4.

Table 2.4: Literature summary of the temperature effects on ABJs

Temperature (°C)	Adherend(s)	Adhesive	Joint/Analysis Type	Source
-50, 25, 90	CFRP	Epoxy	LSJ/Fatigue	[21]
-50, 22, 90	CFRP	Epoxy	DLJ/Fatigue	[20]
-50, 25, 90	CFRP	Epoxy	DCB/Fatigue	[22]
-35, 23, 40	Pultruded GFRP	Epoxy	DLJ/Fatigue	[23]
-40, 90	Steel	Epoxy	SLJ/Static	[26]
20, 40, 50	Steel/CFRP	Epoxy	DLJ/Static	[24]
-30, 25, 80	AA6061 Al/Q235 Steel	Epoxy (3)	SLJ/Static	[27]

### 2.2.3. Dissimilar Adherends

Weight reduction in the automotive, prompted by the CAFE fuel standards in the USA and similar standards in the EU, aircraft, and agricultural industries as well as increasing demand for fiber-reinforced composites in the repair of civil structures [9] has spurred interest in the high strength-to-weight ratios offered by ABJs which are effective in the joining of dissimilar materials in structural applications [1]. Some of the major work which has been conducted in this field include that of Owens and Lee-Sullivan [28, 29] in which SLJs composed of GFRP and aluminum adherends bonded with two different types of two-part epoxy adhesives (EP21LV and EP45HT, Master Bond Inc., Hackensaw, NJ) were studied. A proposed stiffness behavior model was

evaluated with experimental results of monotonic loading. Seong et al. [30] studied SLJs composed of CFRP and aluminum adherends bonded with a toughened epoxy adhesive (FM 73 M, Cytec Industries, Woodland Park, NJ). Parameters including the bonding pressure, overlap length, adherend thickness, and material type were studied for their effects on the failure load and mode of joints failure. The bonding pressure specified by the manufacturer of the adhesive, Cytec Industries, was found to yield the optimal strength. Failure strength increased only slightly with overlap lengths over 30 mm. Adherend thickness increases also resulted in increased failure load. Colombi and Fava [31] studied DSJs composed of steel and CFRP adherends bonded with an epoxy adhesive (SikaDur30, Sika AG, Baar, Switzerland). The joints were subjected to constant amplitude fatigue loading with load (stress) ratios of 0.10 and 0.40 at a frequency of 12 Hz. The study concluded crack propagation was along the interface and the loading ratio had a marginal influence on the fatigue behavior. A summary of these studies along with others which were not drawn upon for development of the present research are presented in Table 2.5.

Table 2.5: Literature summary of dissimilar adherend materials in ABJs

<b>Adherends</b>	<b>Adhesive</b>	<b>Joint Type</b>	<b>Source</b>
6061-T6511 Aluminum/ GFRP	Epoxy (2)	SLJ	[28]
2024-T3 Aluminum/GFRP/CFRP	Epoxy	SLJ	[30]
A5052-F Aluminum/ GFRP	Co-cure (Epoxy)	SLJ/MF	[32]
Steel/CFRP	Epoxy	DLJ	[24]
S275 Steel/CFRP	Epoxy	DLJ	[31]
Steel/CFRP	Epoxy	DLJ	[33]
Q235 Steel/AA6016 Aluminum	Epoxy (3)	SLJ	[27]
Steel/CFRP	Epoxy	SLJ	[34]

MF=Mechanical fastening

### 2.2.4. Stiffness Degradation

Each cycle to which a joint is subjected, assuming the stress amplitude is sufficient, results in the formation and/or propagation of a crack (or cracks) as well as plastic deformation of the adhesive and adherend(s), which will collectively be hereafter referred to as damage accumulation, thereby decreasing joint stiffness. This decrease in stiffness can be monitored through the use of strain gauges, extensometers, or crosshead displacement and used as a non-destructive evaluation method to create a damage metric or design criterion from stiffness-controlled, also known as stiffness-based, curves and are commonly denoted as  $S_c/N$  [35-37]. A brief history of the development of  $S_c/N$  curves for ABJs has been presented in Table 2.6 and summarized in the remainder of this section.

Table 2.6: Literature summary of joint stiffness degradation

Materials/Adherends	Specimen Type	Adhesive	Source
Glass/Polyester, Glass/CF/Polyester	Laminate	-	[38]
E-glass/Polyester	Laminate	-	[39]
E-glass/Polyester	Laminate	-	[37]
Pultruded GFRP	StLJ/DLJ	Epoxy	[36]
Pultruded GFRP	DLJ	Epoxy	[23]

StLJ=Stepped-lap joint

Anderson et al. [38] proposed an empirical model of stiffness degradation for fiber reinforced polymer composites used in the wind energy industry as a function of the number of cycles as:

$$\frac{E}{E_1} = 1 - K \left( \frac{\sigma}{E_0} \right)^n N \quad (2.4)$$

where  $E$  and  $E_1$  are the joint stiffness after  $N$  cycles and during the first cycle, respectively,  $E_0$  is the monotonic joint stiffness,  $\sigma$  is the stress amplitude,  $N$  is the number of cycles, and  $K$  and  $n$  are constants found via curve fitting of experimental data. This model was independently validated by

Philippidis and Vassilopoulos [37, 39] and modified by Zhang et al. [36] to yield the following model for the stiffness degradation of double lap joints (DLJs):

$$\frac{E(N)}{E(0)} = 1 - k_1 \left( \frac{F}{F_u} \right)^{k_2} N \quad (2.5)$$

where  $F$  is the applied load,  $F_u$  is the ultimate tensile load,  $N$  is the number of cycles,  $k_1$  and  $k_2$  are found via fitting to experimental data. Zhang et al. also proposed the following to model the stiffness degradation of stepped-lap joints (StLJs) which exhibited a sigmoid curve:

$$\frac{E(N)}{E(0)} = \left( \frac{N \cdot k^m}{V - N} \right)^{\frac{1}{m}} \quad (2.6)$$

where  $V$ ,  $m$ , and  $k$  are found via fitting to experimental data. The fitting of these parameters to experimental results of StLJs composed of pultruded GFRP laminates bonded with an epoxy adhesive revealed the consistency of the  $m$  and  $k$  parameters regardless of applied loading.  $V$  was dependent on the applied loading.

Equation 2.6 was rearranged to provide the capability of design criterion formation based on a desired reduction in stiffness,  $E(N)/E(0)$ , for StLJs as:

$$N = V \left( \frac{\left( \frac{E(N)}{E(0)} \right)^m}{k^m + \left( \frac{E(N)}{E(0)} \right)^m} \right) \quad (2.7)$$

This formulation allows engineers and designers to create customized failure criterion based on a desired reduction in stiffness which can be non-destructively monitored in-situ.

### 2.3. Impact Response of Adhesively-Bonded Joints

Knowledge and understanding of the conditions to which a structure will be exposed throughout its life allows for the most efficient design and should include the consideration of

impact events as these are highly probable to occur throughout the lifetime of a given structure whether it be debris, hail, falling tools, etc.

There have been a limited number of studies which have involved the low velocity impact (LVI) response of ABJs. Pang et al. [40] studied SLJs composed of Scotchply adherends under transverse impact loads. A 25.4 mm diameter hemispherical tup and a drop mass of 0.75 kg was used during the testing. The drop height was varied to test the joints at varying impact velocities. Specimens were clamped into a jig with a span of 178 mm. The results indicated the adherend thicknesses had a significant influence on the maximum impact load while the overlap length did not. A simplified spring-mass model was used to represent the impactor-joint system. The work of Vaidya et al. [41] has been by far the most noteworthy study completed thus far and studied SLJs composed of CFRP composite adherends bonded with three different types of epoxy. Resinufusion 8604 (an amine cured epoxy system used as a control manufactured by Huntsman Corporation, The Woodlands, TX), a paste epoxy adhesive (Magnabond 6398, Master Bond Inc., Hackensaw, NJ.), and a nanoclay-reinforced Resinufusion 8604 epoxy. The drop mass used was 3.33 kg with impact velocities in the range of 1-2 m/s. Specimens were fixed in a jig with a span of 150 mm. The Magnabond adhesive, which was less stiff but exhibited a higher strain to failure, absorbed more energy prior to failure in comparison to the neat and nanoclay-filled epoxies. The experimental results were also complemented with finite element method (FEM) simulations. The adhesive layer in the static simulation was modeled as a linear, isotropic elastic material in ANSYS and as an elastic-plastic material with kinematic hardening in the dynamic simulation using LS-DYNA 3D. The results of this study provided four main points of interest. The peel stress was tensile on the end of the joint opposite impact and compressive on the side of impact, the failure mode was mixed and the crack initiates at the edge of the lower adherend, the stress distribution

at the crack tip was altered from mixed mode I and II to mainly mode II as the crack propagated through the bond line, and the toughness of the adhesive was found to have considerable influence on the load-carrying capacity of the joint. Liao et al. [42] studied SLJs composed of A5052 aluminum and S45C steel adherends bonded with a two-part epoxy adhesive (ScotchWeld 1838 B/A, 3M Company, St. Paul, MN). The drop mass used was 18.5 kg and was dropped such that the impact was applied in the tensile direction. The results indicated that the strength of joints composed of dissimilar adherends exhibit lower strength than those of similar adherends. A FEM simulation was also performed which indicated the initial failure occurred at the interface of the stiffer adherend. Sayman et al. [43] studied SLJs composed of GFRP composite adherends bonded with a two-party toughened epoxy adhesive (Loctite 9466 A&B, Henkel AG, Germany). The specimens were subjected to transverse impact and simply supported with a span of 85 mm. A 12.7 mm diameter hemispherical tup was used during the testing. After the impact even the specimens were then tested in monotonic tension to determine load-carrying capacity. The results of the study indicated that the load-carrying capacity of the joints decreased at the temperatures of -20°C, 50°C, and 80°C in comparison to that at room temperature. The load-carrying capacity was also greatest for SLJs which were prepared with roughened surfaces. A summary of this literature is presented in Table 2.7, which details the adherend material(s), adhesive used in the manufacture of the joints, type of joint, and the direction in which the samples were loaded during the impact event.

Table 2.7: Literature summary of the impact response of ABJs

<b>Adherend(s)</b>	<b>Adhesive</b>	<b>Joint Type</b>	<b>Loading Direction</b>	<b>Source</b>
GFRP	-	SLJ	Tensile	[40]
CFRP	Epoxy (3)	SLJ	Transverse	[41]
A5052 Aluminum, S45C Steel	Epoxy	SLJ	Tensile	[42]
GFRP	Epoxy	SLJ	Transverse	[43]
CFRP	Epoxy	SLJ	Transverse	[44]

## **CHAPTER 3. OBJECTIVES**

Upon review of the available literature, there is a lack of available data and literature on the fatigue of joints bonded with adhesives other than epoxy, fatigue behavior of SLJs comprised of adherends of dissimilar materials, validation of joint fatigue failure criterion based on stiffness degradation models which have been proposed, and the impact, particularly transverse, behavior of ABJs. This lack of available data and literature is compounded when one wishes to consider the temperature effects in each of these areas. The purpose of this research was to begin to generate data which is currently lacking in these areas as well as provide an understanding of the mechanisms which contribute to the behavior of SLJs when subjected to temperature variations and how they affect said behavior. To accomplish these tasks, the research objectives were separated into experimental and analytical objectives.

### **3.1. Experimental Objectives**

- Evaluation of the temperature effects on polyurethane adhesive characteristics
- Evaluation of the temperature effects on the fatigue behavior of dissimilar material SLJs
- Evaluation of the temperature effect on the impact behavior of dissimilar material SLJs

### **3.2. Analytical Objective**

- Evaluation the applicability of the empirical sigmoidal model proposed by Zhang et al. [36] to dissimilar material SLJs bonded with a structural polyurethane adhesive
- Development of a fatigue failure criterion based on stiffness degradation



## CHAPTER 4. MATERIALS AND METHODS

### 4.1. Materials

#### 4.1.1. Adherends

The adherend materials of interest for SLJ manufacture included a pultruded unidirectional E-glass/polyurethane composite, provided by Tecton Products LLC, USA, bonded to 5052 aluminum and A36 steel. These materials are shown in Figure 4.1 with the relevant thermal, mechanical, and physical property and data available in APPENDIX A. The properties for the composite material were provided by Tecton Products, LLC and those for the 5052 aluminum and A36 steel were obtained from [45] and [46], respectively.

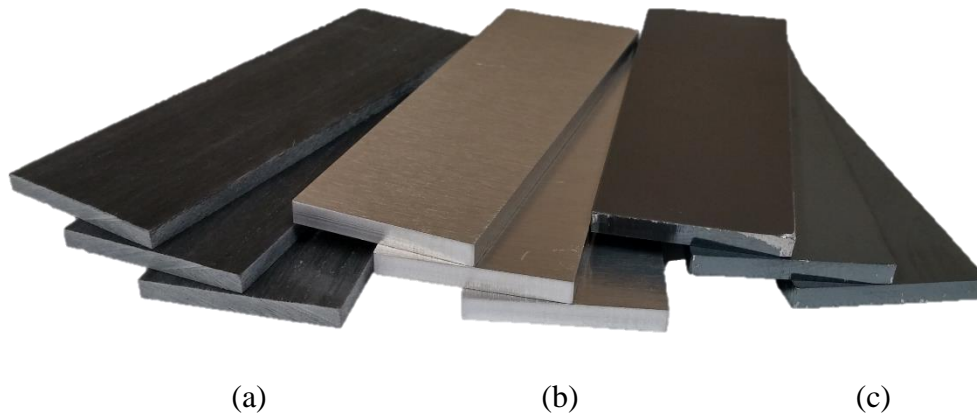


Figure 4.1: (a) Pultruded E-glass/polyurethane composite, (b) 5052 aluminum, (c) A36 Steel

The SLJ adherends will henceforth be identified by the adherend to which the composite adherend is bonded (e.g. composite-aluminum will be identified simply as aluminum).

#### 4.1.2. Adhesive

A commercially available two-part polyurethane structural adhesive, DP620NS (3M Company, St. Paul, MN) [47], shown in Figure 4.2, was selected as a result of a material survey which included Loctite U-10FL and Devcon 14503. The DP620NS yielded joints with the greatest

shear strength of all the surveyed adhesives. The polyurethane chemistry was selected to promote wetting of the polyurethane composite adherend and compatibility with the aluminum and steel adherends.

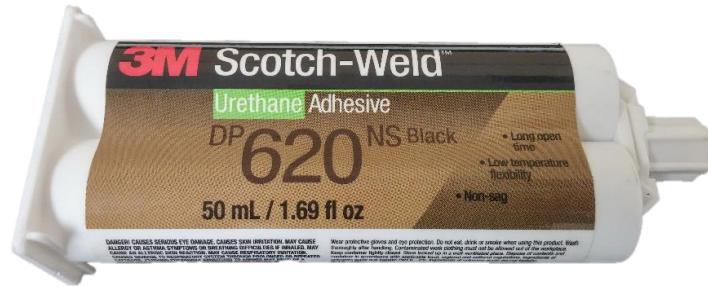


Figure 4.2: DP620NS adhesive manufactured by 3M

#### 4.1.3. Spacing Beads

The bond line thickness was controlled through the incorporation of T-106-125 glass spacing beads (provided by Novum Glass, LLC, Rolla, MO) in the adhesive mixture. The function of the bead was to provide mechanical support between adherends, as shown in Figure 4.3, thereby allowing for the application of increased pressure to the bonding area during joint manufacture without an undesired reduction in bond line thickness. The diameter distribution of the spacing beads consisted of 99% in the range of 106-125  $\mu\text{m}$  and 92% spherical as certified by Novum Glass, LLC, Rolla, MO (see APPENDIX A for the certification report).

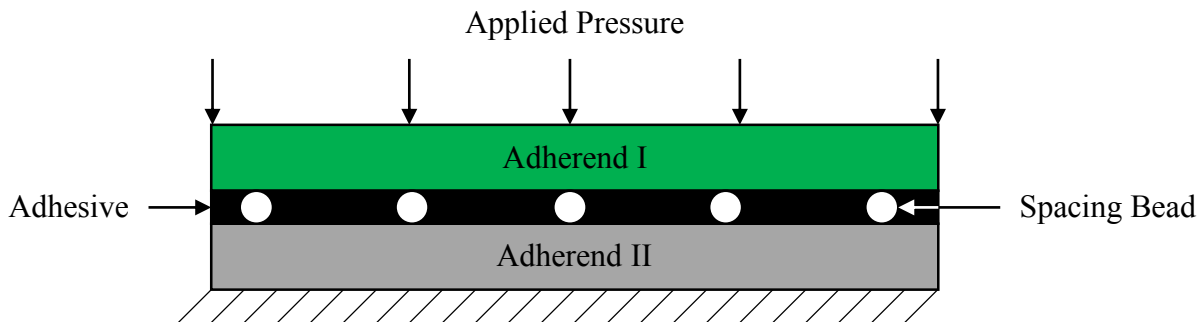


Figure 4.3: Diagram of the mechanical support provided via the incorporation of spacing beads

## **4.2. Experimental Methods**

The experimental methods employed in the present research regarding the equipment used, referenced test standards, procedures used throughout sample manufacture and testing, and data analysis methodology have been described in this section. Variation below 5.00% has been assumed here to be insignificant.

### **4.2.1. Adhesive Characterization**

#### **4.2.1.1. Decomposition**

The degradation temperature, activation energy, and preexponential factor of the adhesive were determined via thermogravimetric analysis (TGA). The experimental procedure was developed referencing ASTM E1641 [48] which required 3.00 mg of cured adhesive to be heated to 650°C at heating rates in the range of 2.5-20°C/min.

The degradation temperature provided an upper temperature limit for the other experimentation methods. The activation energy and preexponential factor were determined to allow for future modelling of the SLJs as an extension of the work of Nguyen et al. [24].

Specimens were prepared by thoroughly mixing the two-part adhesive and applying it to an aluminum plate coated with Teflon release film with a spatula. The adhesive was allowed to cure for a minimum of 48 hours before removal and testing. Testing was conducted using a TGA Q500 (TA Instruments, New Castle, DE) in a nitrogen atmosphere.

The failure criterion,  $\alpha$ , of 5.00% was used to determine the corresponding degradation temperature at each heating rate. The activation energy,  $E$ , and preexponential factor, reported as  $\ln(A)$ , were calculated as described in the test standard.

#### 4.2.1.2. Temperature Effects on Adhesive Stiffness

The effects of temperature on the adhesive stiffness in its bulk form was evaluated via dynamic mechanical analysis (DMA) with which specimens were subjected to a constant amplitude sinusoidal load or displacement at varying temperatures while measuring the storage and loss moduli as a function of temperature were recorded.

Molds for sample manufacture were produced via fused deposition modelling (FDM) using a Lulzbot Taz 6 (Aleph Objects Inc., Loveland, CO) with acrylonitrile butadiene styrene (ABS) filament. The mold was placed in an acetone vapor bath for 24 hours to obtain a smooth finish. The results of this process are shown in Figure 4.4.

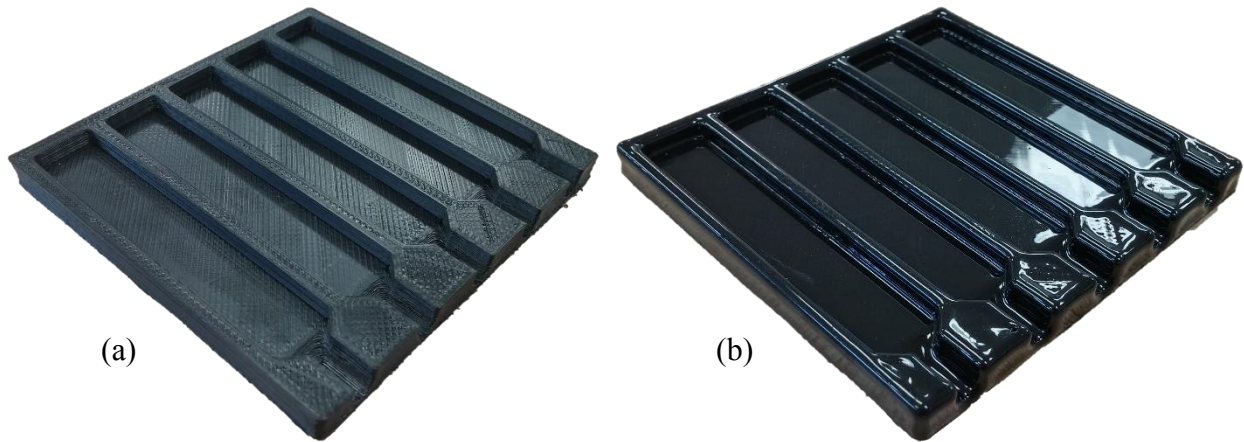


Figure 4.4: (a) Pre- and (b) post-acetone vapor treatment of the DMA sample mold

Samples were manufactured by placing a mold on an aluminum plate, as shown in Figure 4.5, with a nonporous Teflon sheet between the two and injecting the adhesive, using a mixing nozzle, into the mold cavity until filled. The samples were allowed to cure for 24 days prior to testing. The tested sample consisted of 3 specimens.

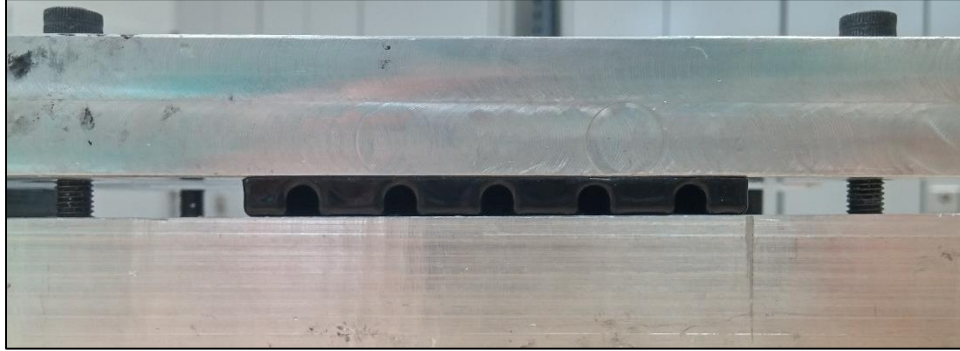


Figure 4.5: DMA sample manufacturing setup

The experimental procedure was developed referencing ASTM D5023 [49] and the work of Bai and Keller [50]. Testing was conducted using a Q800 DMA (TA Instruments, New Castle, DE) with a dual cantilever fixture in a nitrogen atmosphere. Liquid nitrogen was used as a cooling agent. Specimens were secured into the fixture via the application of 56.5 N·cm of torque to the clamping fixtures at room temperature and again once the chamber had reached the initial test temperature of -20°C. A cyclic strain with an amplitude of 0.30% was applied to the specimen at a frequency of 1 Hz while the temperature was ramped from -20°C to 200°C at a rate of 2°C/min.

The  $T_g$  was reported in accordance to ASTM D5023 [49] as the temperature corresponding to the tan delta ( $\tan\delta$ ) peak which indicated the region of rapid change in the storage and loss moduli.

It should be noted that the thickness of the adhesive which comprises the SLJs was much less than that of the bulk adhesive, i.e. just 4.17 % of the bulk specimen thickness, and is therefore not directly comparable [2], but the adhesive has been studied here in bulk form to evaluate the temperature effects on its behavior in isolation.

#### **4.2.1.3. Bond Line Thickness**

The efficacy of the implemented bond line thickness control method was determined via optical microscopy of 5 randomly sampled specimens which were prepared via wet sanding with

increasingly fine sandpaper ranging from 100 to 1200 grit. Microscopy was performed using a Axovert 40Mat (Carl Zeiss AG, Oberkochen, Germany) and images were obtained using a ProgRes C10plus camera (JENOPTIK AG, Jena, Germany), shown in Figure 4.6. Bond line thicknesses were measured at 3 locations on both sides of each specimen using iSolution DT Version 7.9 (IMT i-Solution Inc.) software. Highlighter ink was applied to the area of interest to promote reflectivity and contrast of the composite and adhesive materials as well as to reduce the reflectivity of the metal materials.



Figure 4.6: Zeiss microscope and JENOPTIK camera used to measure bond line thicknesses

The measured bond line thicknesses were then evaluated statistically to determine if they were significantly different than that of the largest diameter within the spacing bead distribution, 125  $\mu\text{m}$ . This was done using a  $t$ -test with the null and alternative hypotheses of:

$$\begin{aligned} H_0 : \mu &= 125 \\ H_1 : \mu &\neq 125 \end{aligned} \tag{4.1}$$

where  $\mu$  is the sample mean. The test statistic,  $t$ , was determined as:

$$t = \frac{\bar{X} - \mu}{\frac{s}{\sqrt{n}}} \quad (4.2)$$

where  $\bar{X}$  is the sample mean,  $s$  is the standard deviation of the sample, and  $n$  was the sample size. The result of this calculation was then compared, using a two-tailed test, with that of the tabulated  $t$  value corresponding to  $n-1$  degrees of freedom and a level of significance of 0.05 to determine if there was statistical evidence for the rejection of the null hypothesis (i.e. if the calculated  $t$  was between the tabulated  $t$  values the hypothesis was not rejected).

## **4.2.2. Temperature Effects on the Monotonic and Fatigue Behaviors of Adhesively-Bonded Dissimilar Material SLJs**

### **4.2.2.1. Sample Manufacture**

Without the availability of an applicable test standard for the fatigue of dissimilar material joints, the specimen geometry was developed referencing the available standards regarding bond strength and fatigue for metal-metal and fiber reinforced plastic (FRP) joints, including ASTM D1002 [51], D3166 [52], D3983 [10], and D5868 [53]. The composite and metal adherends were prepared to the dimensions specified in Figure 4.7 through the use of a wet-tile saw and laser cutting, respectively.

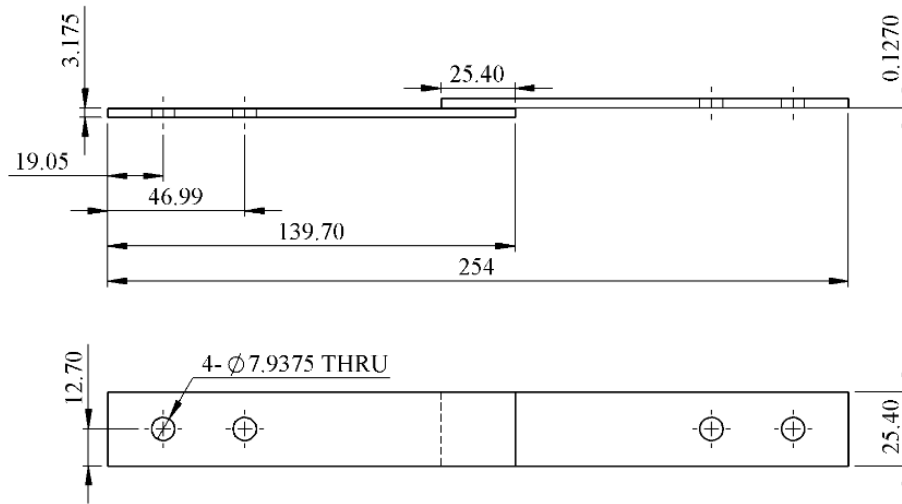


Figure 4.7: Geometry and dimensions of fatigue SLJ specimens (all dimensions in mm)

Once the adherends were cut to shape, the bonding areas were degreased using an acetone soaked cloth and abraded with 100 grit sandpaper. An applied load of approximately 35.0 N was used during abrasion. The procedure included abrasion for 5 seconds in the direction perpendicular to the longitudinal direction and another 5 seconds in an elliptical pattern in the direction perpendicular to the longitudinal direction, as shown in Figure 4.8, after which the bonding surfaces were again cleaned with an acetone soaked cloth.



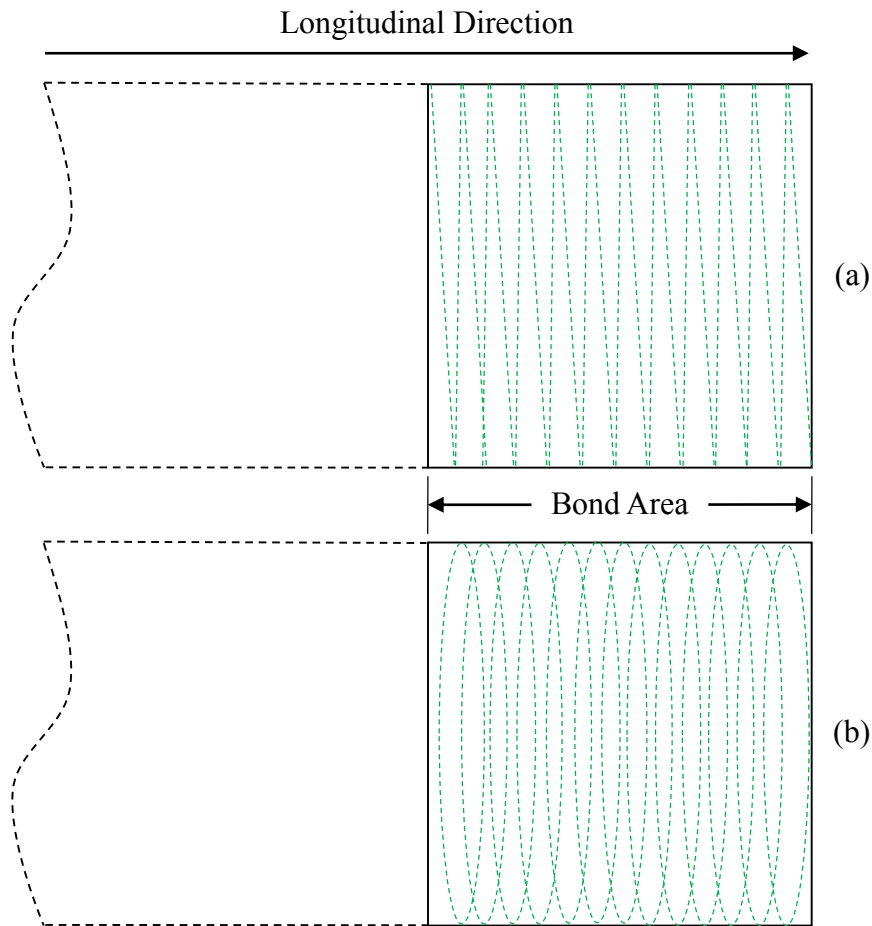


Figure 4.8: Diagram of abrasion path (a) initial horizontal motion and (b) final elliptical motion

Once the adherends were prepared for bonding approximately 1 wt% of spacing beads was mixed with the adhesive until homogeneous. A metal spatula was then used to apply the spacing bead/adhesive mixture to the bonding surface of the metal adherend after which the composite adherend was pressed into place by hand, causing excess adhesive to flow out of the bond line. This excess adhesive was removed using the spatula and used to form the fillets which were incorporated for increased joint performance [54-56]. The fillets on the top and bottom of the joints resulted in differing shapes due to gravitational sagging as shown in Figure 4.9 and Figure 4.10, respectively.

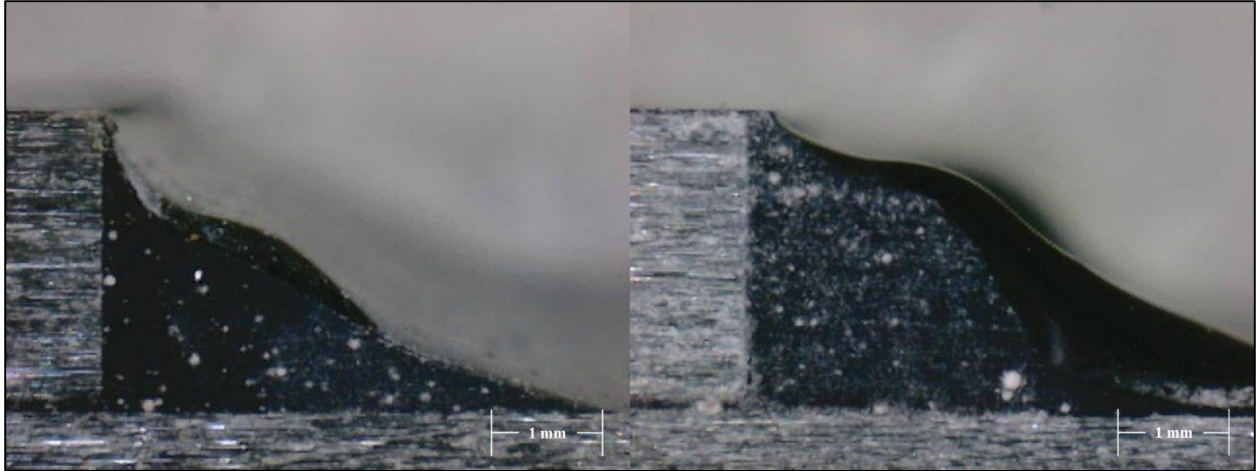


Figure 4.9: Representative upper (nearest the jig clamp) fillets

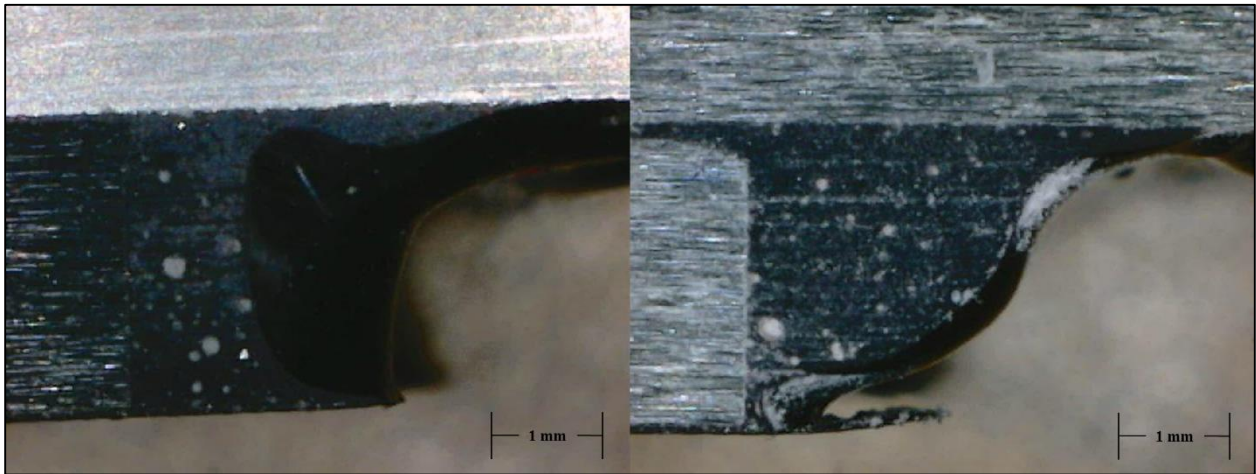


Figure 4.10: Representative lower (nearest the jig base) fillets

The formed SLJs were then placed into a jig such that one side of each adherend was in contact with the alignment pins to ensure parallelism. Clamps were then placed onto the SLJs over the bonding surface to allow for the application of pressure to obtain a consistent bond line thickness. The jig, shown in Figure 4.11 and accompanied with technical drawings in APPENDIX B, was designed, referencing [57], to allow for the simultaneous production of 8 SLJ specimens. The clamping pressure was applied through the application of 1.67 N·m of torque to the clamping bolts, starting from the center and finishing with the outer bolts. The specimens were held under

pressure for a minimum of 24 hours and allowed to cure for at least a total of 48 hours, as per the manufacturer's recommendation [47], prior to testing.



Figure 4.11: Joint assembly jig

The excess adhesive along the edges of the SLJs was removed via belt sanding with 80 grit sandpaper in 3-5 second intervals, to minimize heat build-up within the joint, until both sides were free from excess adhesive and parallel.

#### **4.2.2.2. Apparatus and Fixturing**

The monotonic and fatigue testing was conducted using a model 312.31 servo-hydraulic load frame with a 250 kN load cell and Series 651 environmental chamber (MTS Systems Corporation, Eden Prairie, MN), shown in Figure 4.12. Due to space constraints within the interior of the environmental chamber, fixtures were manufactured to the specifications shown in Figure 4.13 which were developed referencing ASTMs D3983 [58] and D3166 [10].



Figure 4.12: Monotonic and fatigue experimental test setup

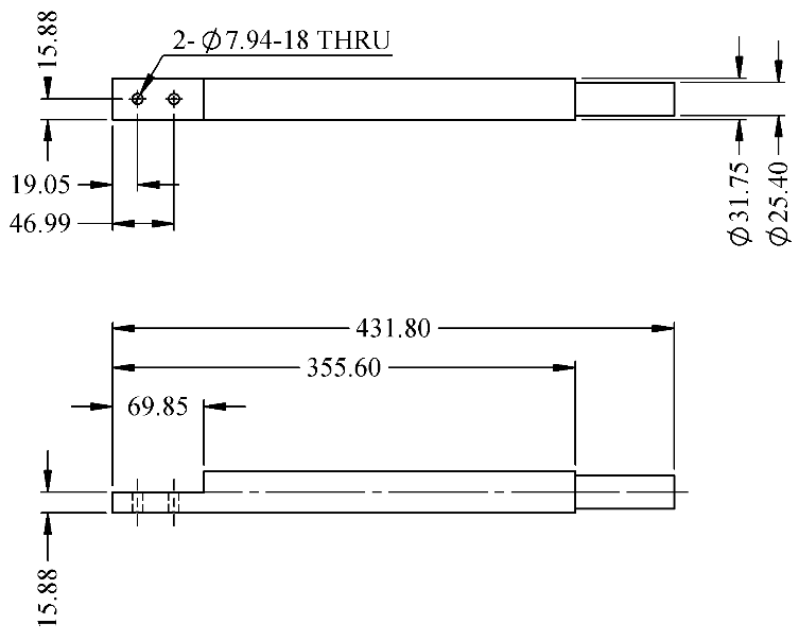


Figure 4.13: SLJ fatigue test fixture (all dimensions in mm)

Specimens were secured into the fixture via a bolt and plate assembly, shown in Figure 4.14, with the bolts being tightened by hand and then loosened a quarter of a turn at which point a 44.48 N tensile load was applied to remove any slack from the system. The bolts were then tightened with a wrench and a torque of 40.67 N·m was applied.

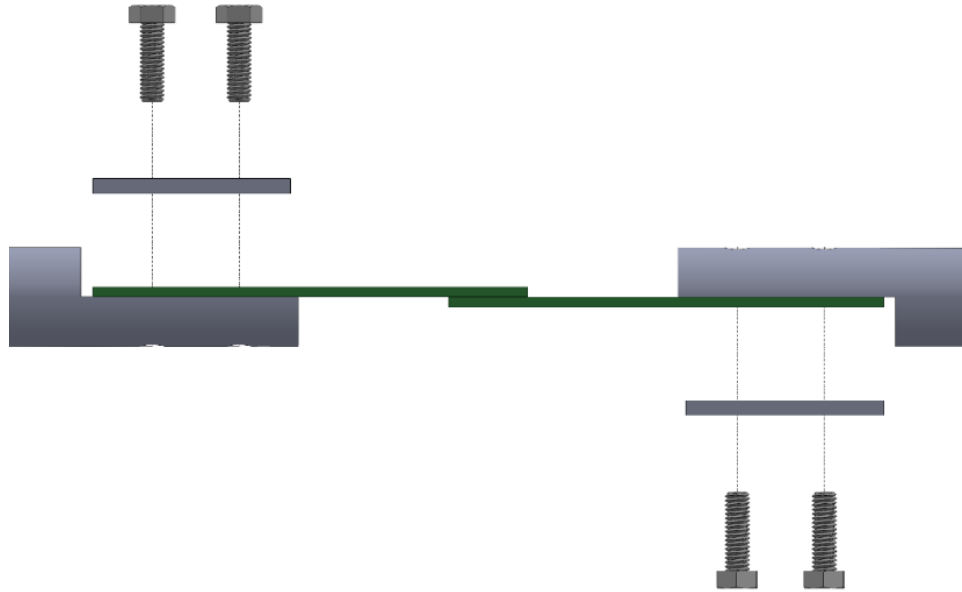


Figure 4.14: Fixture diagram for monotonic and fatigue specimens

#### 4.2.2.3. Experimental Program

The experimental program for the study of fatigue behavior was developed through the use of a full factorial design. The factors of interest included the metal adherends to which the polyurethane composite was bonded, fatigue loading level, and temperature.

The adherends used in joint manufacture included 5052 aluminum and A36 steel, identified in the test program as adherend 1 and 2, respectively. The implemented load levels included 0.50, 0.65, and 0.80, identified in the test program as LL 1, 2, and 3, respectively. The test temperatures included 0°C, 25°C, 50°C, and 75°C, identified in the test program as temperature 1, 2, 3, and 4, respectively. All fatigue testing was performed with a loading ratio,  $R$ , of 0.50 at a frequency of 5

Hz. All experimental samples consisted of a minimum of three specimens except those at 0°C, which consisted of a single specimen. The experimental fatigue test program is listed in Table 4.1.k

Table 4.1: Experimental fatigue test program

<b>Run No.</b>	<b>Adherend</b>	<b>LL</b>	<b>Temperature</b>
1	1	-	1
2	2	-	1
3	1	-	2
4	2	-	2
5	1	-	3
6	2	-	3
7	1	-	4
8	2	-	4
9	1	1	1
10	1	2	1
11	1	3	1
12	2	1	1
13	2	2	1
14	2	3	1
15	1	1	2
16	1	2	2
17	1	3	2
18	2	1	2
19	2	2	2
20	2	3	2
21	1	1	3
22	1	2	3
23	1	3	3
24	2	1	3
25	2	2	3
26	2	3	3
27	1	1	4
28	1	2	4
29	1	3	4
30	2	1	4

#### 4.2.2.4. Experimental Procedure

The experimental procedures were developed referencing ASTM D1002 [51], D3163 [52], and D5868 [53] for monotonic tension and ASTM D3166 [10] for tension-tension fatigue. The experimental procedures were implemented using MPT software (MTS Systems Corporation, Eden Prairie, MN). The following sections describe the implemented procedure for the monotonic tension and tensile-tensile fatigue testing.

##### Monotonic Tension

The implemented test program for monotonic tension consisted of the following:

1. Ramp at 25.0 N/s to 0 N
2. Dwell time of 30.0 minutes at the test temperature
3. Ramp at 1 mm/min to 25.4 mm
  - a. Failure criterion:  $F < 0.75 \cdot F_{max}$
  - b. Record displacement and force data at a rate of 50.0 Hz

##### Tension-Tension Fatigue

The implemented test program for tension-tension fatigue consisted of the following:

1. Ramp at 25.0 N/s to 0 N
2. Dwell time of 30 minutes at the test temperature
3. Ramp at 80 N/s to  $F_{mean}$ 
  - a. Record displacement and force data at rate of 20.0 Hz
4. Apply a sinusoidal load with maximum and minimum loads of  $F_{max}$  and  $F_{min}$ , respectively at a frequency of 5.00 Hz.

- a. Record displacement and force data at a rate of 500 Hz, obtaining approximately 100 data points per load-unload cycle, for 3 consecutive cycles at an interval of 5 cycles or an interval deemed appropriate for the given fatigue life

#### **4.2.2.5. Data Reduction**

Data reduction was performed utilizing MATLAB R2016b (MathWorks, Natick, MA) with which codes were developed to analyze the raw data files obtained from the experimental data acquisition of the MPT software. The overview of how the data was reduced for both monotonic tension and tension-tension fatigue is detailed in the remainder of this section.

##### Monotonic Tension

The ultimate failure load ( $F_{s,ult}$ ), i.e. the maximum load which was supported by the joint throughout the duration of the test, was determined via searching the data set for the max load. The stiffness of each specimen was determined via the application of a linear fit to the data in the range of  $0.25 \cdot F_{s,ult}$  and  $0.75 F_{s,ult}$ . The lower limit was selected to exclude the settling effects of the fixture, grips, or joints while the upper limit was selected to exclude plastic deformation effects.

##### Tension-Tension Fatigue

Joint stiffness was determined via the application of a linear fit to 3 consecutive hysteretic loading response loops, as previously implemented by Zhang et al. [35], each of which consisted of approximately 100 data points. The interval between data acquisition was altered based on the expected fatigue life. The fatigue life was recorded directly from the MPT software cycle counter which reported the final cycle to which the specimen was subjected.

Normalized stiffness and cycle data was obtained by referencing initial stiffness and final cycle, respectively and allowed for an analysis of the effects of the loading and temperature variables on the failure behavior.



### 4.2.3. Temperature Effects on the Low Velocity Transverse Impact Behavior of Adhesively-Bonded Dissimilar Material SLJs

#### 4.2.3.1. Sample Manufacture

The transverse LVI specimens were manufactured to the dimensions shown in Figure 4.15 using the same methodology as described in section 4.2.2.1 with the addition of clamping bars over the end tab bond areas.

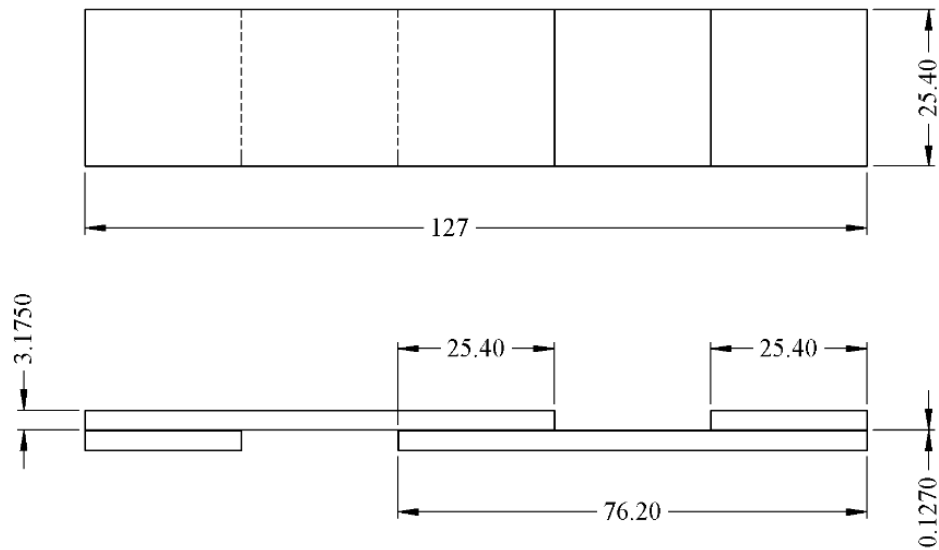


Figure 4.15: Geometry and dimensions of impact SLJ specimens (all dimensions in mm)

#### 4.2.3.2. Apparatus and Fixturing

Testing was conducted using a model 9250HV drop weight tower and EC8250A environmental chamber (Instron, Norwood, MA), shown in Figure 4.16, using liquid nitrogen for cooling, a 12.7 mm diameter hemispherical steel tup, and total mass of 7.19 kg.



Figure 4.16: LVI testing apparatus setup

Fixed boundary conditions were implemented via fixing the specimen end tabs using a pneumatic clamp, shown in Figure 4.17. A diagram of the transverse impact event is shown in Figure 4.18.



Figure 4.17: Pneumatic clamping mechanism used to secure impact specimens

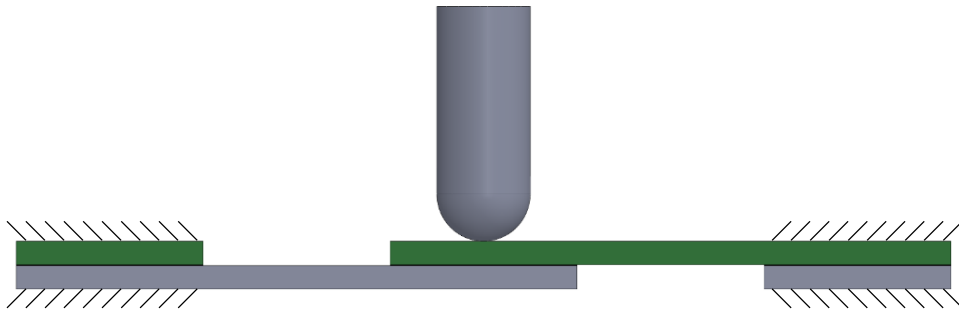


Figure 4.18: Diagram of transverse SLJ impact

A jig, used to ensure specimen alignment and placement consistency, was manufactured using FDM with a Mark 2 printer (Markforged, Cambridge, MA) with Markforged Onyx filament, composed of carbon filled nylon, which allowed for use at elevated temperatures. The jig was designed for pressure fitting within the 76.2 mm hole of the pneumatic clamps as well as the pressure fitting of aluminum inserts to provide the linear support, as opposed to the curved support offered by the pneumatic clamping mechanism, and is shown in Figure 4.19. Technical drawings of both the upper and lower jig components are available in APPENDIX B.

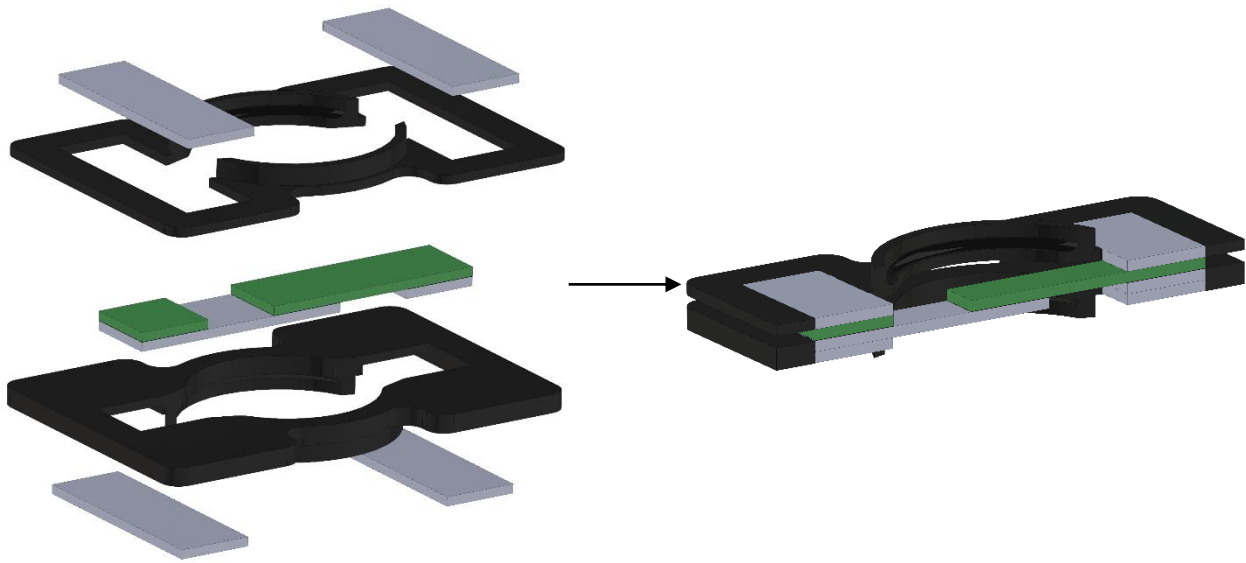


Figure 4.19: Schematic of LVI specimen and clamping jig

To ensure consistency and comparability, the specimens were placed in the jig such that the impact surface would be that of the composite adherend, thereby eliminating the differing plastic deformation effects within the impact zone which would have arisen from differing materials.

#### 4.2.3.3. Experimental Program

The experimental program for the study of LVI behavior was developed through the use of a full factorial design. The factors of interest included the metal adherends, to which the polyurethane composite was bonded, and temperature.

The adherends used in joint manufacture included 5052 aluminum and A36 steel, identified in the test program as adherend 1 and 2, respectively. The test temperatures included  $-20^{\circ}\text{C}$ ,  $0^{\circ}\text{C}$ ,  $25^{\circ}\text{C}$ ,  $40^{\circ}\text{C}$ ,  $80^{\circ}\text{C}$ , and  $120^{\circ}\text{C}$ , identified in the test program as temperature 1, 2, 3, 4, 5, and 6, respectively. The target impact velocity of the testing apparatus was set to 1 m/s for all specimens. All experimental samples consisted of a minimum of five specimens except those at  $0^{\circ}\text{C}$ , which consisted of a single specimen. The experimental LVI test program is listed in Table 4.2.

Table 4.2: Experimental LVI test program

Run No.	Adherend	Temperature
1	1	1
2	2	1
3	3	1
4	1	2
5	2	2
6	3	2
7	1	3
8	2	3
9	3	3
10	1	4
11	2	4
12	3	4
13	1	5
14	2	5
15	3	5
16	1	6
17	2	6
18	3	6

#### 4.2.3.4. Experimental Procedure

The experimental LVI procedure was developed referencing ASTM D7136 [59] and the work of Vaidya et al. [41] and consisted of the following:

1. Place the specimen into the jig such that the impact surface is that of the composite
2. Equilibrate at the test temperature for a minimum of 30 minutes
3. Move the impact tup to a height such that the impact velocity is 1 m/s
4. Initiate clamp closure
5. Release the impact tup
6. Record data for 20 ms after initial contact

#### 4.2.3.5. Data Reduction

The data obtained from the LVI testing included time, load, energy, velocity, and deflection. These data were reduced using MATLAB R2016b (MathWorks, Natick, MA) to obtain insight into the failure progression and response behaviors of the studied SLJs.

The impact velocity was determined via obtaining the velocity when time is zero, which is the time data point before a force on the load cell was registered as reported by the Impulse Data Acquisition Version 3.4.59 (Instron, Norwood, MA) software.

The initial failure load,  $F_{if}$ , was determined via the application of a moving average filter, via the built in smooth MATLAB function with a span of 10, to the force response data in order to reduce data noise. A higher accuracy central-difference approximation of slope was used to further reduce the influence of data noise and is given as:

$$F'_{i+2} = \frac{-F_{i+2} + 8F_{i+1} - 8F_{i-1} + F_{i-2}}{12\Delta\delta} \quad (4.3)$$

where  $F$  is the force at the  $i^{\text{th}}$  data point and  $\Delta\delta$  is the change in displacement between the  $i+2$  and  $i-2$  data points. The approximated slope was then used to approximate the initial failure load at which point the slope would be near zero. This approximation was then used as a basis to find the initial failure force in the acquired data knowing that the approximation would always be low due to the averaging of data points giving more weight to those occurring before initial failure. The maximum load was then determined by searching the data within the smoothing span for the highest load. Once the initial failure load was determined, the corresponding initial failure displacement,  $\delta_v$ , was also known, being the corresponding displacement at the time of initial failure.

The initial stiffness (stiffness being defined by the slope of the force-displacement response curve) was determined via the application of a linear fit to the force-displacement response data prior to initial failure. The secondary stiffness was determined via the application of a linear fit to the force-displacement response data between 25% and 75% of the subsequent peak load which was determined using the same methodology as was used for the determination of initial failure.

The maximum impact load,  $F_{max}$ , and displacement,  $\delta_{max}$ , were determined via searching the data for the maximum of the entire data set for each respective result. The absorbed energy was determined to be the energy at which point the impact force returned to zero, indicating complete release of any remaining elastic strain energy.

These parameters have been demonstrated on a representative SLJ LVI response curve shown in Figure 4.20.

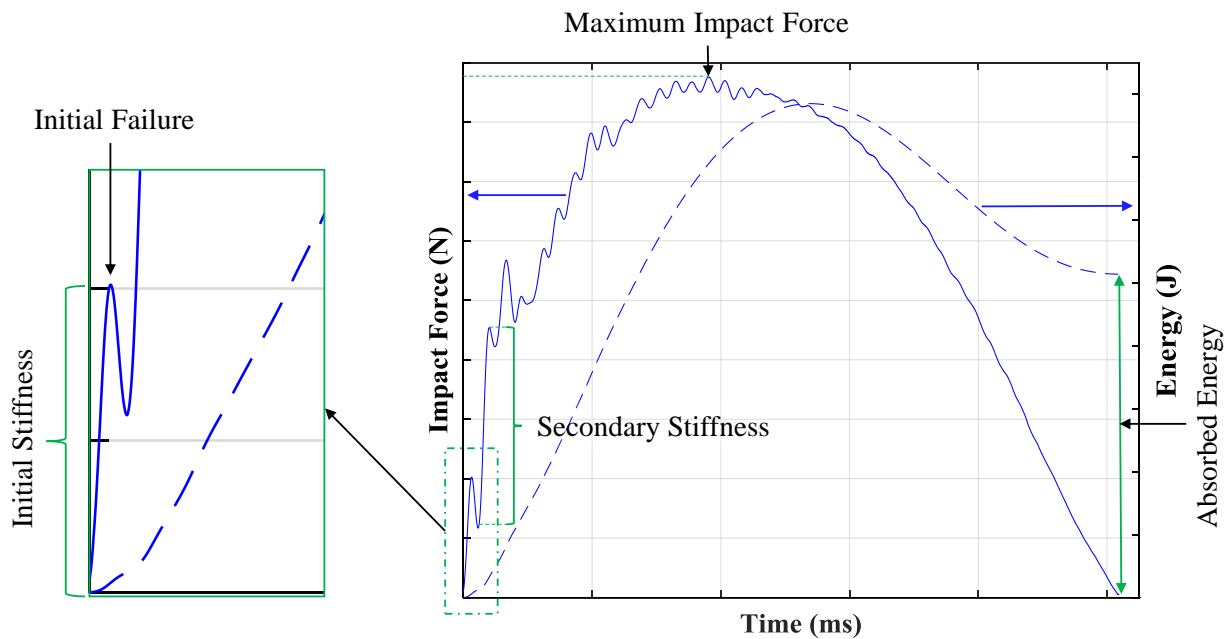


Figure 4.20: Identification of the reduced LVI data

## CHAPTER 5. RESULTS AND DISCUSSION

### 5.1. Adhesive Characterization

#### 5.1.1. Decomposition

The analysis of the rate dependent weight reduction as a function of temperature, shown in Figure 5.1, allowed for the determination of the upper temperature threshold for the adhesive to be 244°C, 259°C, 265°C, and 279°C at heating rates of 2.5°C/min, 5°C/min, 10°C/min, and 20°C/min, respectively.

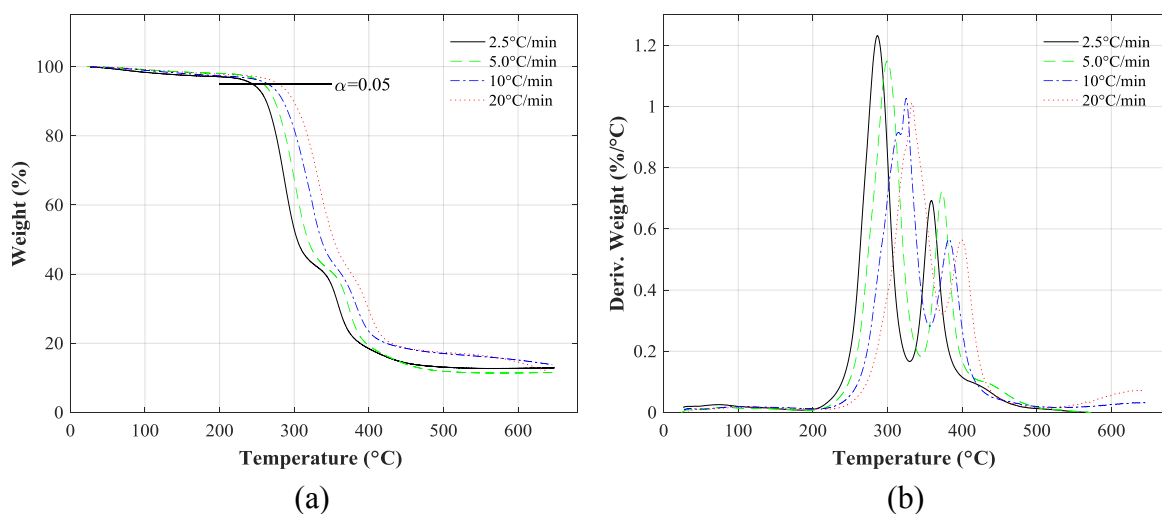


Figure 5.1: (a) TGA and (b) DTGA curves

The analysis of the data, requiring a linear fit and data manipulation as shown in Figure 5.2, yielded an activation energy of 136 kJ/mol and a preexponential factor,  $\ln(a)$ , of 26.8.



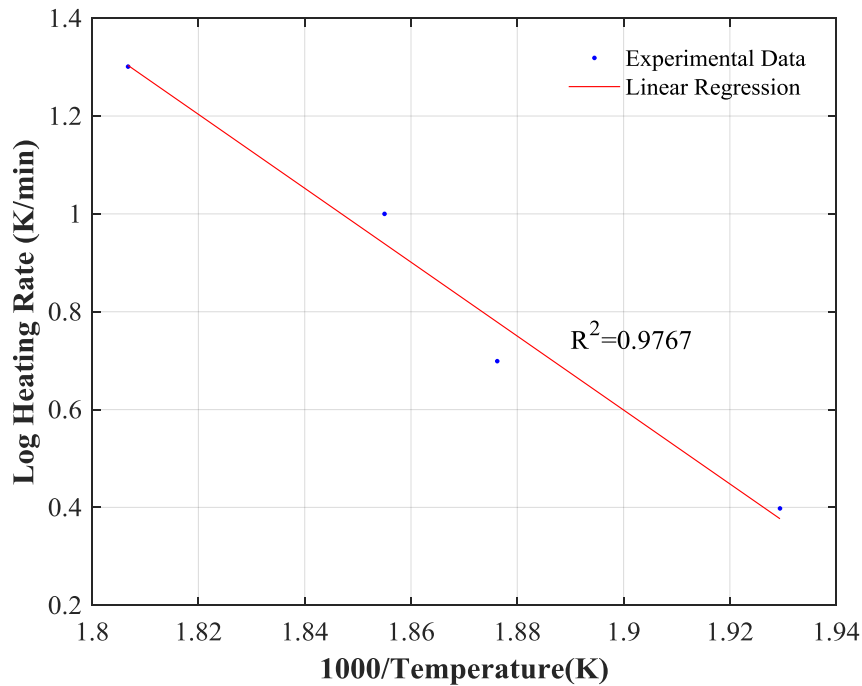


Figure 5.2: Linear fit of the degradation results

### 5.1.2. Temperature Effects on Adhesive Stiffness

The dynamic mechanical analysis of the bulk adhesive yielded a  $T_g$  of 60.2°C with a variance coefficient of 0.748%. The analysis also demonstrated the adverse effects of temperature on the stiffness of the adhesive which can be understood by considering free volume theory which provides an effective explanation of  $T_g$  [2]. The thermal expansion of the polymer due to elevated temperatures, which is generally more than that of a majority of engineering materials [2], increases the free volume, or the volume which is not occupied by atoms which make up the polymer network of the material. This increase in free volume allows for greater mobility of the polymer network [2, 60]. The effect of this increase in free volume on the bulk adhesive demonstrated by the obtained storage modulus and  $\tan\delta$  DMA data and has been shown in Figure 5.3.

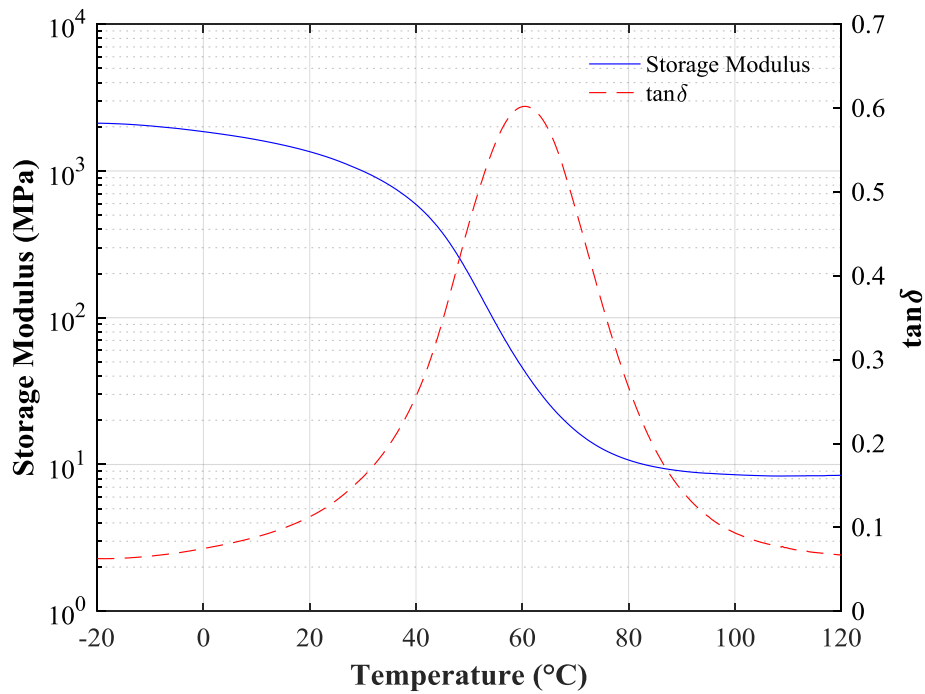


Figure 5.3: Storage modulus and tan delta vs temperature of a representative two-part polyurethane adhesive specimen

### 5.1.3. Bond Line Thickness

The microscopy of the bond line thicknesses yielded average thicknesses of 157  $\mu\text{m}$ , 138  $\mu\text{m}$ , and 109  $\mu\text{m}$  for the composite, aluminum, and steel joints, respectively. The statistical analysis indicated that the thicknesses were not significantly different from that of the maximum spacing bead diameter of 125  $\mu\text{m}$ . The results of the bond line thickness measurements are shown in Figure 5.4 with the corresponding data available in APPENDIX C. Representative images of the composite, aluminum, and steel SLJ bond lines are also shown in Figure 5.5, Figure 5.6, and Figure 5.7, respectively.

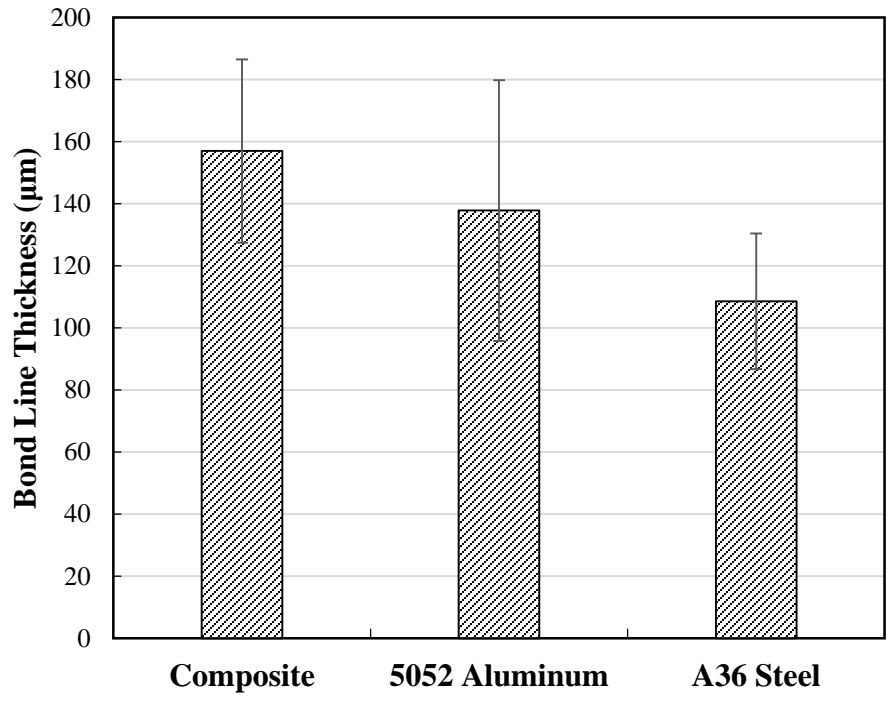


Figure 5.4: Comparison of bond line thickness between SLJ adherends

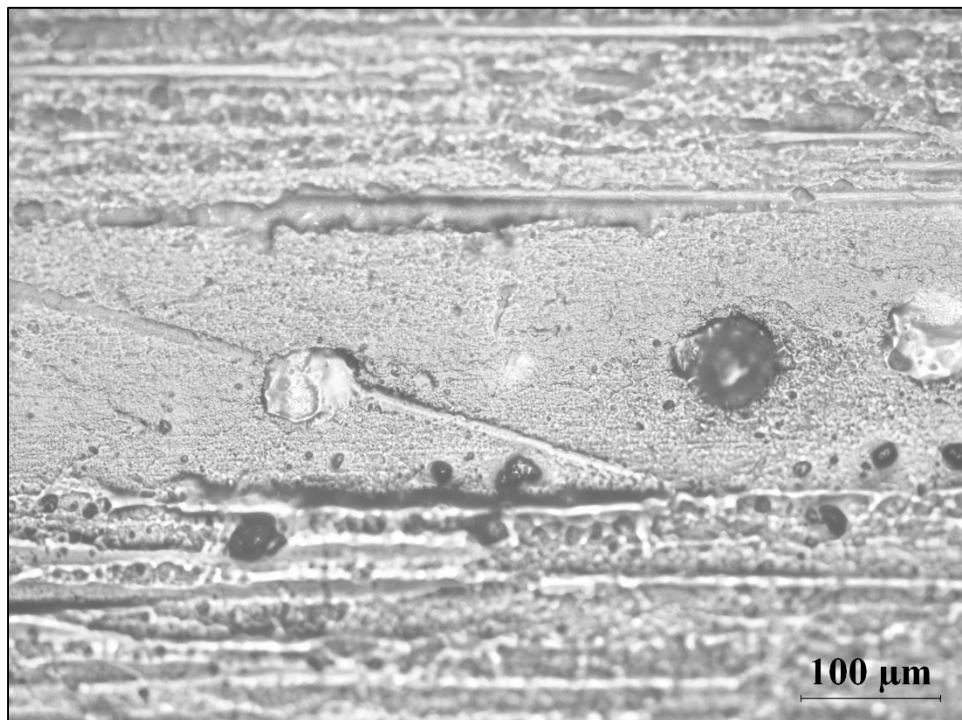


Figure 5.5: Microscopy image of a composite SLJ bond line

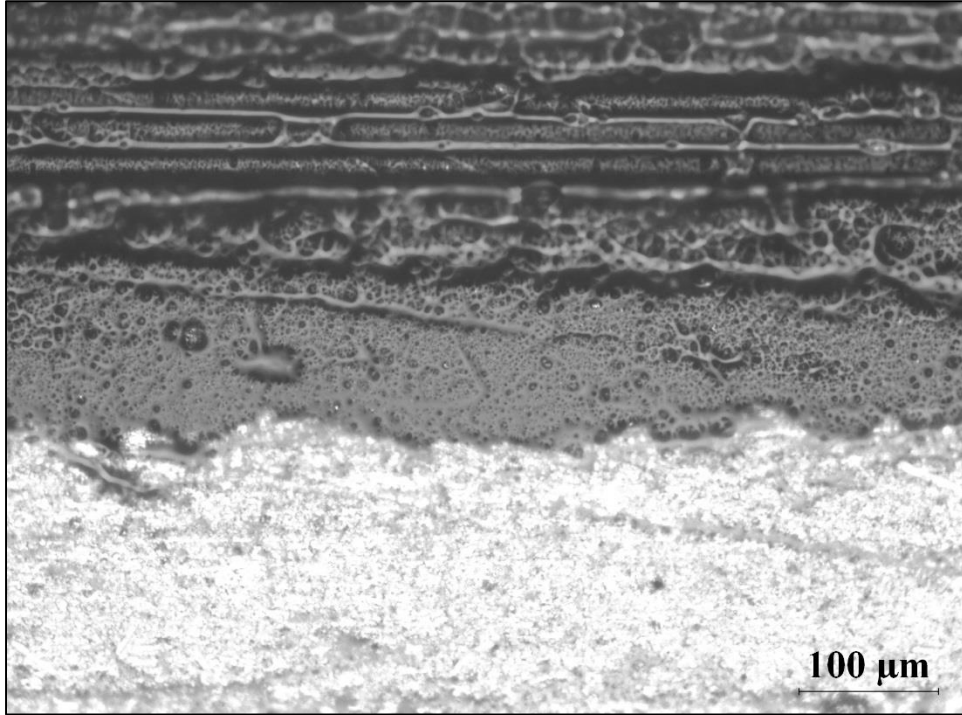


Figure 5.6: Microscopy image of an aluminum SLJ bond line

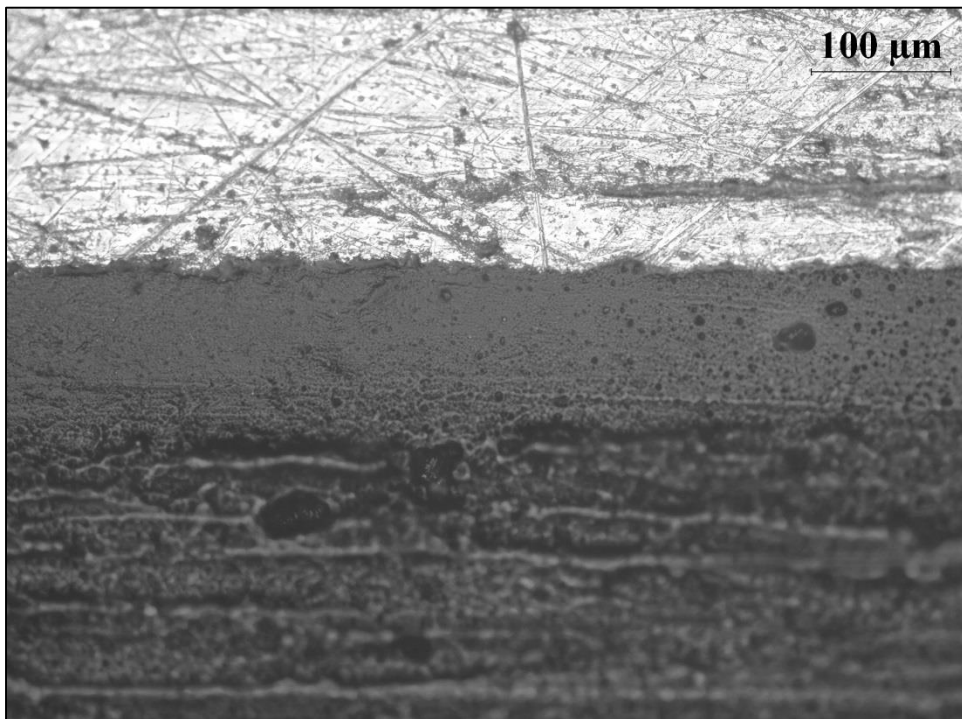


Figure 5.7: Microscopy image of a steel SLJ bond line

## 5.2. Temperature Effects on the Monotonic and Fatigue Behaviors of Adhesively-Bonded Dissimilar Material SLJs

### 5.2.1. Monotonic Tension

The steel and aluminum SLJs exhibited brittle fracture at the temperatures of 0°C and 25°C and exhibited ductile fracture at the temperatures of 50°C and 75°C. Representative load-displacement response curves at each test temperature are shown in Figure 5.8 and Figure 5.9 for steel and aluminum SLJs, respectively.

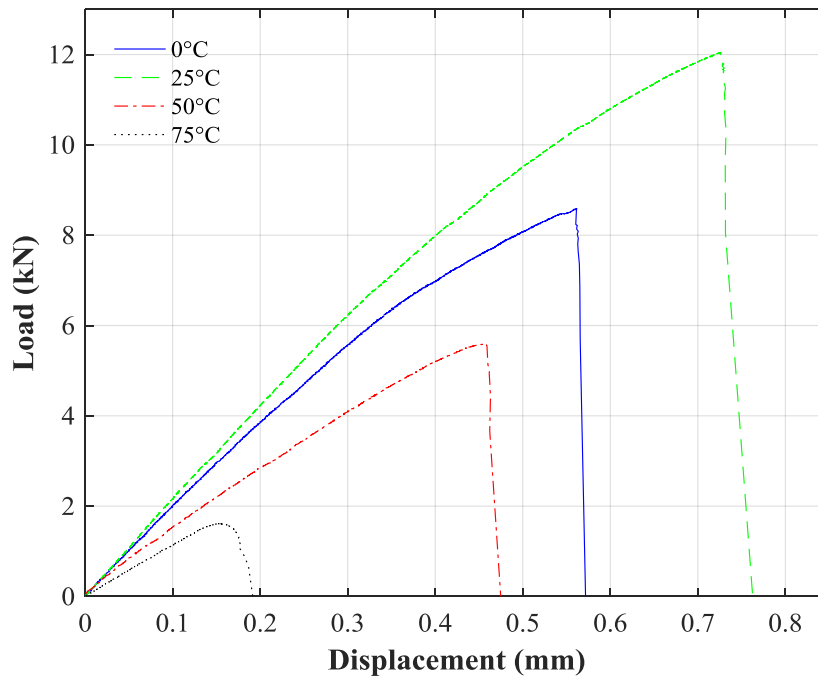


Figure 5.8: Representative monotonic load vs displacement of steel SLJs

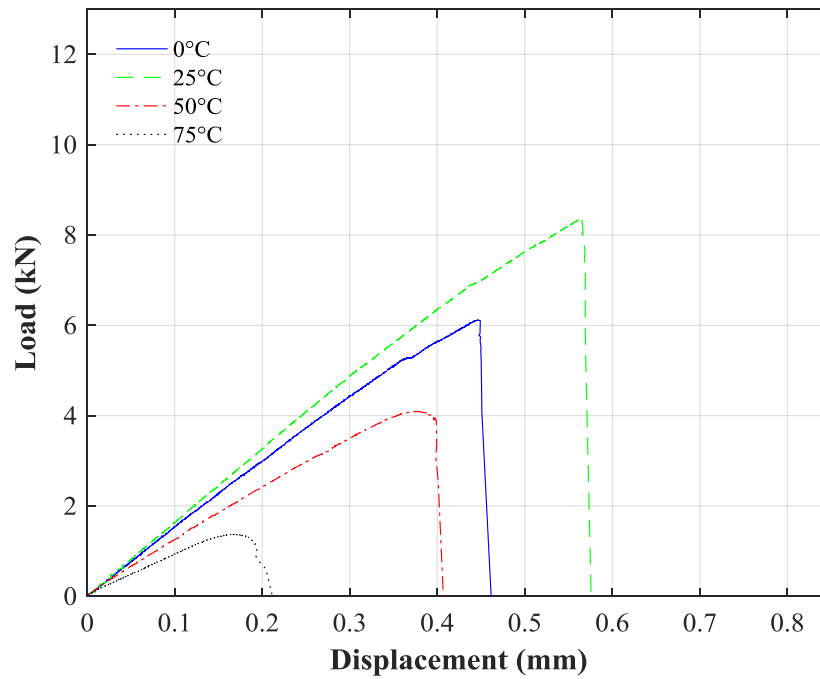


Figure 5.9: Representative monotonic load vs displacement of aluminum SLJs

The analysis of the monotonic force-displacement curve data yielded ultimate loads, displacements at failure, and stiffnesses at each temperature level, shown in Figure 5.10, Figure 5.11, and Figure 5.12, respectively which demonstrated reductions of all properties at non-ambient temperatures.

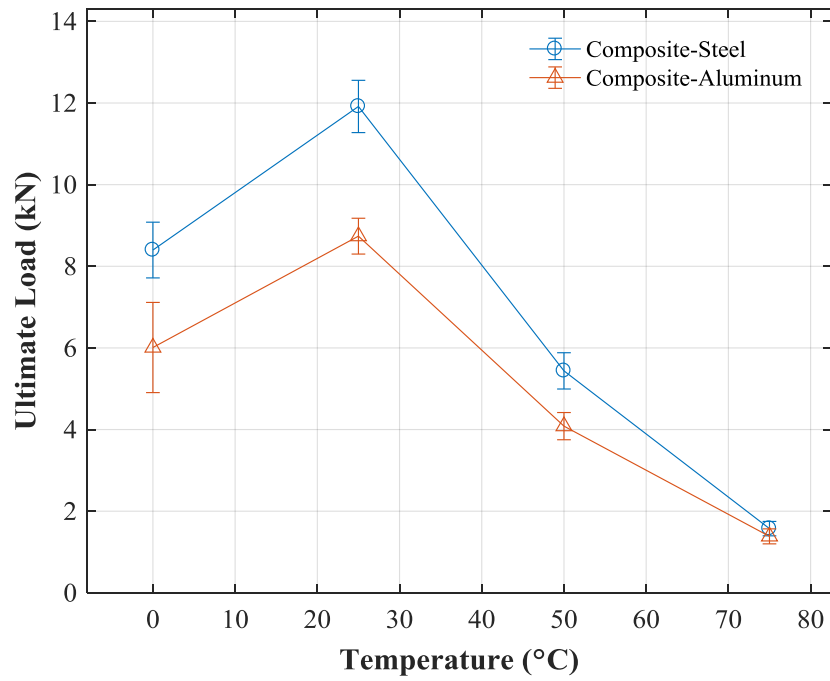


Figure 5.10: Ultimate load versus temperature of steel and aluminum SLJs

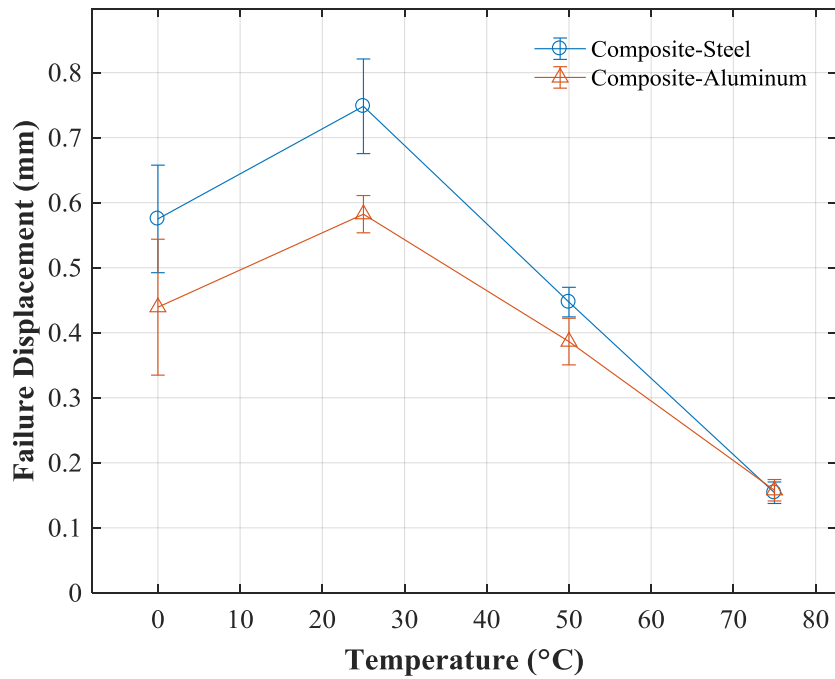


Figure 5.11: Failure displacement versus temperature of steel and aluminum SLJs

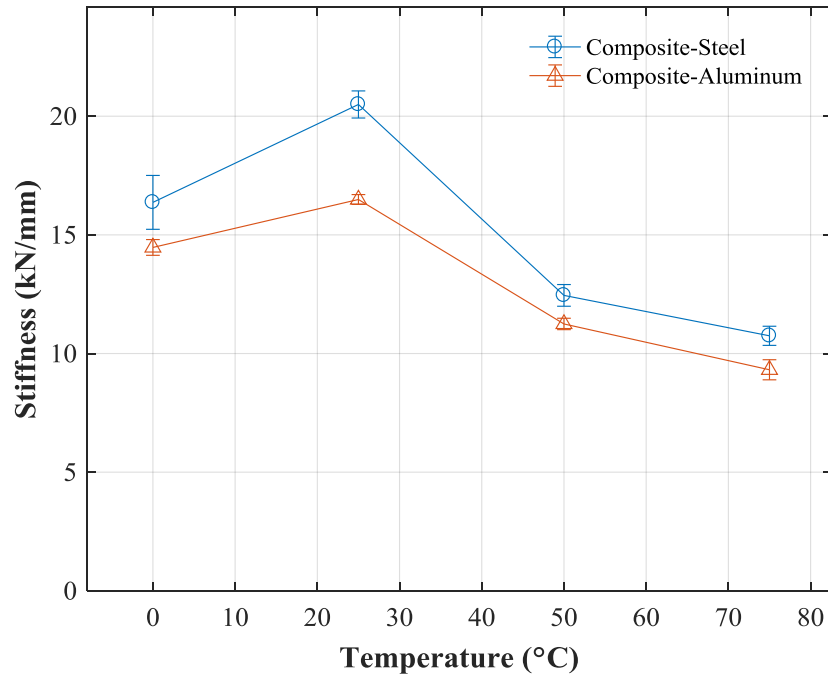


Figure 5.12: Stiffness versus temperature of steel and aluminum SLJs

The reduction of strength of the SLJs at non-ambient temperatures follow trends previously demonstrated in adhesively bonded joints by [24, 61-64] and can be attributed to the combination of the dissimilar coefficients of thermal expansion of the joined materials, unbalanced adherend stiffnesses, and embrittlement, thermal softening, and mechanical property degradation of the adhesive.

The dissimilarity of the adhesive and adherend coefficients of thermal expansion, which were 297% and 95.9% larger than that of the composite for the aluminum and steel, respectively, induces stresses within the joint due to the differing thermal strains resulting from the expansion or contraction of each material. The adhesive thus constricts this expansion or contraction which alters the bending moments at the joint ends thereby causing variations in the shear and peel stress distributions throughout the bond line [65]. The variation in stress distributions, which are no longer symmetric along the bond line when the coefficients of thermal expansion of the adherends



differ, alters the curvature of the eccentric loading path and affects one end more than the other, generally contributing to a reduction in joint performance [65, 66].

The imbalance of adherend stiffness reduces the load carrying capacity of a joint by imparting a stress concentration on the adherend which is more compliant. The stress concentration is due to the greater resulting deformation of the more compliant adherend in comparison to that of the stiffer adherend [54, 65]. This effect has been demonstrated in Figure 5.13.

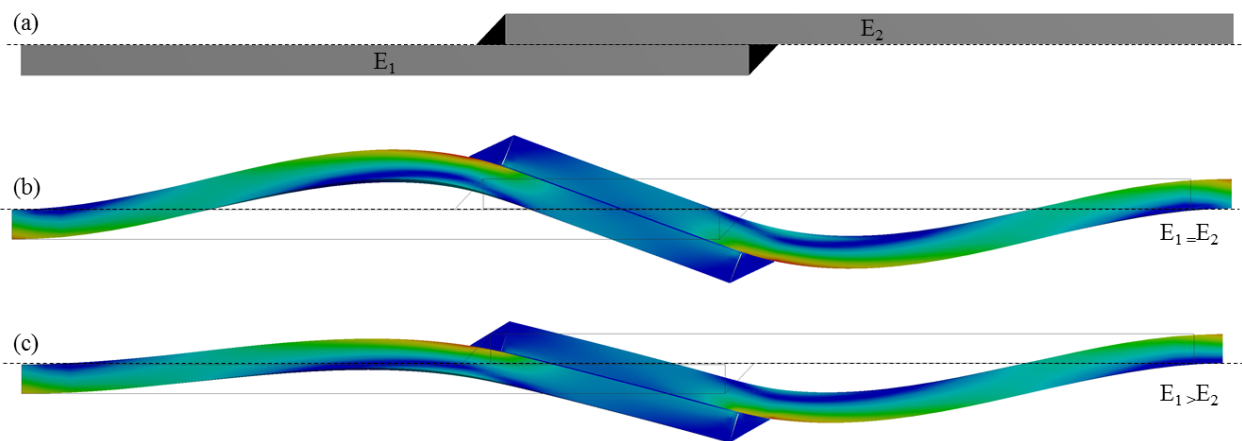


Figure 5.13: Demonstration of the effect of stiffness imbalance on SLJ stress distribution and deformation when loaded in tension. (a) Undeformed SLJ, (b) SLJ with adherends of equivalent stiffness, (c) SLJ with adherend 1 having a greater stiffness than adherend 2

Temperatures below that of a thermoset adhesive's  $T_g$  do not have a significant effect due to the limited mobility of the crosslinked network where the free volume is small. This is due to the restriction of the freedom of movement of the polymer chains, which results in a maintained stiffness and load carrying capacity. When the temperature is increased to and above the  $T_g$ , however, the free volume becomes large enough for the polymer network to begin to move with less restriction, resulting in a decrease in stiffness and load carrying capacity [2, 60].

The evaluation of the sample fracture surfaces revealed a mixed failure mode consisting of interfacial failure, at the adhesive-metal adherend interface, and cohesive failure of the adhesive

and within the resin rich surface layer of the composite adherend at the temperatures of 0°C and 25°C. The failure mode transitioned to interfacial failure, at the adhesive-metal adherend interface, at the temperatures of 50°C and 75°C. The fracture surfaces are shown in Figure 5.14 and Figure 5.15 for the steel and aluminum SLJs, respectively.

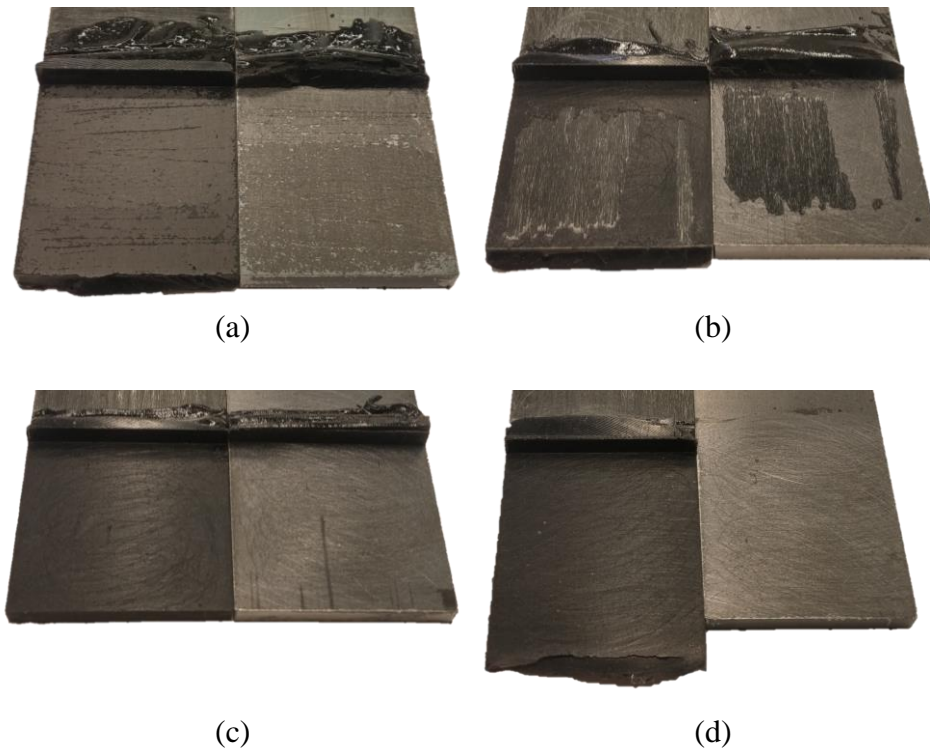


Figure 5.14: Representative monotonic fracture surfaces of steel SLJs at (a) 0°C, (b) 25°C, (c) 50°C, and (d) 75°C

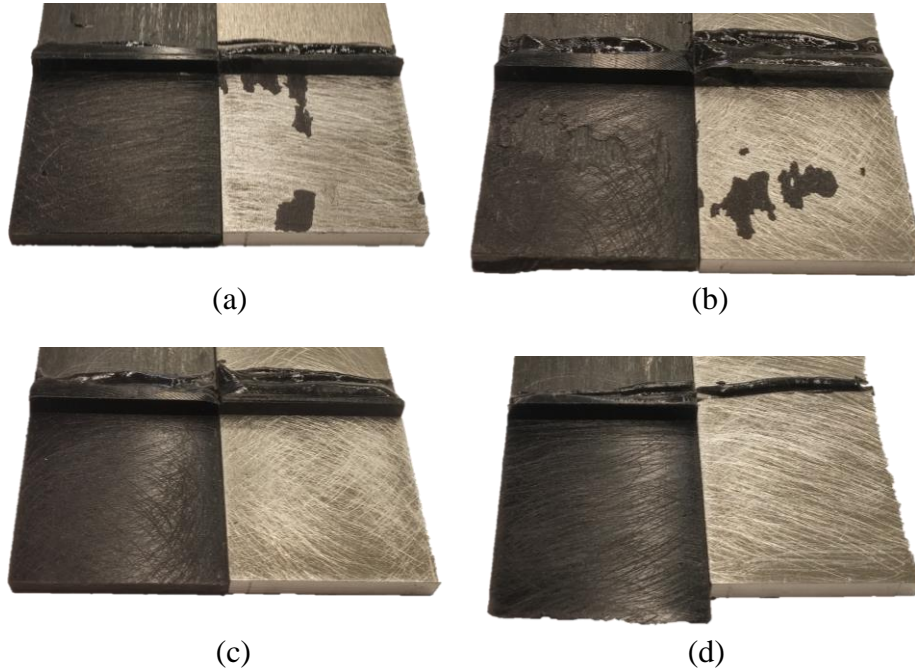


Figure 5.15: Representative monotonic fracture surfaces of aluminum SLJs at (a) 0°C, (b) 25°C, (c) 50°C, and (d) 75°C

### 5.2.2. Tension-Tension Fatigue

The fatigue loading parameters which were determined via the analysis of the monotonic data regarding the sample ultimate load and load levels yielded the applied sinusoidal loading parameters to which each fatigue sample was subjected are listed in Table 5.1.

Table 5.1: Fatigue loading parameters

<b>Adherend</b>	<b>Temperature (°C)</b>	<b><math>F_{s,ult}</math> (kN)</b>	<b><math>LL</math></b>	<b><math>F_{max}</math> (kN)</b>	<b><math>F_{mean}</math> (kN)</b>	<b><math>F_{min}</math> (kN)</b>
Aluminum	0	5.471	0.50	2.735	2.052	1.368
			0.65	3.556	2.667	1.778
			0.80	4.377	3.282	2.188
	25	8.738	0.50	4.369	3.277	2.185
			0.65	5.680	4.260	2.840
			0.80	6.991	5.243	3.495
	50	4.084	0.50	2.042	1.531	1.021
			0.65	2.654	1.991	1.327
			0.80	3.267	2.450	1.633
	75	1.383	0.50	0.692	0.519	0.346
			0.65	0.899	0.674	0.450
			0.80	1.107	0.830	0.553
Steel	0	8.128	0.50	4.064	3.048	2.032
			0.65	5.283	3.962	2.641
			0.80	6.502	4.877	3.251
	25	11.92	0.50	5.958	4.468	2.979
			0.65	7.745	5.809	3.872
			0.80	9.532	7.149	4.766
	50	5.438	0.50	2.719	2.039	1.359
			0.65	3.535	2.651	1.767
			0.80	4.350	3.263	2.175
	75	1.573	0.50	0.786	0.590	0.393
			0.65	1.022	0.767	0.511
			0.80	1.258	0.944	0.629

The observed fatigue lives of the SLJs composed of steel and aluminum adherends exhibited a trend of reduction as the temperature was increased above ambient with the exception of aluminum at 25°C and a loading level of 0.80. This trend indicates that elevated temperature not only negatively affects the strength of the dissimilar material joints but the fatigue life as well. This trend, however, was not observed at the sub-ambient test temperature at which fatigue lives noticeably increased. These results have been shown in Figure 5.17 and Figure 5.16 for aluminum and steel SLJs, respectively.

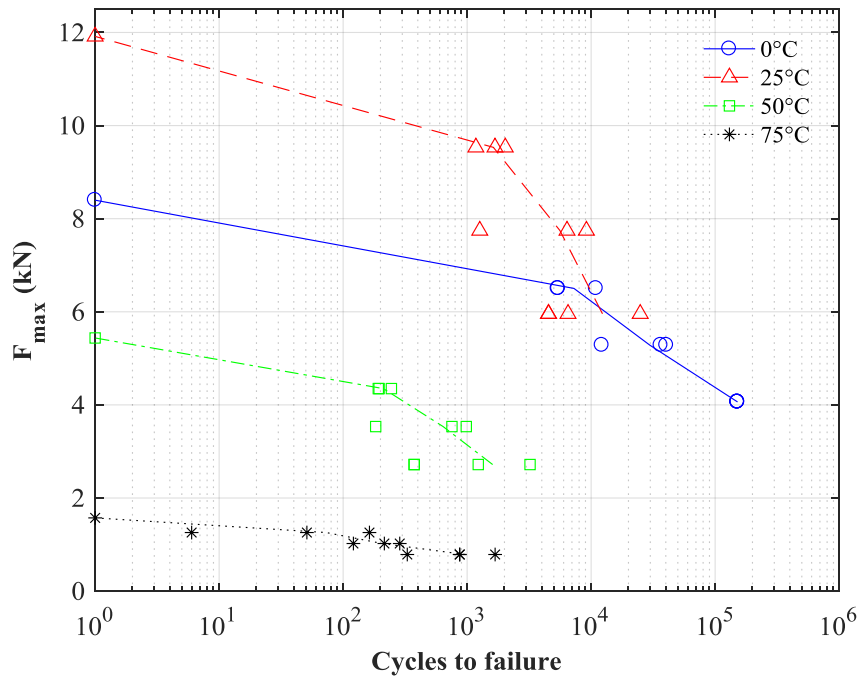


Figure 5.16: F-N diagram for steel SLJs at each test temperatures

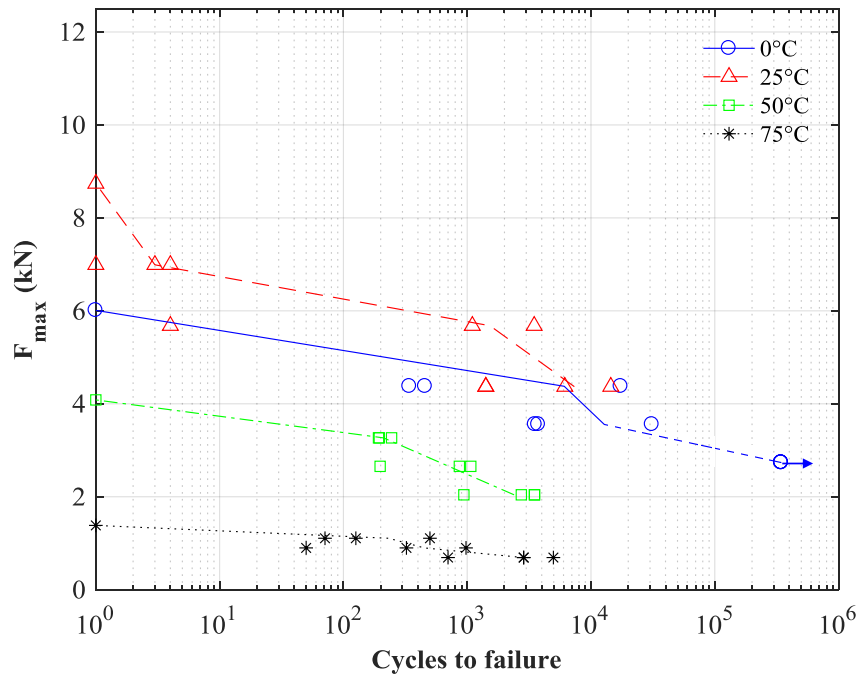


Figure 5.17: F-N diagram for aluminum SLJs at each test temperatures

The fatigue life behavior of the studied SLJs offers an interesting deviation from the trends of the monotonic results at the sub-ambient temperature level, exhibiting similar trends as the work done by Zhang et al. [23], and leads one to inquire as to the cause of such an increase in fatigue performance when the ultimate load carrying capacity of the joint has been reduced. One such explanation for this behavior is to consider heat build-up within the joint throughout the duration of the test due to friction among the two separate interfaces as well as among the molecular network within the adhesive and adherends themselves. This heat build-up would contribute to a degradation of mechanical properties of the adhesive, as discussed previously in sections 5.1.2 and 5.2.1, and result in a decreased life. At lower ambient temperatures the surrounding air would remove a greater amount of heat via convection from the joint than at elevated temperatures which would delay the degradation of the strength and stiffness of the adhesive. This effect was observed in the fatigue life data and the stiffness degradation throughout the fatigue life of the SLJs and was evaluated to further understand the effects of temperature and loading on the fatigue lives of adhesively-bonded SLJs. Zhang et al. [23] tested this hypothesis by monitoring the temperature of the specimen throughout the duration of the test and observed no increase greater than 2°C but did not describe the methodology used in doing so. It is therefore not possible at this time to conclusively confirm nor repudiate these claims. If the temperature was taken from the outside of the joint, this would be a misrepresentation of the actual temperature increase within the joint.

The hysteresis loops which were used to determine joint stiffness throughout the duration of a fatigue test were found to provide a reasonable approximation of stiffness, e.g. consistent loops with minimal energy loss throughout the majority of life, throughout the duration of life. A representative example of such changes in these loops at quarterly normalized cycles throughout a test is shown in Figure 5.18.

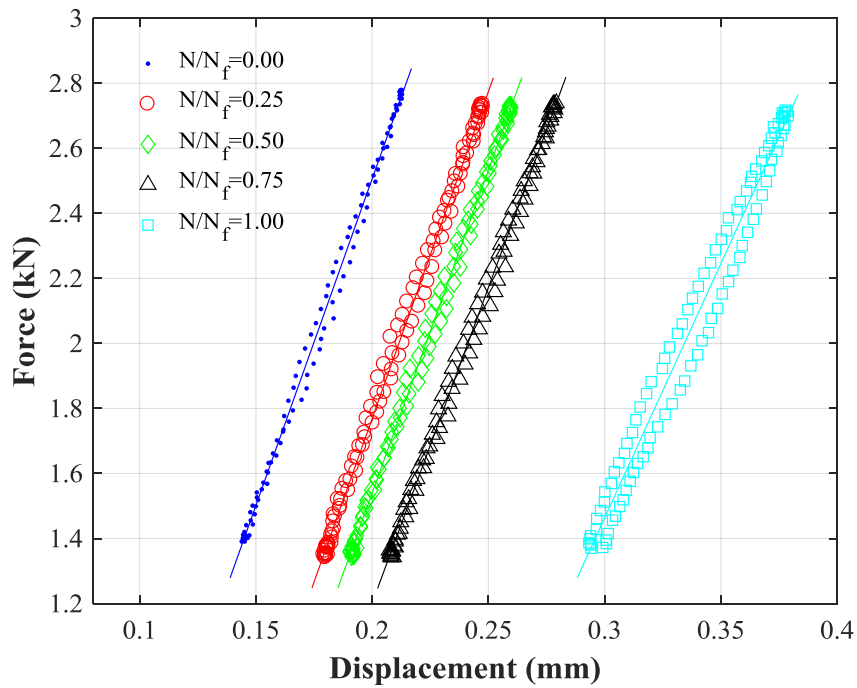


Figure 5.18: Representative hysteretic fatigue loading loops at quarterly normalized cycles used in the determination of stiffness

The evaluation of the effects of adherend material and load level on the stiffness degradation indicated no trend or correlation between the parameters of study, besides the effects on the initial stiffness of the joint, throughout the majority of life. The stiffness reduction at the end of life, however, was observed to generally decrease with increasing load level at each temperature. These results have been shown in Figure 5.19, Figure 5.21, Figure 5.23, and Figure 5.25. Data evaluation has been made easier by comparison of the normalized stiffness degradation against the normalized number of cycles for each adherend material and load level as shown in Figure 5.20, Figure 5.22, Figure 5.24, and Figure 5.26.

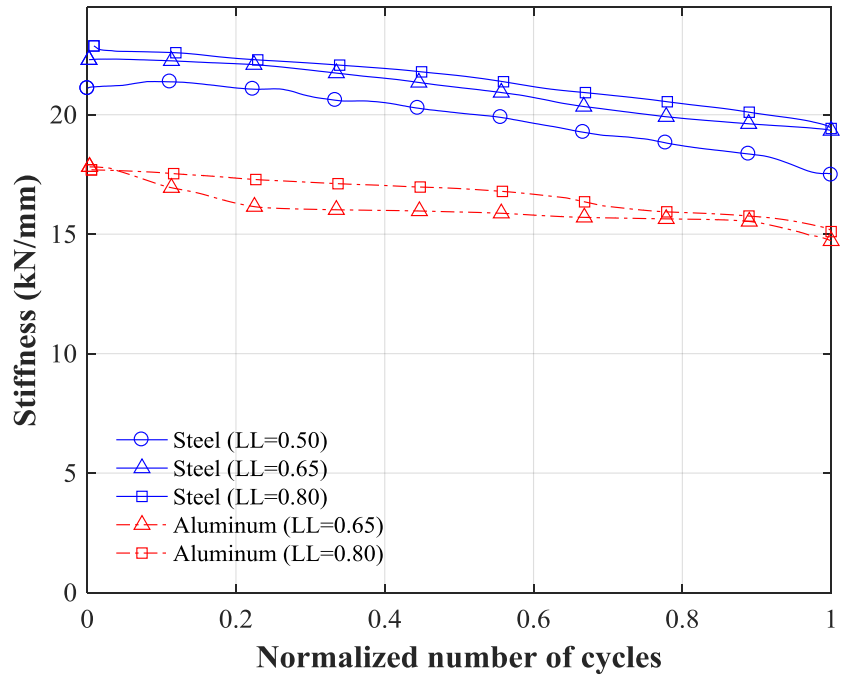


Figure 5.19: Stiffness vs normalized number of cycles of steel and aluminum SLJs at 0°C

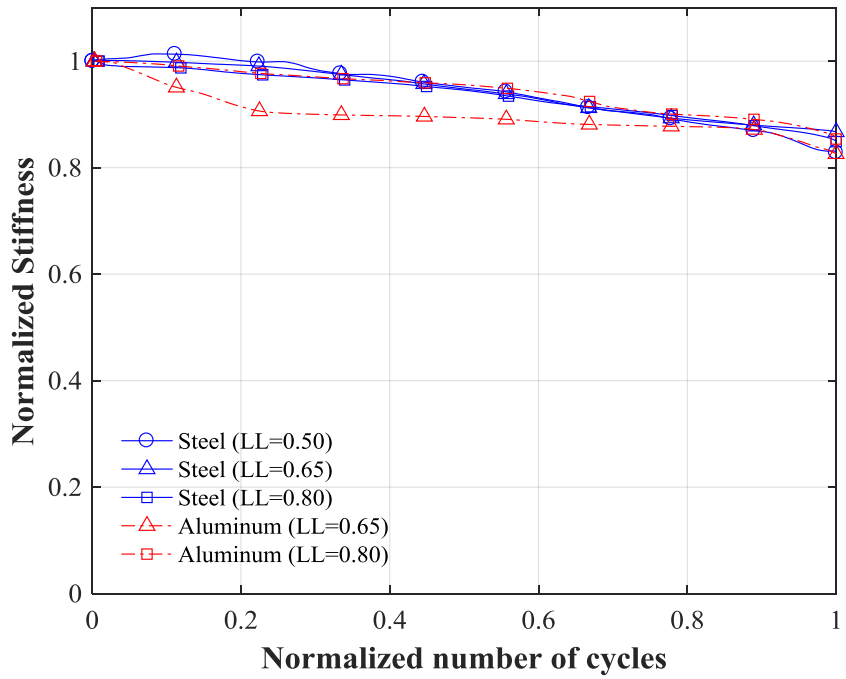


Figure 5.20: Normalized stiffness vs normalized number of cycles of steel and aluminum SLJs at 0°C



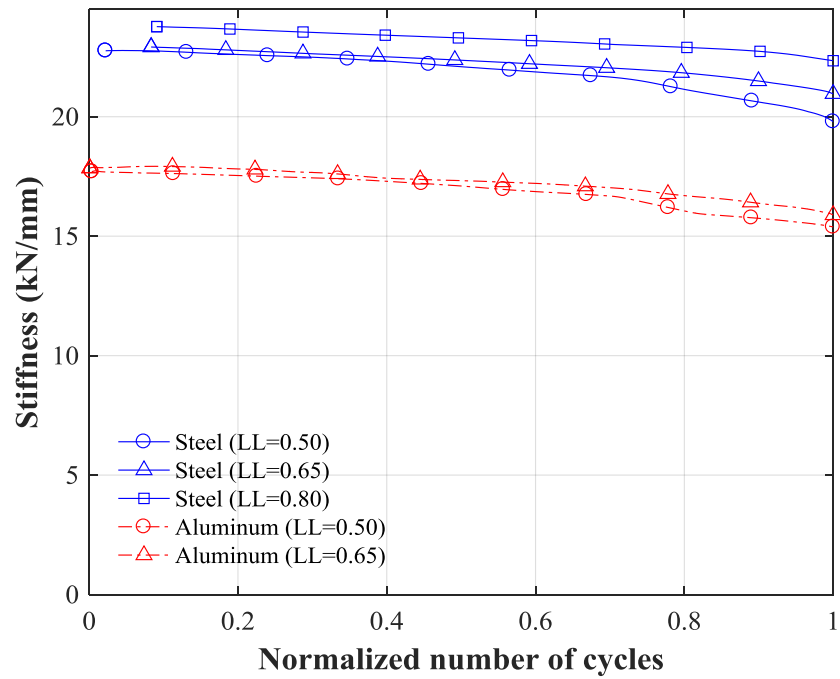


Figure 5.21 Stiffness vs normalized number of cycles of steel and aluminum SLJs at 25°C

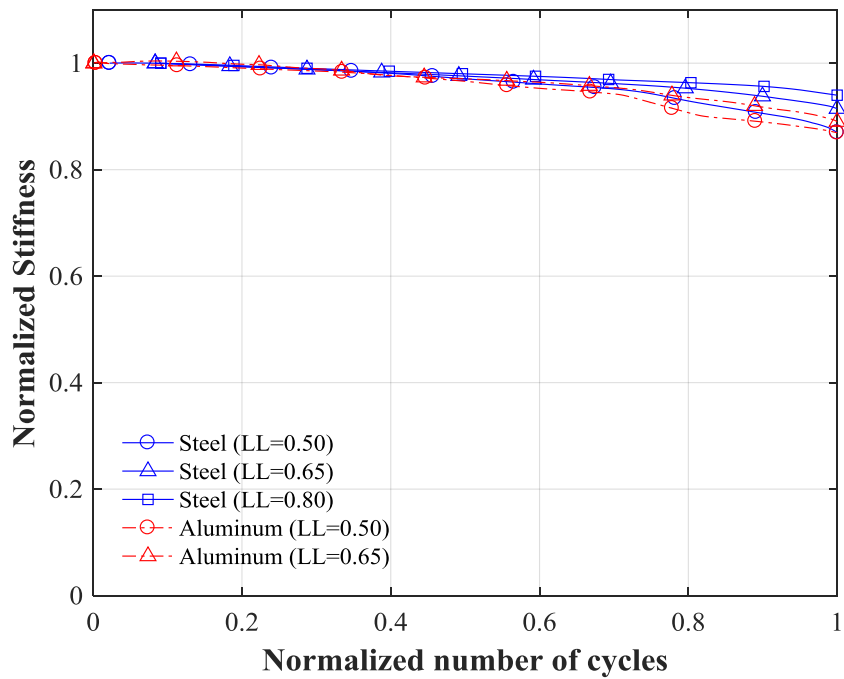


Figure 5.22: Normalized stiffness vs normalized number of cycles of steel and aluminum SLJs at 25°C

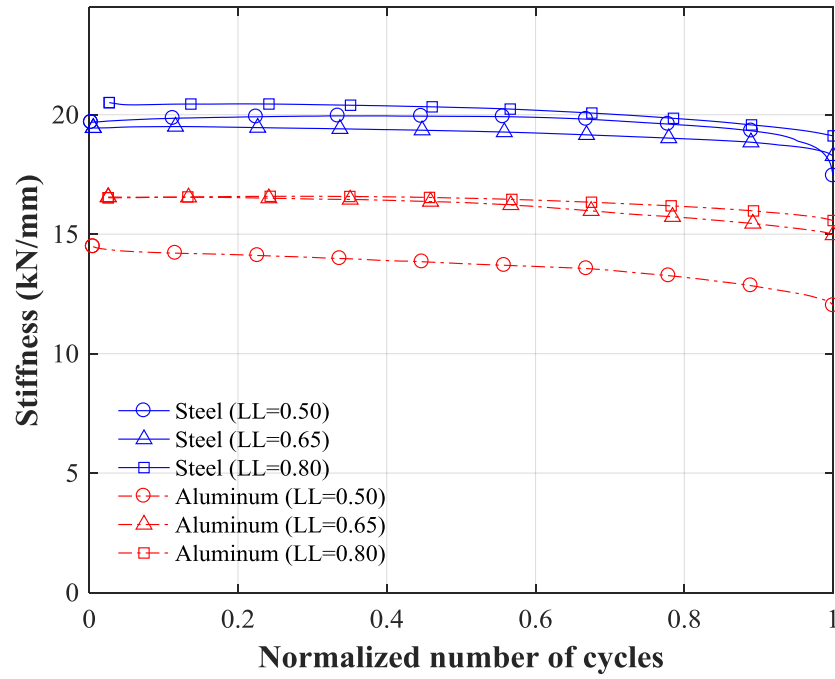


Figure 5.23: Stiffness vs normalized number of cycles of steel and aluminum SLJs at 50°C

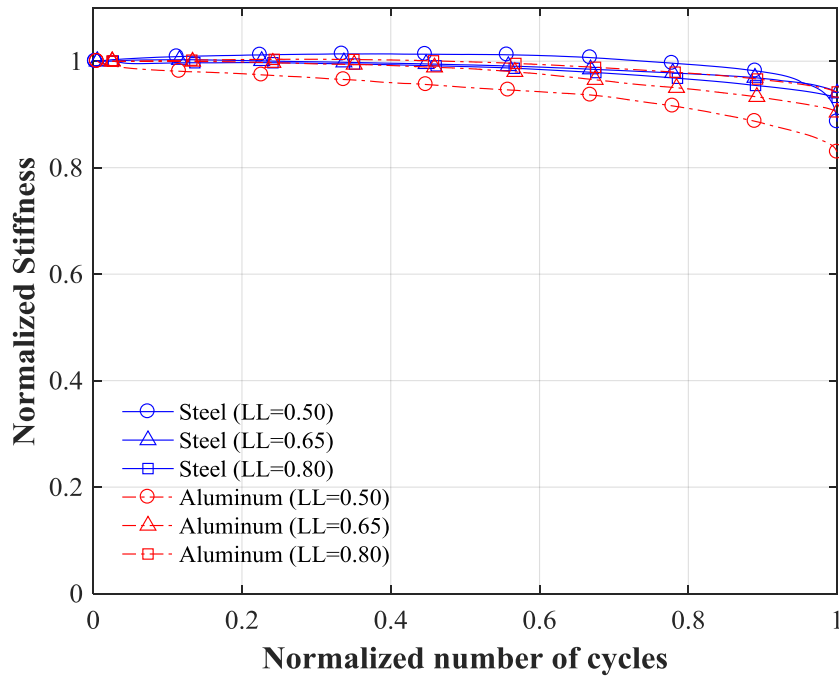


Figure 5.24: Normalized stiffness vs normalized number of cycles of steel and aluminum SLJs at 50°C

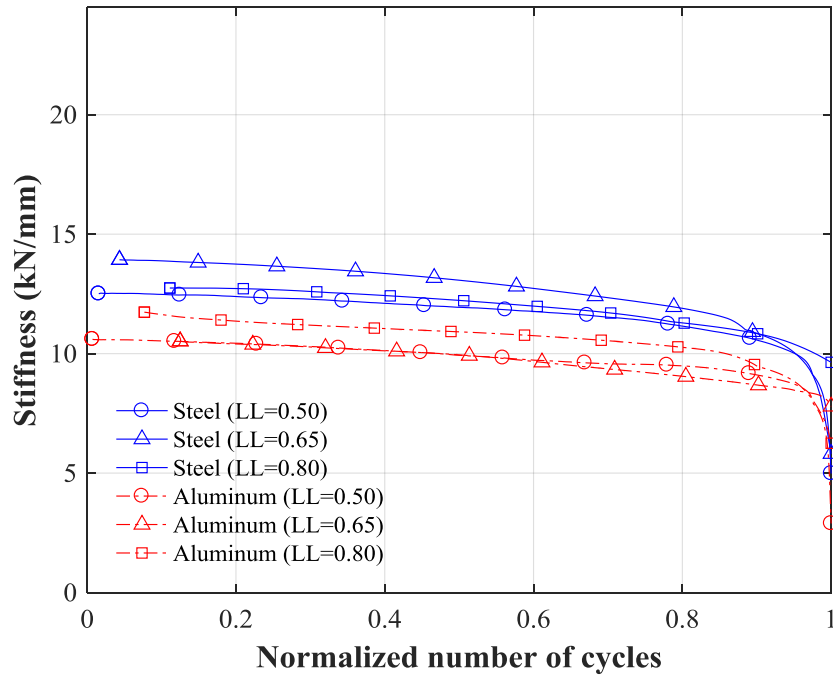


Figure 5.25: Stiffness vs normalized number of cycles of steel and aluminum SLJs at 75°C

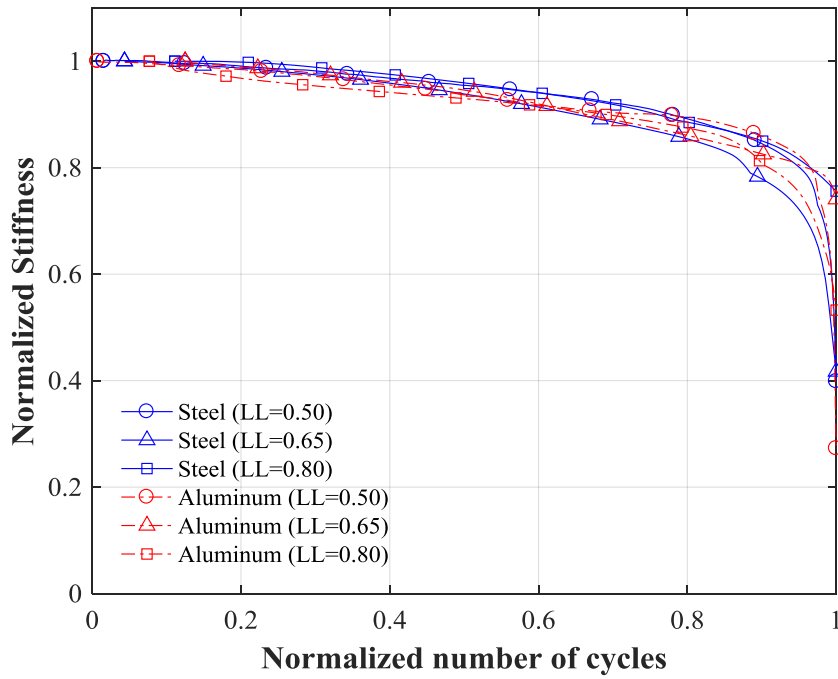


Figure 5.26: Normalized stiffness vs normalized number of cycles of steel and aluminum SLJs at 75°C

After observing no effects on the stiffness degradation behavior of the studied SLJs due to the adherend material or load level, the effect of temperature was evaluated in the same way as those of adherend material and load level, i.e. via the comparison of the stiffness and normalized stiffness with the normalized number of cycles. This evaluation indicated small effects below the  $T_g$  but also indicated an increase in rate of degradation and more degradation at the end of life. These results are shown in Figure 5.27 and Figure 5.29, for stiffness, and Figure 5.28 and Figure 5.30, normalized stiffness in comparison to the normalized number of cycles for steel and aluminum SLJs, respectively.

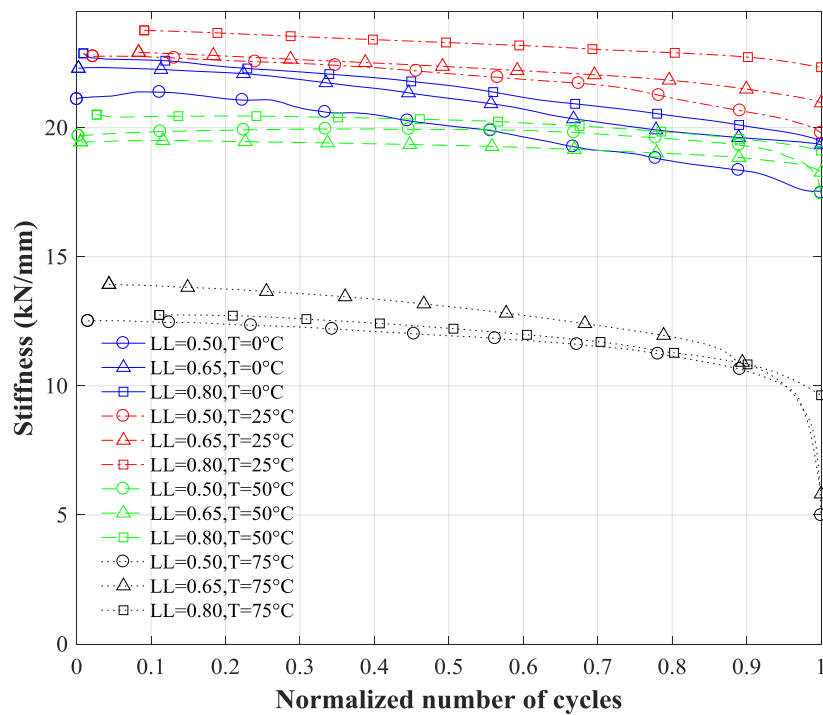


Figure 5.27: Stiffness vs normalized number of cycles of steel SLJs

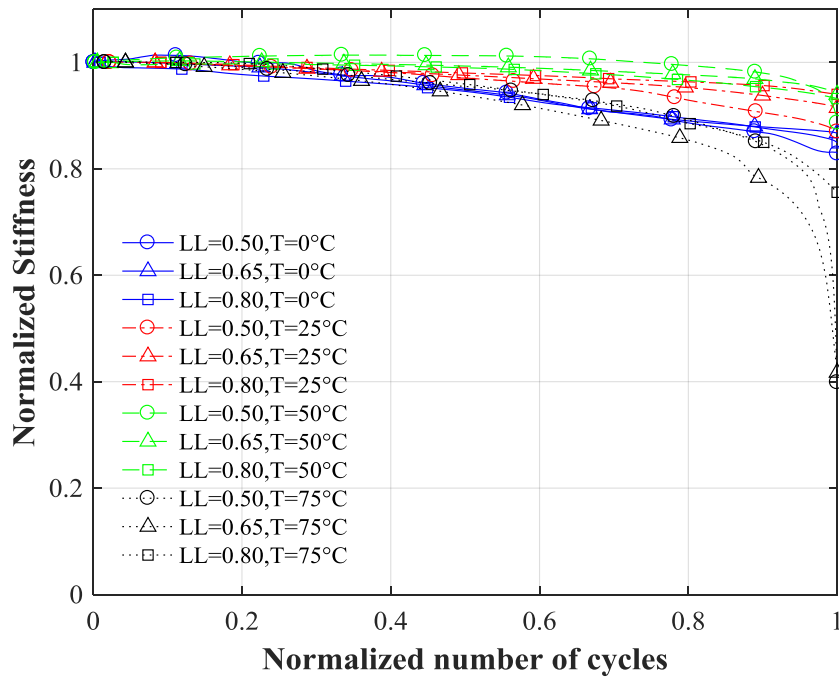


Figure 5.28: Normalized stiffness vs normalized number of cycles of steel SLJs

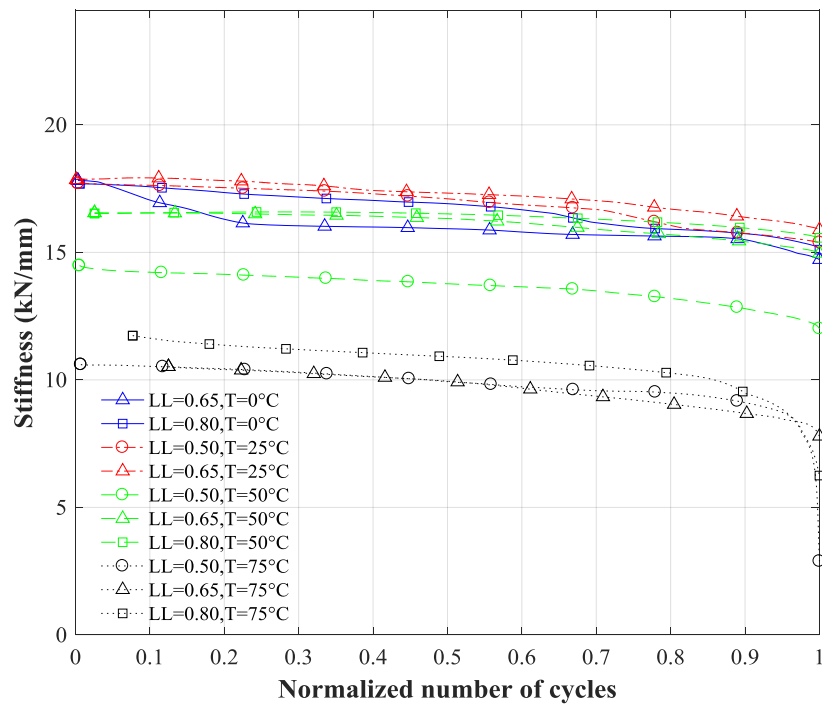


Figure 5.29: Stiffness vs normalized number of cycles of aluminum SLJs

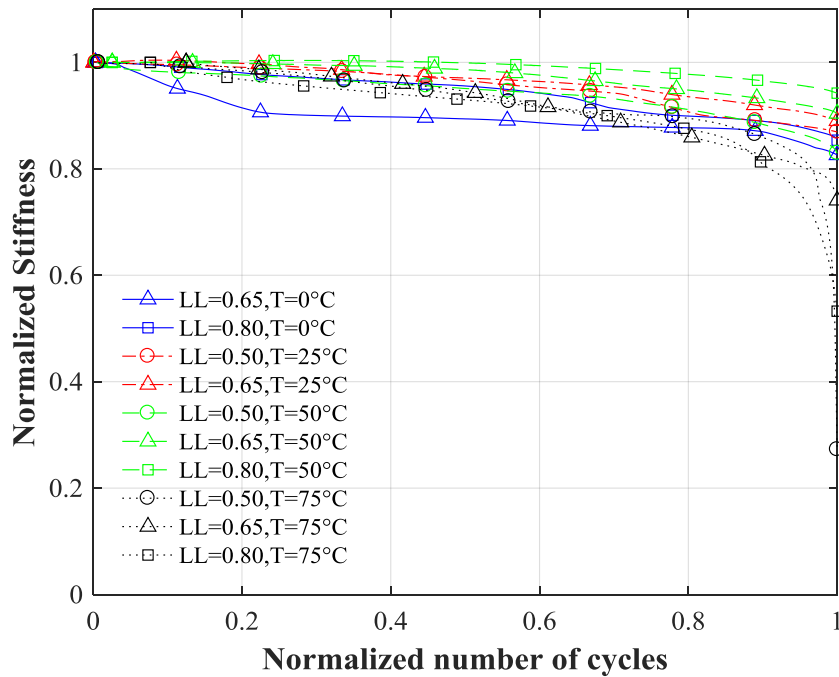


Figure 5.30: Normalized stiffness vs normalized number of cycles of aluminum SLJs

The stiffness degradation of the SLJs of study did not exhibit a sigmoid behavior as that of Zhang et al. [36] and the model which they proposed for StLJs was found to be inapplicable to the stiffness degradation of the studied dissimilar material SLJs. The SLJs did however exhibit near linear stiffness degradation throughout the majority of life indicating stable crack growth

Upon review of the averaged degradation results, listed in APPENDIX C, it was found that the lowest stiffness degradation was exhibited by the aluminum SLJs at 50°C and was 5.80% and thus a conservative failure criterion for the studied joints was proposed as a stiffness reduction of 5%.

The evaluation of the sample fracture surfaces revealed similar modes of failure as observed in the monotonic testing, i.e. the fracture surfaces consisted of interfacial failure at the adhesive-metal adherend interface and cohesive failure within adhesive and resin rich surface layer of the composite adherend at the temperatures of 0°C and 25°C and transitioned to interfacial

failure at the adhesive-metal adherend interface at the temperatures of 50°C and 75°C. The fracture surfaces are shown in Figure 5.31Figure 5.14 and Figure 5.32Figure 5.15 for the steel and aluminum SLJs, respectively.

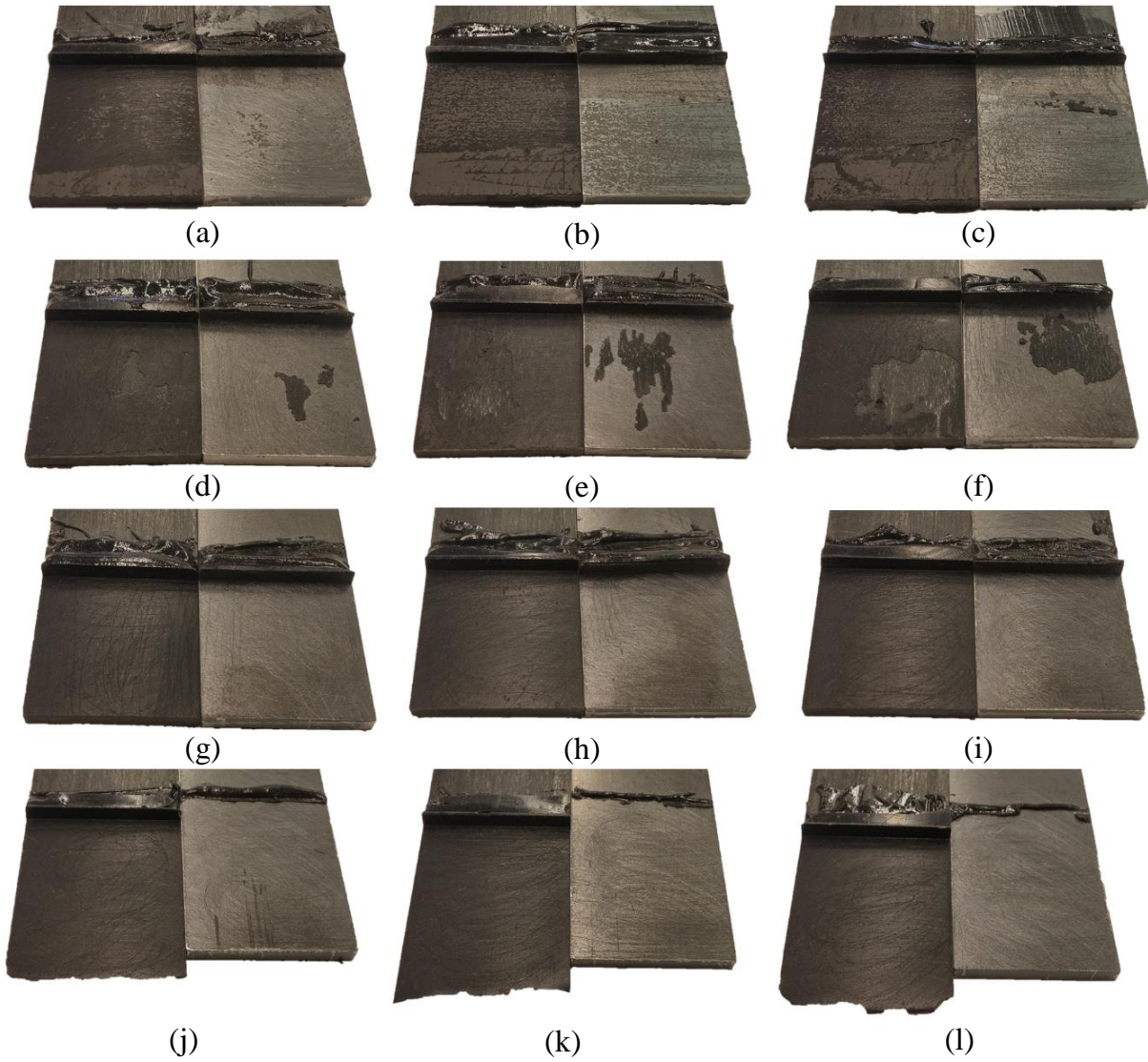


Figure 5.31: Representative fatigue fracture surfaces of steel SLJs at (a) 0°C and LL=0.50, (b) 0°C and LL=0.65, (c) 0°C and LL=0.80, (d) 25°C and LL=0.50, (e) 25°C and LL=0.65, (f) 25°C and LL=0.80, (g) 50°C and LL=0.50, (h) 50°C and LL=0.65, (i) 50°C and LL=0.80, (j) 75°C and LL=0.50, (k) 75°C and LL=0.65, and (l) 75°C and LL=0.80

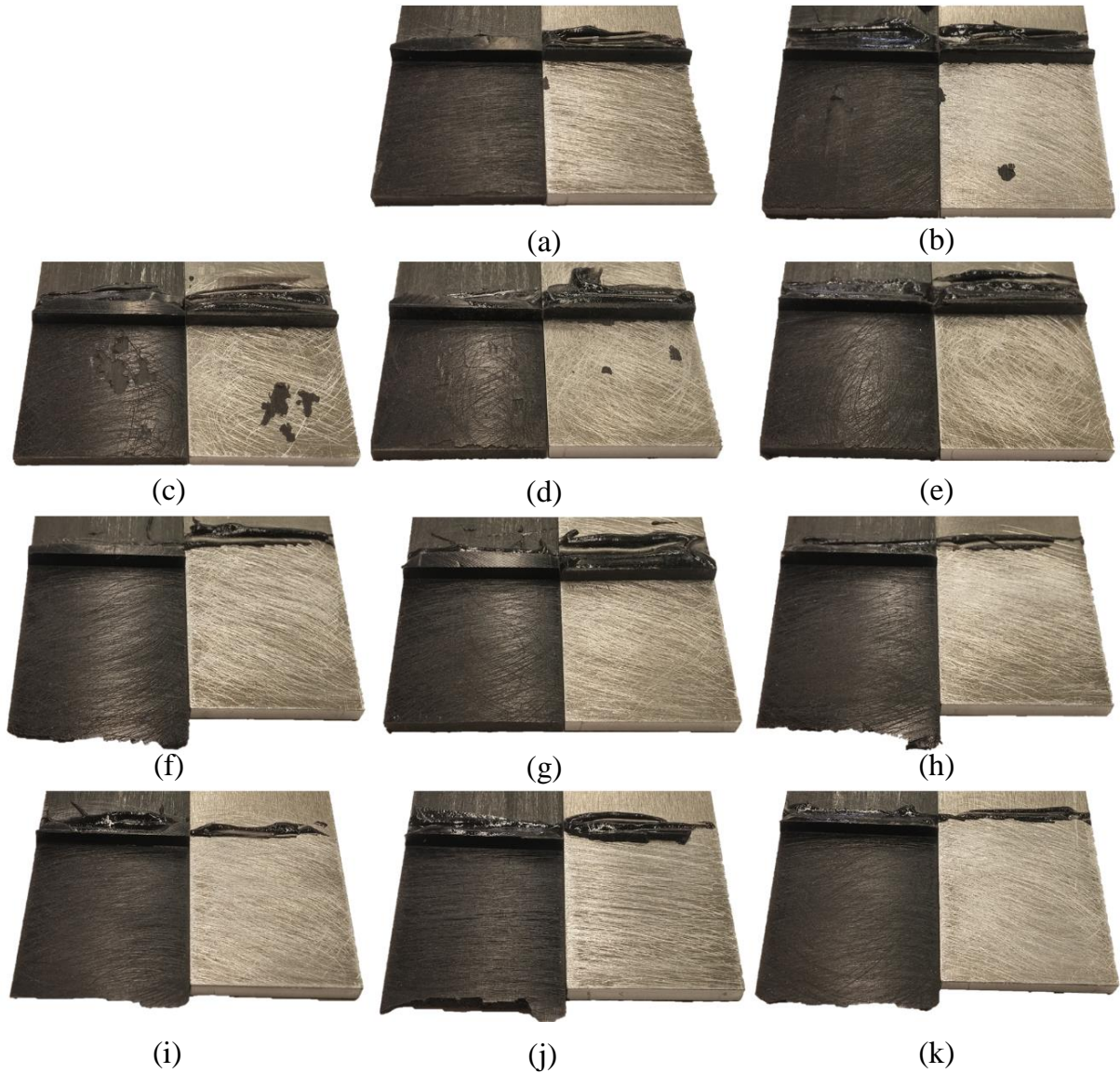


Figure 5.32: Representative fatigue fracture surfaces of aluminum SLJs at (a) 0°C and LL=0.65, (b) 0°C and LL=0.80, (c) 25°C and LL=0.50, (d) 25°C and LL=0.65, (e) 25°C and LL=0.80, (f) 50°C and LL=0.50, (g) 50°C and LL=0.65, (h) 50°C and LL=0.80, (i) 75°C and LL=0.50, (j) 75°C and LL=0.65, and (k) 75°C and LL=0.80



### 5.3. Temperature Effects on the Low Velocity Transverse Impact Behavior of Adhesively-Bonded Dissimilar Material SLJs

The impact velocity of 1 m/s, which was set as the apparatus target velocity for all specimens, was evaluated to ensure sample data comparability and found to vary by 0.849% about the mean of 1.01 m/s, as shown in Figure 5.33.

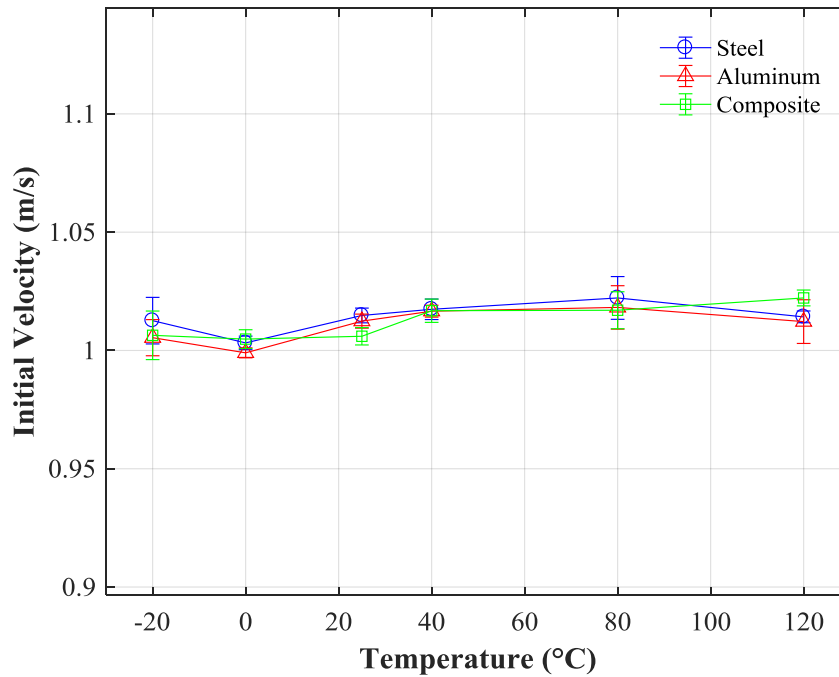


Figure 5.33: Initial impact velocity for all LVI samples

The energy to which a given SLJ exposed, including that stored via elastic and plastic deformations, was evaluated as the maximum energy which was registered during the impact event to ensure data comparability and is shown in Figure 5.34. The variation among the samples as a whole was 2.19% and indicated, in conjunction with the variance of impact velocities, that the fixed boundary conditions were maintained for all samples and comparison of sample data was valid.

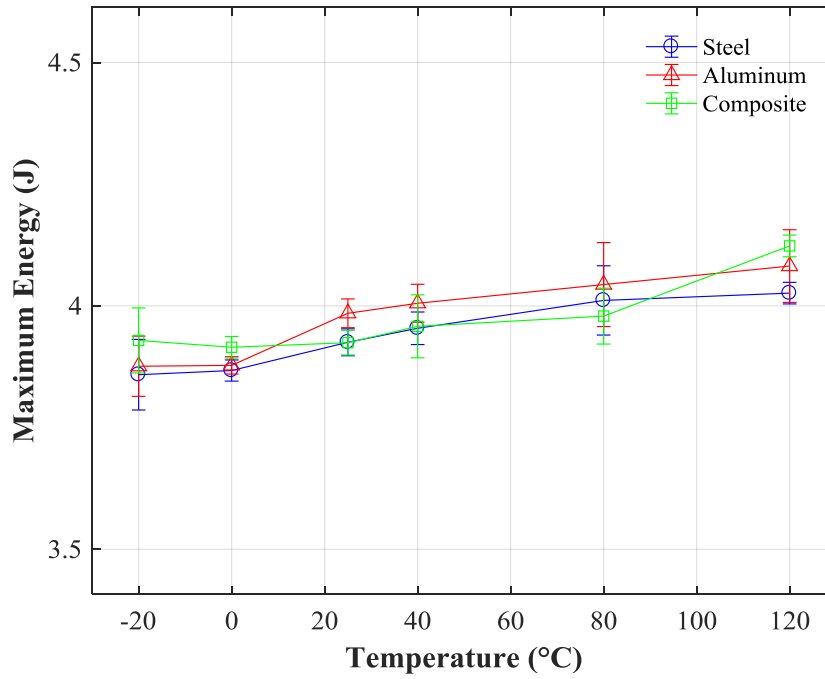


Figure 5.34: Maximum energy vs temperature of all SLJ samples

Representative impact force-energy-time response curves are shown in Figure 5.35, Figure 5.36, and Figure 5.37 for steel, aluminum, and composite SLJs, respectively. Representative impact force-displacement response curves are shown in Figure 5.38, Figure 5.39, and Figure 5.40 for steel, aluminum, and composite SLJs, respectively.

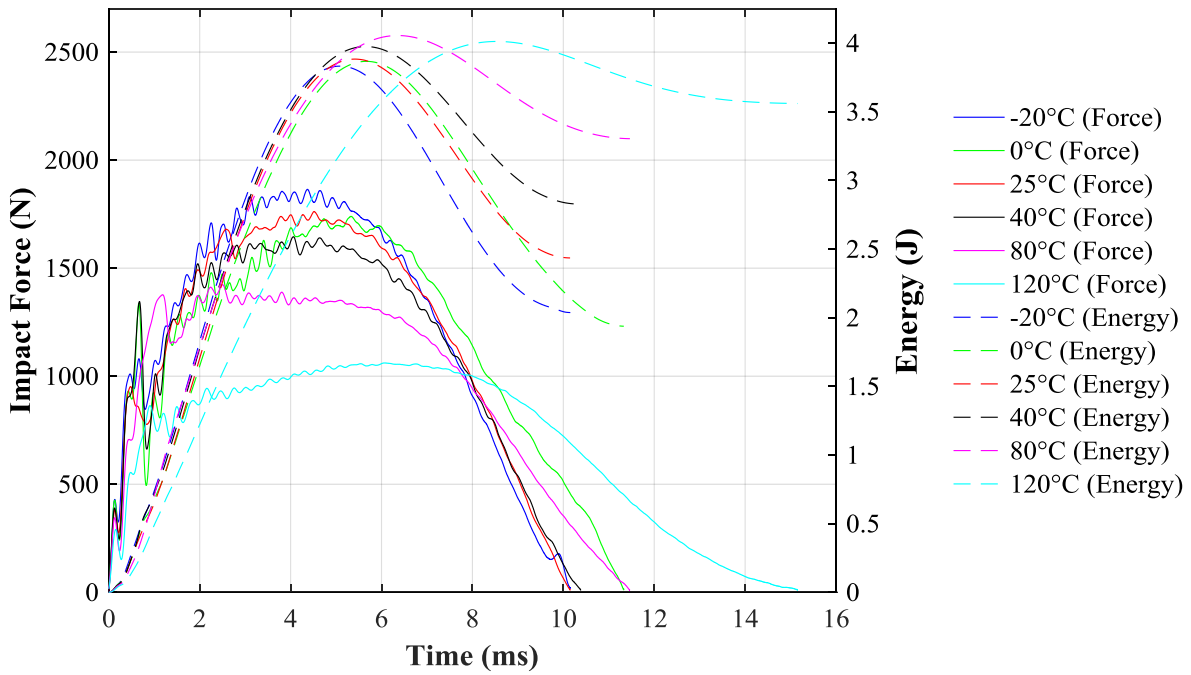


Figure 5.35: Representative impact force-energy-time response curves of steel SLJs at each test temperature

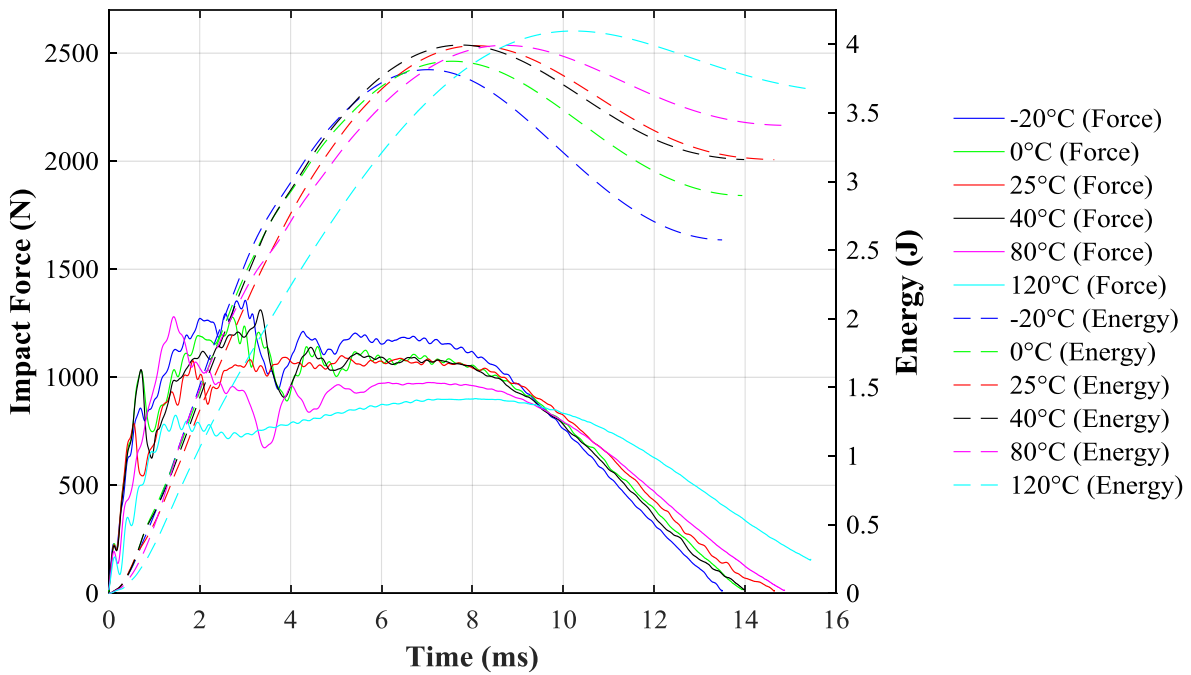


Figure 5.36: Representative impact force-energy-time response curves of aluminum SLJs at each test temperature

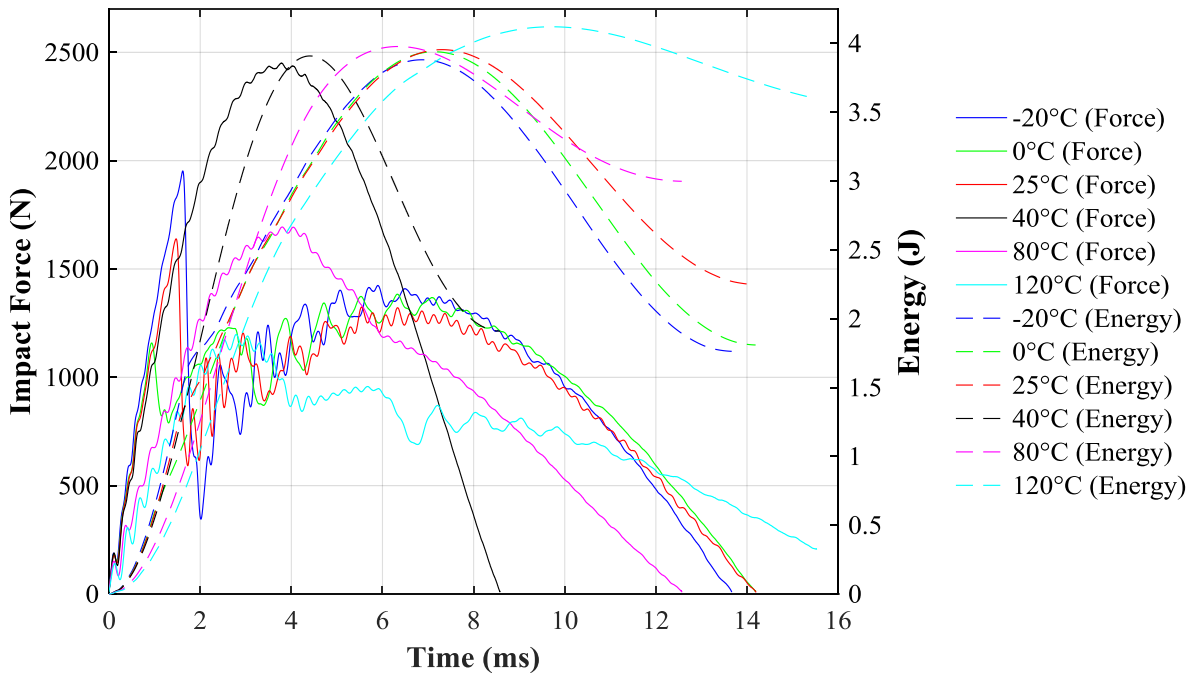


Figure 5.37: Representative impact force-energy-time response curves of composite SLJs at each test temperature

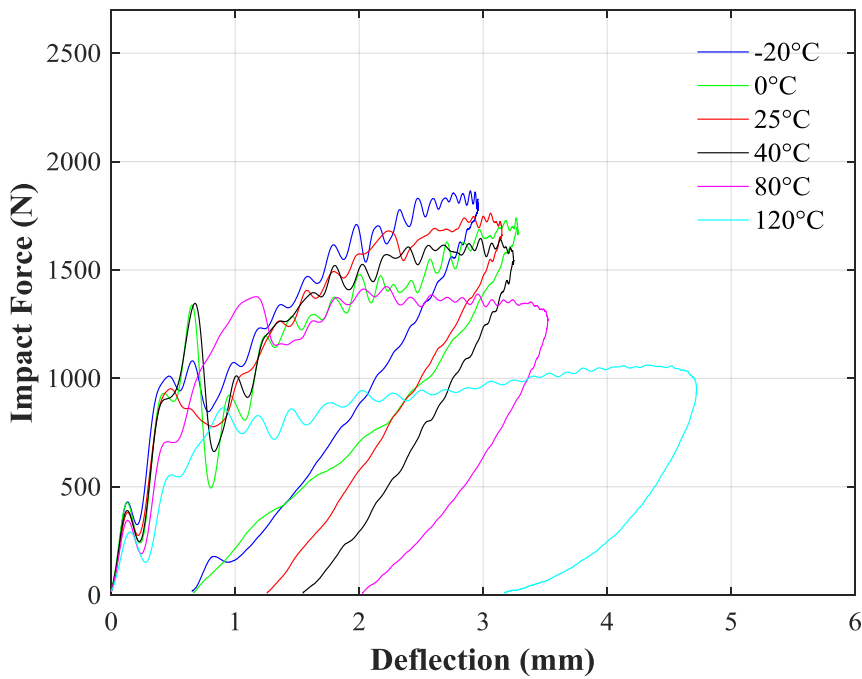


Figure 5.38: Impact force vs deflection of representative steel SLJs at each test temperature

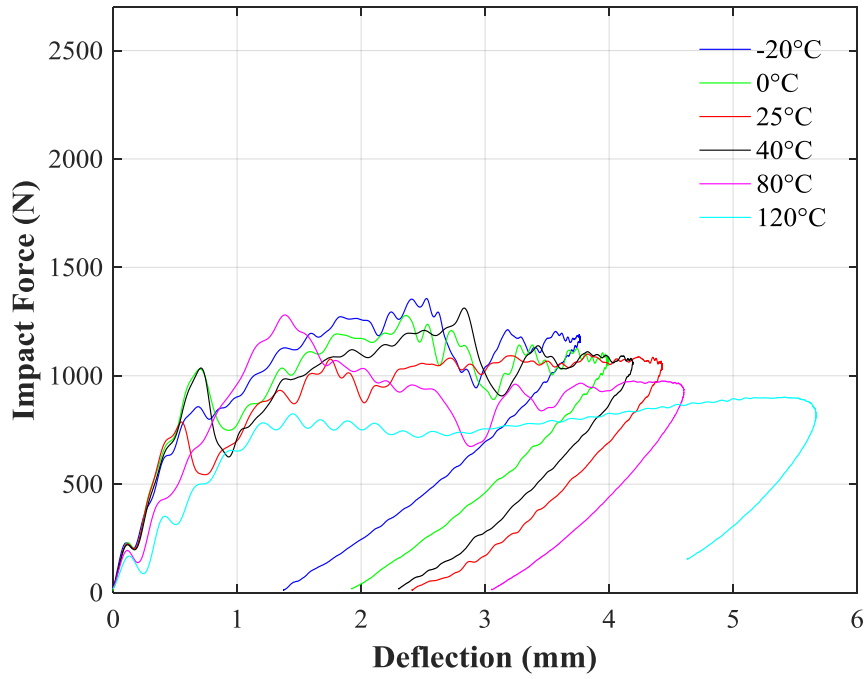


Figure 5.39: Impact force vs deflection of representative aluminum SLJs at each test temperature

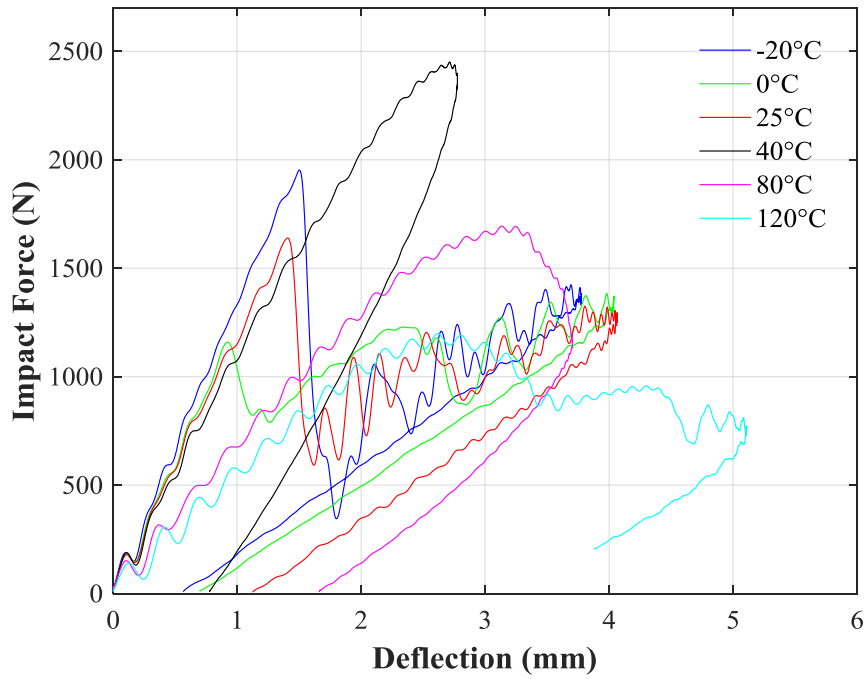


Figure 5.40: Impact force vs deflection of representative composite SLJs at each test temperature

The initial stiffness of each adherend combination was found, as would be expected from the stiffness of the corresponding adherends, to be highest for steel, then aluminum, and finally composite SLJs. Stiffnesses of all substrate combinations also exhibited an inverse relation to temperature, i.e. as temperature increased, stiffness decreased, as shown in Figure 5.41. This response can be understood, at least in part, by considering the previously discussed degradation of the mechanical properties of the adhesive itself. Another aspect to consider again is the effect of temperature on the adhesion at the interface of the adhesive and metal adherends where interfacial failure was observed.

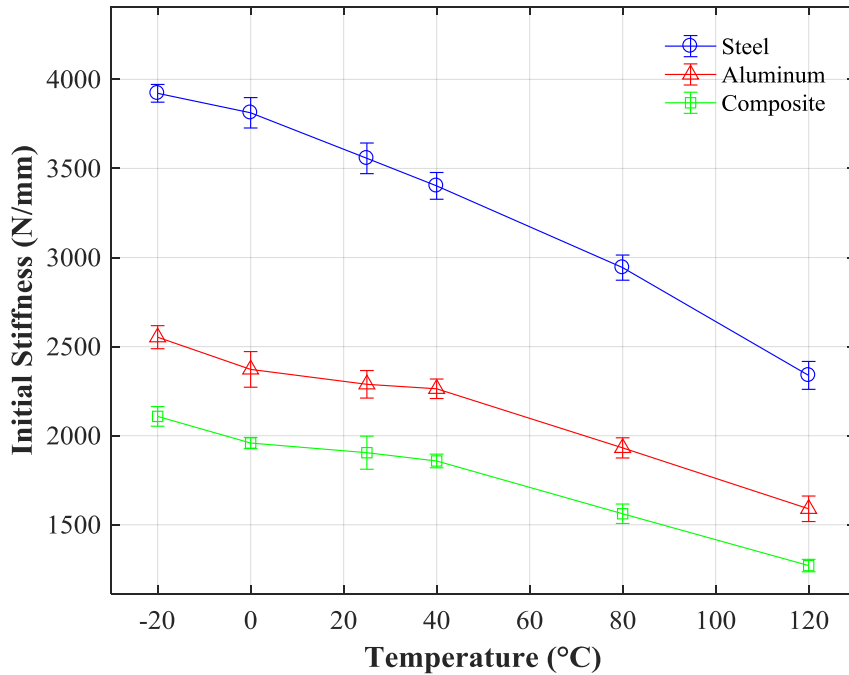


Figure 5.41: Initial stiffness vs temperature for all SLJ adherend materials

The initial failure was observed to exhibit a general decreasing trend in failure load and energy with little decrease at temperatures below  $T_g$  and significant decreases at temperatures above  $T_g$ . This has been shown for failure load and energy in Figure 5.42 and Figure 5.43, respectively.

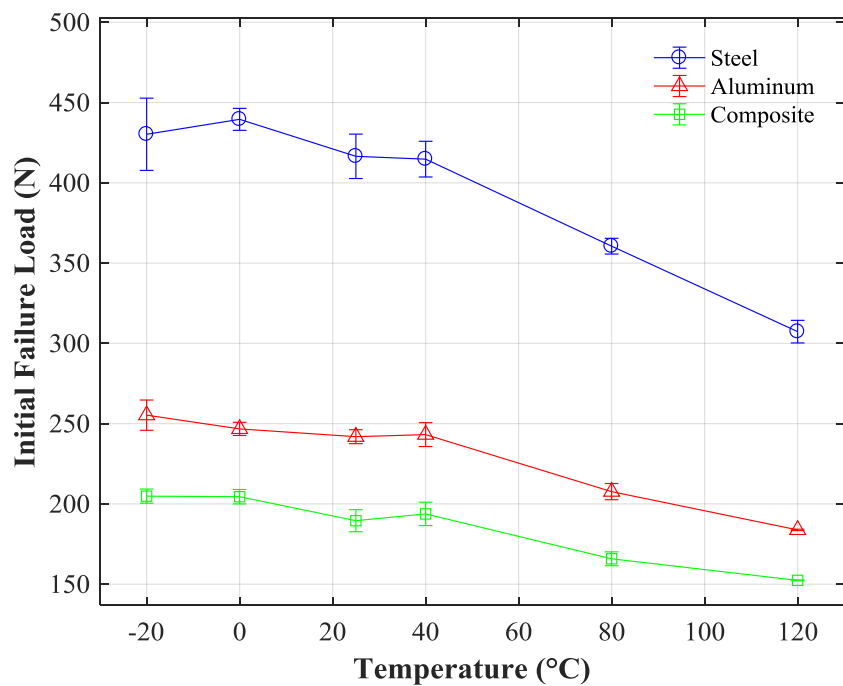


Figure 5.42: Initial failure load vs temperature for all SLJ adherend materials

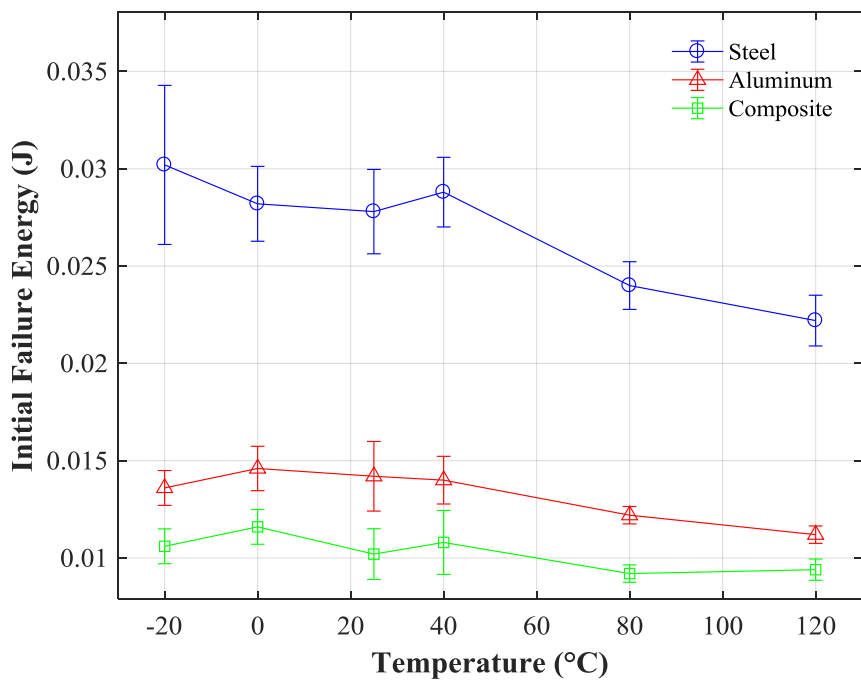


Figure 5.43: Initial failure energy vs temperature for all SLJ adherend materials

The review of the composite SLJs which were tested at 80°, which exhibited crack propagation through a majority of the joint but not complete failure as shown in Figure 5.44, indicated that failure initiation occurred in the fillet opposite impact. The crack propagation, indicated by consecutive arrows, for each SLJ type, assuming crack propagation in steel and aluminum SLJs was similar to that of composite SLJS in terms of initiation and propagation direction, has been shown in Figure 5.45 and Figure 5.46 for composite and metal adherends, respectively.

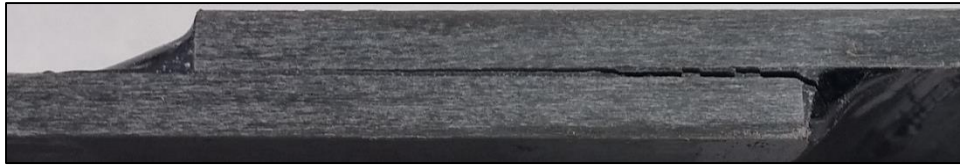


Figure 5.44: Resulting crack formation in a composite SLJ at 80°C under LVI loading

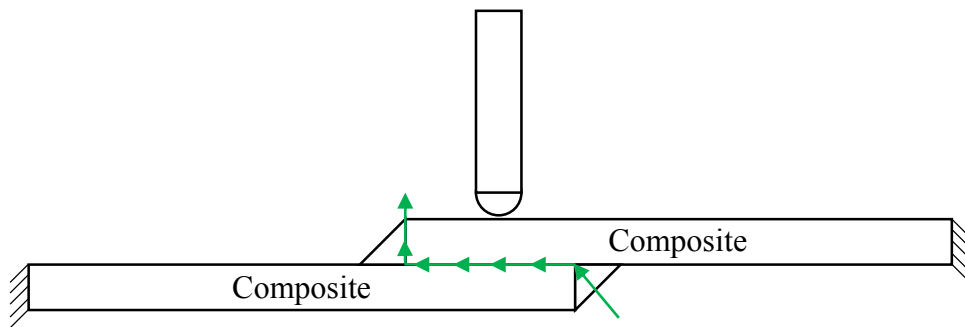


Figure 5.45: 2D crack propagation diagram of a typical composite SLJ

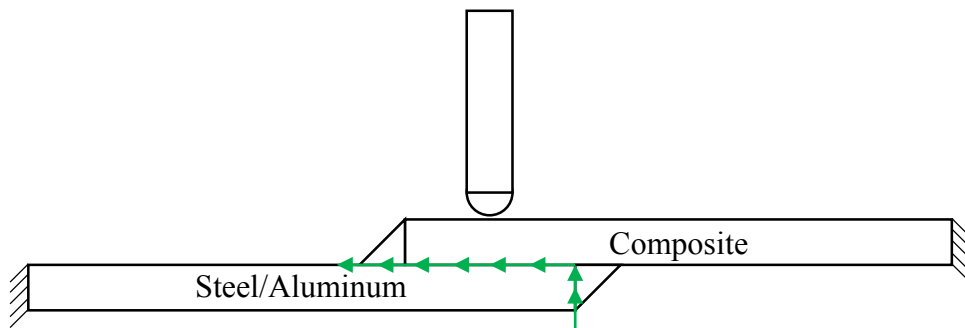


Figure 5.46: 2D crack propagation diagram of a typical metal SLJ



The hypothesis that crack initiation takes place within the lower fillet of a given LVI specimen was further evaluated by determining whether or not the initial failure was solely due to crack formation within the composite adherend, which was also observed. This was accomplished by conducting additional LVI testing, consisting of 2 steel specimens and 1 aluminum specimen at 25°C, in which the impact surface was changed to that of the metal adherend as opposed to that of the composite. The methodology used was the same as that described in section 4.2.3.4. The results indicated that crack formation in the composite adherend was not the cause of the observed initial drop in load corresponding to initial failure. These results have been demonstrated with the impact force- displacement response, narrowed to include the initial portion of the impact event, for the aluminum and steel SLJs in Figure 5.47 and Figure 5.48, respectively.

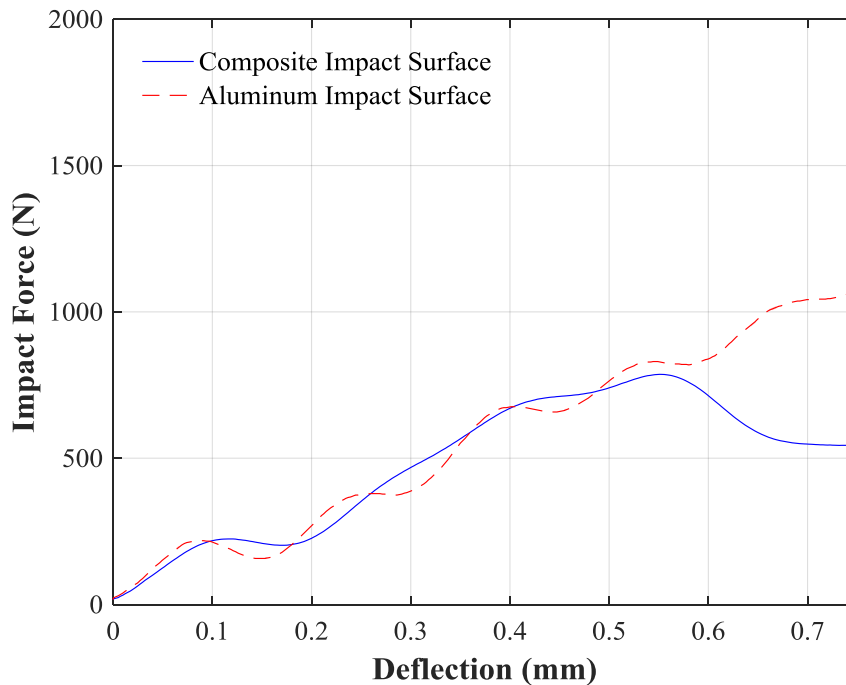


Figure 5.47: Impact force vs deflection for aluminum SLJs in which the impact surface was varied between the composite and aluminum adherend

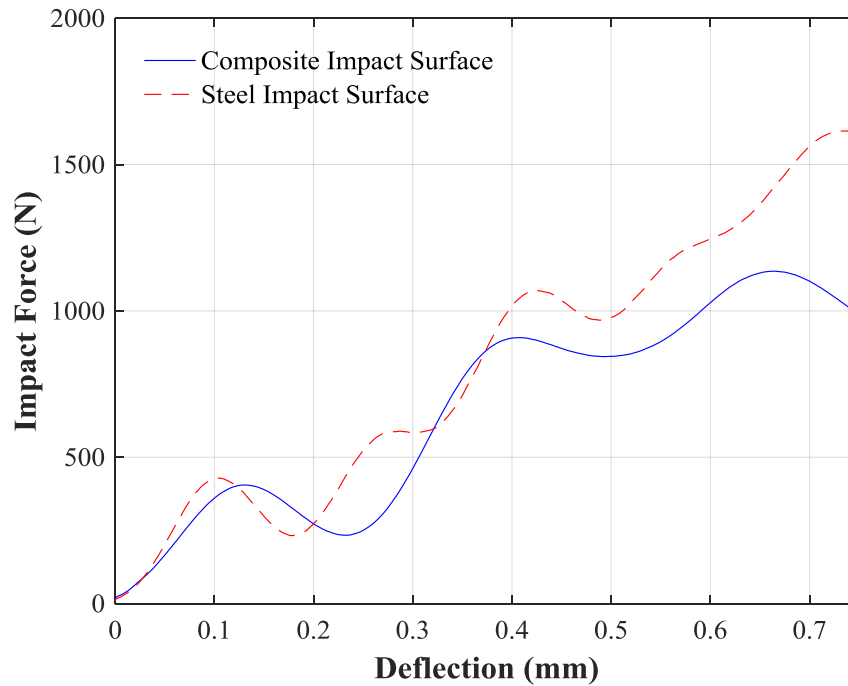


Figure 5.48: Impact force vs deflection for steel SLJs in which the impact surface was varied between the composite and steel adherend

The hypothesis has not thus far been proven to be true and requires additional testing and would be complemented through the use of a high-speed camera to conclusively identify the location of initial failure and finite element method (FEM) simulations. The results obtained through the current research has indicated that initial crack formation occurs in the lower fillet but has not conclusively proven where. This is an important consideration. The 2D crack propagation diagrams shown in Figure 5.45 and Figure 5.46 indicated that crack propagation is thought to occur from the outer most surface and propagates through the fillet, in the case of composite SLJs, or along the interface, in the case of metal SLJs, but this currently has no experimental support. Another possible crack initiation location is at the end corner of the lower adherend, hence the necessity for additional testing.

As one may have noticed in Figure 5.45, the crack propagation of the composite SLJ is through the lower fillet and not along the adhesive-adherend interface observed in the metal SLJs and is a result of the better adhesion between the composite material and that of the adhesive, as observed from the mixed cohesive and adherend failure modes. This increased adhesion performance causes the fillet to be the critical component as opposed to the interface. A representative fillet crack in a composite SLJ has been shown in Figure 5.49 and was obtained using a Scalar USB Microscope M2 (ProScope, Wilsonville, OR).

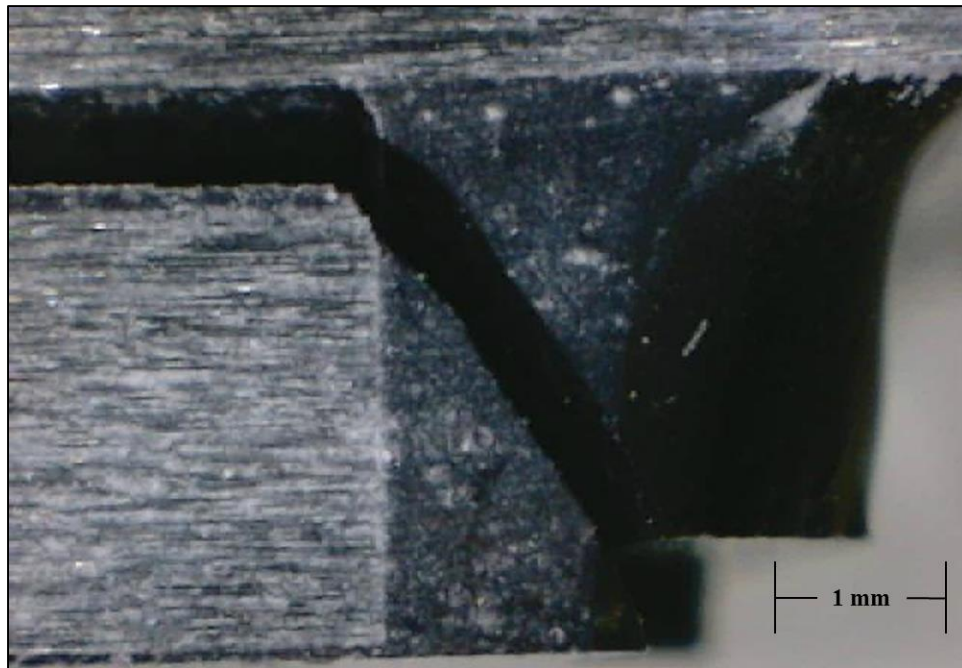


Figure 5.49: Image of a representative fillet crack in a composite SLJ

Evaluation of overall joint performance was accomplished via the determination of the secondary stiffness, maximum impact force, and energy absorbed by the joint during the impact event. These parameters allowed for a comparison of the studied SLJ types in terms of the parameters in which they excelled and those which they underperformed the other materials.

The secondary stiffness was found to exhibit similar trends as the initial stiffness in that it did not exhibit a significant amount of change at sub- $T_g$  temperatures, decreased with elevated temperatures, and was dependent on the adherend material as shown in Figure 5.50. The causes of the initial stiffness degradation also contributed to the degradation of the secondary stiffness. The steel SLJs exhibited the greatest stiffness due to the larger stiffness of the steel SLJ adherend, followed by the aluminum SLJs and finally the composite SLJs.

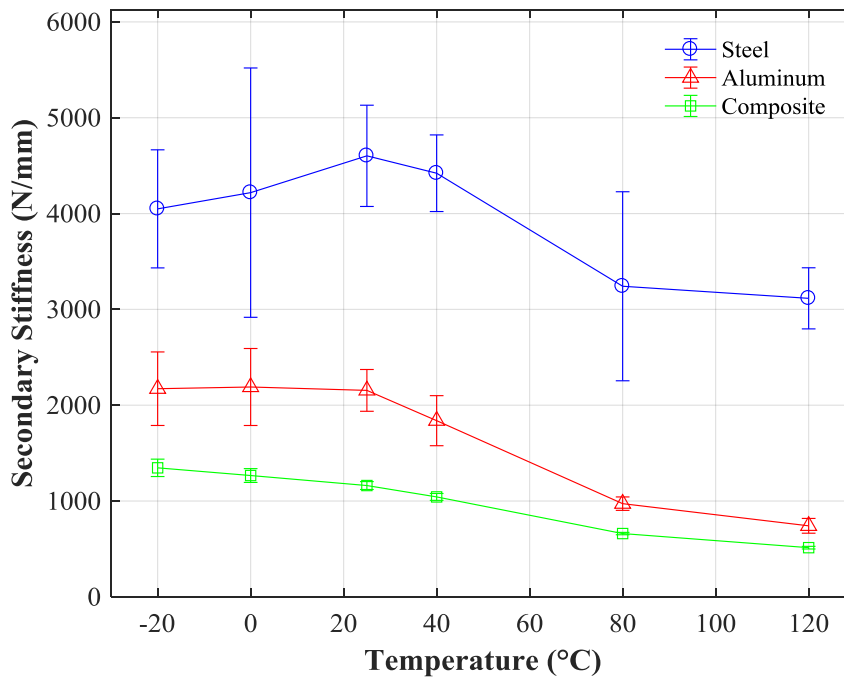


Figure 5.50: Secondary stiffness vs temperature for all SLJ adherend materials

The evaluation of the maximum impact force which was supported by the SLJs throughout the impact events indicated similar performance of the composite and steel SLJs in the range of -20°C to 25°C, after which the composite SLJs outperformed the steel SLJs. The aluminum SLJs supported less load than their composite and steel counterparts at all temperatures with the

exception of steel at 80°C; at which point the two supported similar loads. These results are shown in Figure 5.51.

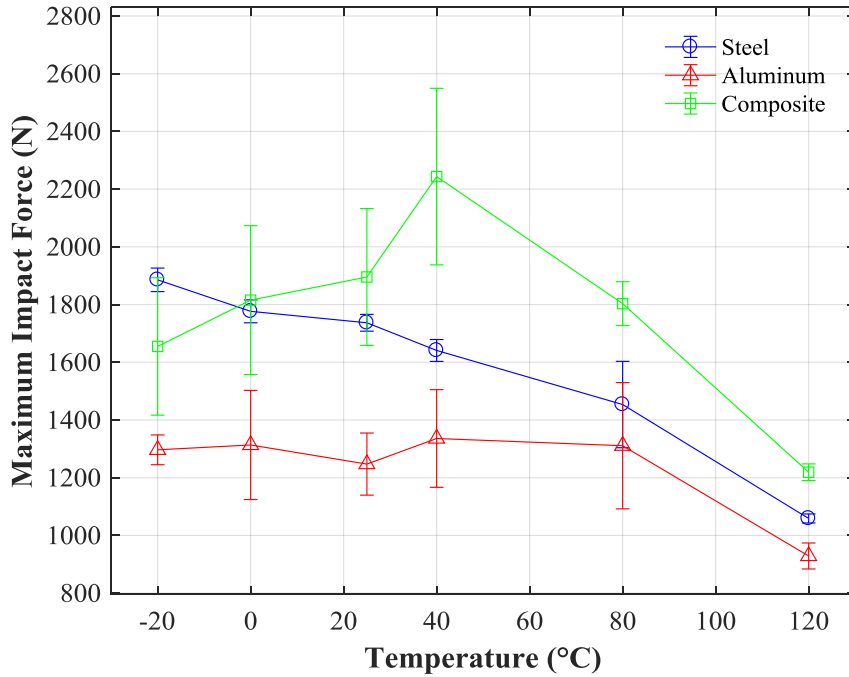


Figure 5.51: Maximum impact force vs temperature for all SLJ adherend samples

The LVI behavior of the SLJs can be understood by considering the viscoelastic nature of the polymer adhesive. At lower temperatures the adhesive is in a glassy, i.e. brittle, state which limits the ability of the adhesive to deform in the areas of concentrated stress, such as that at the end of the joints, which lower the load carrying capacity of the joint. This was apparent in the composite samples where the maximum load was dictated by the strength of the joint and the mode of failure was a mixture of cohesive and adherend failure as opposed to the metal samples where it was influenced not only by joint failure, which the failure mode interfacial, but also the plastic deformation of the metal adherend. As the temperature was increased near the  $T_g$  of the adhesive it begins to transition into a leathery state in which the lattice network begins to have more freedom

of movement [67, 68] and is more compliant in the areas of high stress concentration resulting in a redistribution of stresses, delay of crack formation, and increased toughness [54].

The evaluation of the energy absorbed by the SLJs during the impact event indicated the greatest energy absorption capacity was for aluminum, then steel, and finally composite SLJs, except at 40°C at which point the all SLJs types absorbed similar amount of energy as shown in Figure 5.52.

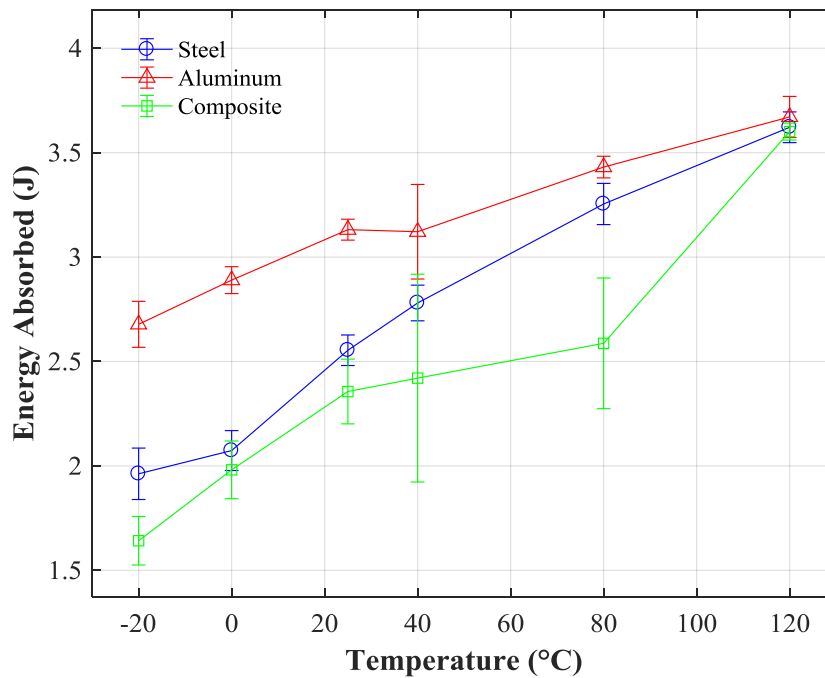


Figure 5.52: Energy absorbed vs temperature of all SLJ adherend samples

This energy absorption behavior can be understood by examining the modes of failure for the studied SLJs. The SLJs composed of composite adherends exhibited failure only in the joint area, limiting their absorption capacity to that of the joint, while the metal SLJs exhibited failure in both the adhesive area and in the metal adherend in the form of plastic deformation. Though the composite SLJs exhibited better adhesion throughout the joint, as was evident by the observed

mixed modes of failure (cohesive and adherend), they were observed to absorb lower amounts of energy than that of their metal counterparts and did not exhibit any noticeable form of adherend failure outside of the bond area. As to the higher energy absorption exhibited by the aluminum SLJs, this was attributed to the lower yield strength of the aluminum adherend (106 MPa), in comparison to that of steel adherend (330 MPa), which resulted in an earlier onset of plastic deformation. This difference in energy absorption among SLJ types reduces as the temperature increases indicating the failure of the joint becomes increasingly dominated by adhesive failure with increasing temperature due to the corresponding increasing toughness of the adhesive.

The evaluation of the sample fracture surfaces revealed similar modes of failure as observed in the monotonic and fatigue testing for the joints composed of a metal adherend, i.e. the fracture surfaces consisted of interfacial failure at the adhesive-metal adherend interface and cohesive failure within adhesive at sub- $T_g$  temperatures and transitioned to interfacial failure at the adhesive-metal adherend interface at the temperatures above  $T_g$ . The observed mode of failure in the composite SLJs at sub- $T_g$  temperatures was mixed between cohesive failure within the adhesive and resin rich surface of the composite adherend. The mode of failure of the composite SLJs transitioned to purely cohesive failure within the adhesive at temperatures above  $T_g$ . The fracture surfaces are shown in Figure 5.53, Figure 5.54, and Figure 5.55 for the steel, aluminum, and composite SLJs, respectively.

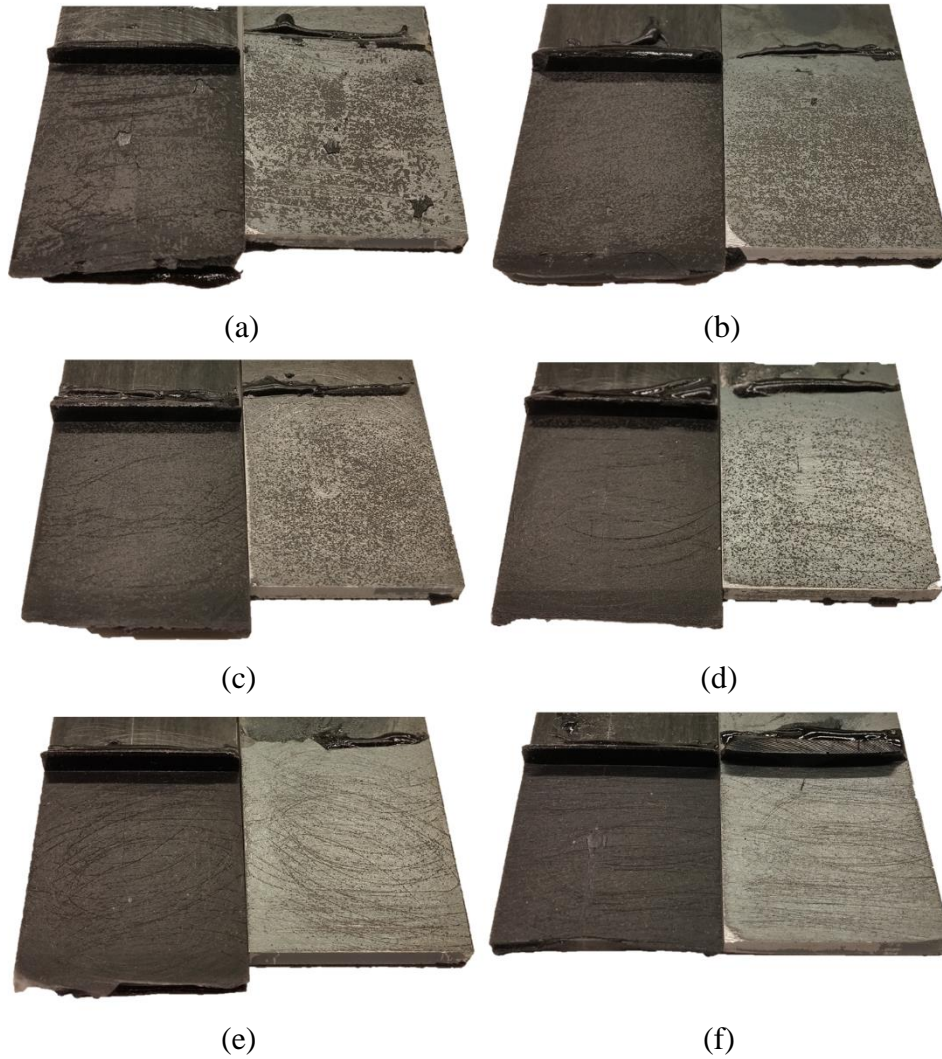


Figure 5.53: Representative LVI fracture surfaces of steel SLJs at (a)  $-20^{\circ}\text{C}$ , (b)  $0^{\circ}\text{C}$ , (c)  $25^{\circ}\text{C}$ , (d)  $40^{\circ}\text{C}$ , (e)  $80^{\circ}\text{C}$ , and (f)  $120^{\circ}\text{C}$



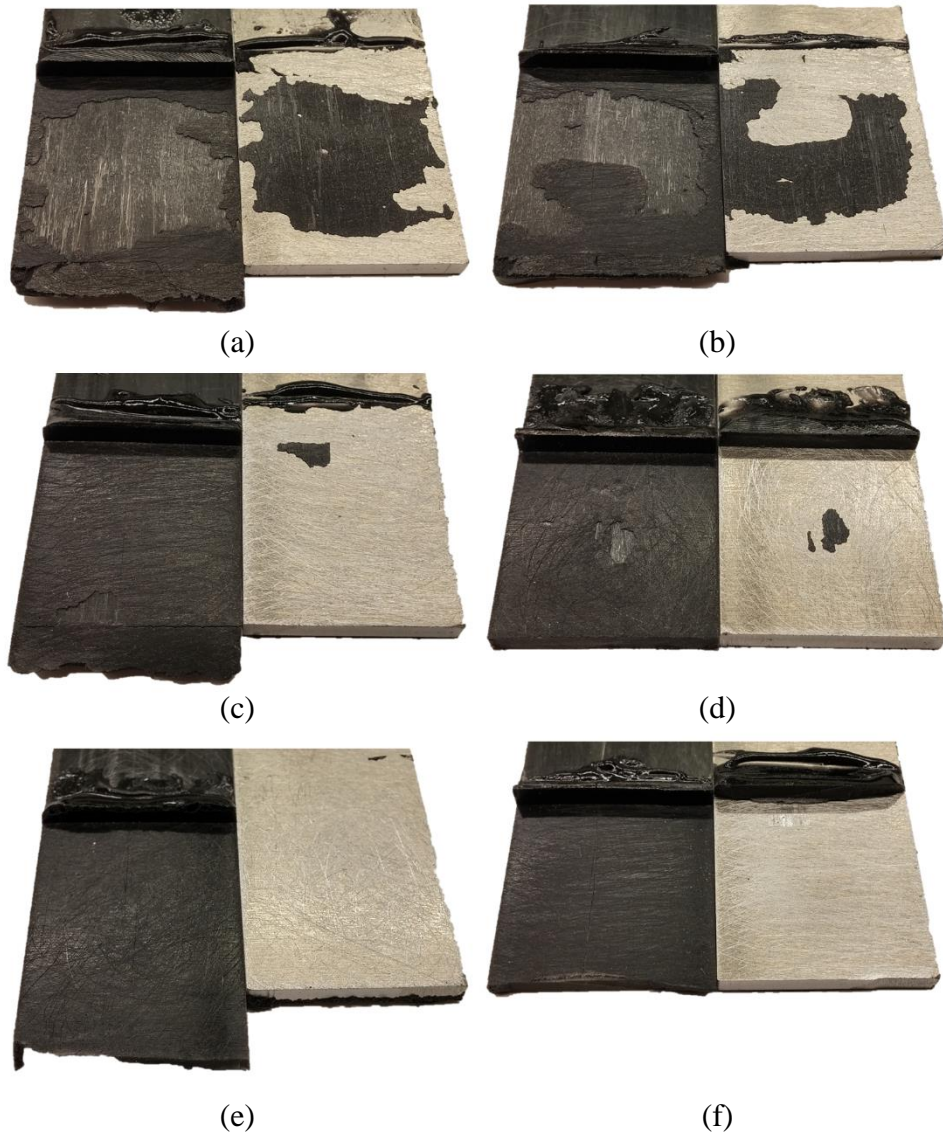


Figure 5.54: Representative LVI fracture surfaces of aluminum SLJs at (a)  $-20^{\circ}\text{C}$ , (b)  $0^{\circ}\text{C}$ , (c)  $25^{\circ}\text{C}$ , (d)  $40^{\circ}\text{C}$ , (e)  $80^{\circ}\text{C}$ , and (f)  $120^{\circ}\text{C}$

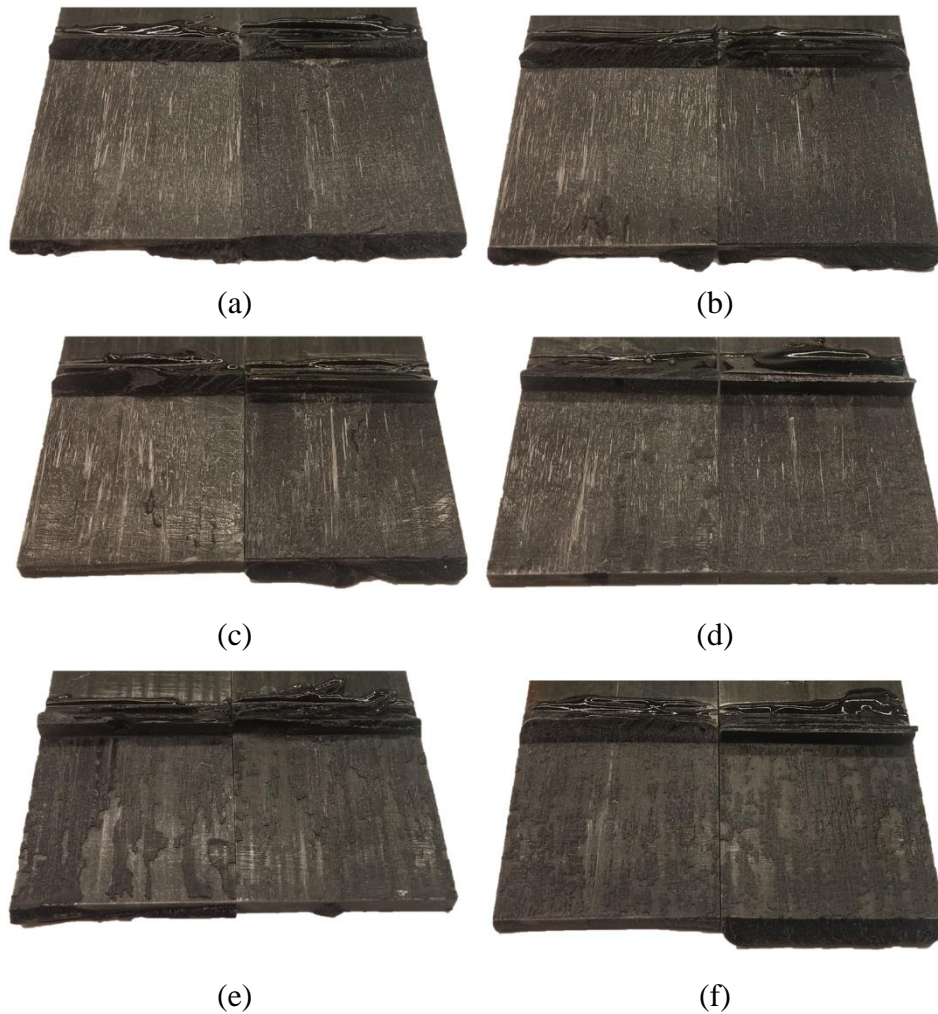


Figure 5.55: Representative LVI fracture surfaces of composite SLJs at (a)  $-20^{\circ}\text{C}$ , (b)  $0^{\circ}\text{C}$ , (c)  $25^{\circ}\text{C}$ , (d)  $40^{\circ}\text{C}$ , (e)  $80^{\circ}\text{C}$ , and (f)  $120^{\circ}\text{C}$

#### 5.4. Sources of Error

The potential sources of error which may have contributed to variation in data, as is inherent in all experimental endeavors, were many and a few of these which were thought to be of particular importance have been discussed in this section.

The preparation of the bonding surfaces plays an important role in the performance of an ABJ due to its influence on the adherence between adhesive and substrate [2, 55, 69]. Although care was taken to subject the bonding surface of each adherend to the same process, the sanding

of these surfaces was inherently inconsistent in terms of the pressure applied as well as abrasion paths which traversed the entirety of the bonding area. The cleaning and degreasing of the bonding areas also differed between specimens due to the infeasibility of manufacturing the joints at the same time. The variation in time between cleaning and adhesive application could have allowed for the formation of an oxidized layer on the bonding surfaces of the joints which were prepared at a later time. Once the joints were formed, the formation of the fillets offered another noteworthy source of potential error. Not only were these formed by hand, which did not allow for consistent angle formation and adhesive volume application, but two additional factors also greatly influenced the resulting shape of the fillets. The first being gravitational sagging. Gravitational sagging was observed in both the upper fillets, i.e. those nearest the clamp, and lower fillets, i.e. those nearest the base, as shown in Figure 4.9 and Figure 4.10, respectively. Gravitational sagging could be ideally considered a constant source of error, since the joints were all manufactured with the metal adherends in contact with the base and composite in contact with the clamps, but the second factor which affected the fillet formation also affected the gravitation sagging. This second factor was time. As it took time to manufacture each SLJ, the mixed adhesive, required to be previously mixed in order to incorporate the glass spacing beads, was in the process of curing and resulted in a variation in viscosity of the adhesive applied to each specimen within a given sample. This variation in viscosity would also affect the wetting characteristics of the adhesive and therefore the quality of the adhesive bond [2].

Once the joints had been manufactured they required finishing via belt sanding to ensure parallel edges. This introduced heat into the joint which was limited by abrading the joints in durations of 3-5 seconds. Nevertheless the temperature of the joint was elevated during this process

which could have had the potential to alter the interfacial bonds between the adhesive and metal adherends.

The test fixtures used in the study of the fatigue behavior of the SLJs also increased the compliance of the test system which could have potentially altered the load path through the joints and artificially increased joint strength by decreasing the stress concentrations caused by the eccentric loading path of SLJs.

The strength of the SLJs at elevated temperatures decreased such that the loading which was applied throughout the cyclic fatigue test program were very low, i.e. <1.00% of the load cell capacity, which may have caused control errors in the application of the sinusoidal loading waveform and thus a misrepresentation of the behavior of the studied joints at increasingly elevated temperatures.

## CHAPTER 6. CONCLUSIONS AND RECOMMENDATIONS

### 6.1. Conclusions

The effects of temperature on the fatigue, specifically life and stiffness degradation, and low velocity transverse impact behaviors of dissimilar material SLJs, composed of a pultruded E-glass/polyurethane composite adherend bonded to 5052 aluminum and A36 steel adherends with a two-part polyurethane adhesive, were experimentally investigated throughout this research. To obtain a better understanding of the underlying causes of the observed behavioral changes, the temperature effects on the adhesive was also studied in isolation in its bulk form.

The evaluation of the two-part polyurethane adhesive characteristics consisted of three portions which included decomposition, temperature effects on stiffness, and efficacy of the spacing beads in controlling the bond line thickness.

The decomposition temperatures were found was to be 244°C, 259°C, 265°C, and 279°C at heating rates of 2.5°C/min, 5°C/min, 10°C/min, and 20°C/min, respectively. These temperatures were used as an upper limit in the design of experiments for the remainder of the research. Analysis of the data using the Ozawa/Flynn/Wall method described in ASTM E1641[48] yielded an activation energy of 136 kJ and a preexponential factor of 26.8. These values were obtained to allow for future modeling of joint performance to be performed which was not within the scope of this research.

The temperature effects on the stiffness of the adhesive were evaluated using dynamic mechanical analysis and yielded a  $T_g$  of 60.2°C. The majority of stiffness degradation was observed to occur in the range of 40°C to 80°C. The results of this study allowed for the better understanding of the temperature effects on the behavior of the studied SLJs. .

The efficacy of controlling the bond line thickness with glass spacing beads and the application of a 1.67 N·m torque to the clamping bolts was evaluated via statistical analysis of the microscopy measurements. It was found that the implemented method produced bond line thicknesses which were not statistically different from the maximum diameter of the spacing bead distribution of 125  $\mu\text{m}$ , hence it was concluded to be an effective method to control bond line thickness.

The evaluation of the temperature effects on the fatigue behavior of the adhesively-bonded SLJs consisted of the study of the monotonic tension, fatigue life (in the form of F-N diagrams), and stiffness degradation behaviors.

The monotonic tensile strength, stiffness, and displacement at failure of the studied SLJs were found to decrease at non-ambient temperatures which was consistent with the literature and was caused by the combination of the dissimilarity in thermal expansion coefficients and stiffnesses of the adherends as well as the mechanical property degradation of the adhesive at temperatures above its  $T_g$ .

The fatigue lives of the studied SLJs were generally found to decrease with increasing temperature, when comparing at normalized load levels. This effect was observed at temperatures below the  $T_g$  of the adhesive as well. Therefore, Temperature should always be considered throughout the design process, as any change in temperature will affect the fatigue life of the joint.

The fatigue lives and stiffness degradation behavior of the studied SLJs were found to be independent of the adherend materials of which they were composed, when comparing lives and degradation at normalized load levels. If validated by further experimental work, this would allow for a decrease in the time and cost of the fatigue testing and design of adhesively-bonded dissimilar materials by reducing the variables required to be evaluated to only the adhesive.

The loading level was observed to affect the stiffness reduction at failure, such that a higher load level generally resulted in lower stiffness reduction at failure. The variation in reduction when comparing between load levels was generally insignificant. Sub- $T_g$  temperatures were observed to have a negligible effect on the stiffness degradation behaviors. Once the temperature was elevated above the  $T_g$ , however, there was a significant change in stiffness degradation behavior towards the end of life which was observed to be an acceleration of the rate of stiffness degradation accompanied with a greater stiffness reduction at failure. These results have indicated that the use of such joints should be confined to sub- $T_g$  temperatures to ensure stable crack growth throughout the majority of life, thereby allowing for simplified in-situ stiffness reduction failure determinations, i.e. the ability to define failure at the time/cycle after which the observed in-situ stiffness degradation rate is no longer linear.

The sigmoid model proposed by Zhang et al. [36] for StLJs was found not to apply to the studied SLJs as they did not exhibit a sigmoid curve but did yield trends similar to those demonstrated by Zhang et al. [23]. A conservative failure criterion was determined to be at a stiffness reduction of 5%.

The results of this research have also indicated that the adverse effects of the mismatch of adherend CTEs and stiffnesses, which govern the monotonic mechanical properties, do not have a corresponding effect on the fatigue lives and failure behavior of adhesively-bonded dissimilar materials (i.e. lower fatigue lives at all non-ambient temperatures). These insights, pending further validation, would allow for the simplification of joint fatigue design by allowing for the prediction of fatigue life and stiffness degradation by considering load levels normalized with the ultimate static load of the joint.

The evaluation of the temperature effects on the LVI behavior of the adhesively-bonded SLJs consisted the study of the initial failure in terms of stiffness, load, and energy and overall joint performance in terms of secondary stiffness, maximum supported impact force, and absorbed energy.

The load and energy at initial failure along with the stiffness prior to initial failure were analyzed to evaluate the effects of temperature on the failure initiation behaviors of the studied SLJs. All SLJ types were found to exhibit the same general trends. The results indicated negligible variation in the load and energy at initial failure at temperatures below the  $T_g$  of the adhesive and decreasing load and energy with increasing temperatures above  $T_g$ . The initial stiffness exhibited greater stiffnesses at sub-ambient temperatures and lower stiffnesses at temperatures elevated above ambient. The steel SLJs exhibited the highest properties followed by aluminum and finally composite SLJs.

To determine whether the observed initial failure was a result of crack formation in the composite adherend additional specimens were tested such that the metal adherend was the point of contact with the impact tup. Similar initial failure behavior was observed when the impact surface was that of the composite and that of the metal adherend which indicated that initial failure could not be attributed to the crack formation in the composite adherend. It was hypothesized that the initial failure was caused by crack formation in the fillet opposite that of the impact tup. This hypothesis was supported by the examination of the composite SLJs tested at 80°C, in which complete joint failure did not occur, which allowed for the evaluation of the crack propagation.

Although the results obtained in this research indicate the initial failure occurring in the lower fillet it has not provided insight into the precise location within the fillet region and therefore requires further validation.



The results of this study have demonstrated the influence of adherend stiffness on the initial failure behavior of dissimilar material SLJs. Stiffer adherends yield higher failure loads and energies as well as initial stiffnesses. They have also demonstrated the importance of the temperature dependent mechanical properties of the adhesive on the performance of dissimilar material SLJs under LVI loading.

The secondary stiffness was found to exhibit negligible variation below the  $T_g$  and decreasing stiffnesses at temperatures above  $T_g$ . The same influence of adherend stiffness was observed for secondary stiffness as well, i.e. higher adherend stiffnesses translates into higher SLJ stiffness at all temperatures.

The maximum impact force supported by the steel and composite SLJs were similar at temperatures below 40°C, above which the composite SLJs supported higher maximum impact forces. The peak for the composite SLJs was at 40°C above which the maximum force began to decrease with increasing temperature and below which the force remained relatively constant. The steel SLJs exhibited a consistent decrease in maximum impact force as temperature was increased while the aluminum SLJs exhibited nearly constant maximum impact force until 80°C. This was understood by considering the viscoelastic nature of the polymeric adhesive. As the temperature approached the  $T_g$ , the material became more compliant in the areas of high stress, such as those which occur at the ends of the joint. This deformation allowed the stress in those critical areas to be redistributed and thus increased the load carrying capacity of the joints.

The energy absorbed by the joint during the impact event was found to increase with temperature for all SLJ types. The aluminum SLJs yielded the greatest absorption, followed by steel, and then composite. This was due to the plastic deformation which occurs in the metal adherends. The aluminum yielded at a lower load than the other materials and therefore plastically

deformed through a larger portion of the impact event. The steel also plastically deformed, but not to the same extent as the aluminum and is reflected by the lower amount of absorbed energy. The composite SLJs absorb the least because they did not exhibit any plastic deformation and stored all the energy which was not absorbed by the fracture of the adhesive fillet and bond line as elastic strain energy within the adherends. The strain energy was released once the drop weight reached zero velocity. The increasing trend of energy absorption was due to the corresponding increase in toughness of the adhesive which accompanies an increase temperature.

The results of this study have demonstrated that joint stiffness is mostly dependent upon the stiffness of the adherend materials of which it is composed and decreases above the  $T_g$  of the adhesive, that the load carrying capacity was greatest for the composite SLJs, and that the lower the temperature, the more influence the yielding of the adherends has on the energy absorption of the joint due to the increasing embrittlement of the adhesive. These results have also demonstrated the importance of not only the adherend materials, but of the temperature effects on the adhesive on the behavior of SLJs under transverse LVI. Consider, for instance, an automotive bumper where the design goals are to absorb the maximum amount of energy with the lightest weight structure possible. These criteria could be addressed via the consideration of an adhesively-bonded structure joined with an adhesive (or multiple adhesives) which is flexible (i.e. temperatures near or above  $T_g$ ) throughout the expected range of operating temperatures. The multitude of potential adhesive-adherend combinations would allow for such structures to be designed for specific impact events or standards while reducing weight.

## **6.2. Recommendations for Future Work**

This work has provided a basis upon which additional work can be developed to further the understanding of the behavior of dissimilar material joints. One such area is the creep behavior

of the SLJs. In this work the joints were under constant tensile loading (although the loading varied, it was constantly varied within the tensile region) and would thus result in creep of the polymeric adhesive. This influence of this creep behavior on the joint fatigue performance is not well understood and would be of interest when developing an understanding of the various factors which affect joint performance and to what degree. The creep behavior would be affected by not only time but also temperature and could be studied through the use of time-temperatures superposition on the adhesive in bulk form. The results from studying the creep behavior of the adhesive in bulk form could then be used to further develop methods of correlation to that of manufactured joints.

Furthering the understanding and predictability of the temperature effects on the monotonic strength and stiffness of dissimilar materials joints could also be achieved through the extension of the of the work done by Nguyen et al. [24], which studied the stiffness and strength degradation modelling of DSJs, to SLJs composed of similar and dissimilar adherends.

The temperature effects on the fatigue behavior of dissimilar material joints could be further understood by determining the effect of temperature rise, or heat build-up, within the joint throughout fatigue life which would become especially important as test temperatures near the  $T_g$  of the adhesive. The F-N diagrams of the current work could also be extended via further experimentation at lower load levels and additional temperatures to determine their effects of on the fatigue threshold of the joints. The effects of thermal cycling on the monotonic and fatigue behaviors of dissimilar material SLJs would also be of interest in future work to determine how temperature cycling affects joint performance to better reflect practical applications in which temperature variations throughout use are cyclical, e.g. daily temperature changes, or inconsistent.

A stiffness degradation model could then be developed to allow for the formation of a failure criterion which would be allow for the inclusion of temperature dependent parameter.

The temperature effects on the LVI behavior of dissimilar material joints could be further understood via FEM simulation with the inclusion of viscoelastic modeling of the adhesive to accurately reflect the behavioral changes. Future work would also be complemented by the use of high speed imaging of experimental impact events to determine the crack initiation and propagation behavior. The boundary conditions could also be changed to simply supported to further separate the effects of adherend plastic deformation from the fracture of the adhesive fillet and bond line. The current work could also be expanded by considering additional impact velocities, or strain rates, and bond areas, i.e. differing lengths and widths.

## REFERENCES

- [1] A. J. Kinloch, "Adhesives in engineering," *Proceedings of the Institution of Mechanical Engineers, Part G: Journal of Aerospace Engineering*, vol. 211, no. 5, pp. 307-335, 1997.
- [2] L. F. da Silva, A. Öchsner, and R. D. Adams, *Handbook of adhesion technology*. Springer Science & Business Media, 2011.
- [3] J. Schultz, M. Nardin, A. Pizzi, and K. Mittal, "Handbook of adhesive technology," *Marcel Decker, New York*, 1994.
- [4] I. M. Daniel, O. Ishai, I. M. Daniel, and I. Daniel, *Engineering mechanics of composite materials*. Oxford university press New York, 1994.
- [5] T. Vallée, J. R. Correia, and T. Keller, "Optimum thickness of joints made of GFPR pultruded adherends and polyurethane adhesive," *Composite Structures*, vol. 92, no. 9, pp. 2102-2108, 8// 2010.
- [6] T. Vallée, T. Tannert, J. Murcia-Delso, and D. J. Quinn, "Influence of stress-reduction methods on the strength of adhesively bonded joints composed of orthotropic brittle adherends," *International Journal of Adhesion and Adhesives*, vol. 30, no. 7, pp. 583-594, 10// 2010.
- [7] J. A. B. P. Neto, R. D. S. G. Campilho, and L. F. M. da Silva, "Parametric study of adhesive joints with composites," *International Journal of Adhesion and Adhesives*, vol. 37, pp. 96-101, 9// 2012.
- [8] J. Na, Y. Liu, Y. Wang, L. Pan, and Y. Yan, "Effect of Temperature on the Joints Strength of an Automotive Polyurethane Adhesive," *The Journal of Adhesion*, vol. 92, no. 1, pp. 52-64, 2016.
- [9] A. Brunner, "Investigating the performance of adhesively-bonded composite joints: standards, test protocols, and experimental design," *Fatigue and Fracture of Adhesively-Bonded Composite Joints*, vol. 52, p. 1, 2014.
- [10] *ASTM D3166-99 Standard Test Method for Fatigue Properties of Adhesives in Shear by Tension Loading (Metal/Metal)*, 2012.
- [11] R. Sarfaraz, "Understanding fatigue loading conditions in adhesively-bonded composite joints," *Fatigue and Fracture of Adhesively-Bonded Composite Joints*, p. 73, 2014.
- [12] A. J. Curley, H. Hadavinia, A. J. Kinloch, and A. C. Taylor, "Predicting the service-life of adhesively-bonded joints," *International Journal of Fracture*, journal article vol. 103, no. 1, pp. 41-69, 2000.

- [13] H. Hadavinia, A. J. Kinloch, M. S. G. Little, and A. C. Taylor, "The prediction of crack growth in bonded joints under cyclic-fatigue loading I. Experimental studies," *International Journal of Adhesion and Adhesives*, vol. 23, no. 6, pp. 449-461, // 2003.
- [14] M. Quaresimin and M. Ricotta, "Fatigue behaviour and damage evolution of single lap bonded joints in composite material," *Composites Science and Technology*, vol. 66, no. 2, pp. 176-187, 2006.
- [15] V. Shenoy, I. A. Ashcroft, G. W. Critchlow, A. D. Crocombe, and M. M. Abdel Wahab, "Strength wearout of adhesively bonded joints under constant amplitude fatigue," *International Journal of Fatigue*, vol. 31, no. 5, pp. 820-830, 5// 2009.
- [16] H. Khoramishad, A. D. Crocombe, K. B. Katnam, and I. A. Ashcroft, "A generalised damage model for constant amplitude fatigue loading of adhesively bonded joints," *International Journal of Adhesion and Adhesives*, vol. 30, no. 6, pp. 513-521, 9// 2010.
- [17] J. A. M. Ferreira, P. N. Reis, J. D. M. Costa, and M. O. W. Richardson, "Fatigue behaviour of composite adhesive lap joints," *Composites Science and Technology*, vol. 62, no. 10-11, pp. 1373-1379, 8// 2002.
- [18] P. N. B. Reis, J. F. R. Monteiro, A. M. Pereira, J. A. M. Ferreira, and J. D. M. Costa, "Fatigue behaviour of epoxy-steel single lap joints under variable frequency," *International Journal of Adhesion and Adhesives*, vol. 63, pp. 66-73, 12// 2015.
- [19] H. Khoramishad, A. D. Crocombe, K. B. Katnam, and I. A. Ashcroft, "Predicting fatigue damage in adhesively bonded joints using a cohesive zone model," *International Journal of Fatigue*, vol. 32, no. 7, pp. 1146-1158, 7// 2010.
- [20] I. A. Ashcroft, D. J. Hughes, S. J. Shaw, M. A. Wahab, and A. Crocombe, "Effect of Temperature on the Quasi-static Strength and Fatigue Resistance of Bonded Composite Double Lap Joints," *The Journal of Adhesion*, vol. 75, no. 1, pp. 61-88, 2001/02/01 2001.
- [21] I. A. Ashcroft, M. M. A. Wahab, A. D. Crocombe, D. J. Hughes, and S. J. Shaw, "The effect of environment on the fatigue of bonded composite joints. Part 1: testing and fractography," *Composites Part A: Applied Science and Manufacturing*, vol. 32, no. 1, pp. 45-58, 1// 2001.
- [22] I. A. Ashcroft and S. J. Shaw, "Mode I fracture of epoxy bonded composite joints 2. Fatigue loading," *International Journal of Adhesion and Adhesives*, vol. 22, no. 2, pp. 151-167, // 2002.
- [23] Y. Zhang, A. P. Vassilopoulos, and T. Keller, "Environmental effects on fatigue behavior of adhesively-bonded pultruded structural joints," *Composites Science and Technology*, vol. 69, no. 7-8, pp. 1022-1028, 6// 2009.
- [24] T.-C. Nguyen, Y. Bai, X.-L. Zhao, and R. Al-Mahaidi, "Mechanical characterization of steel/CFRP double strap joints at elevated temperatures," *Composite Structures*, vol. 93, no. 6, pp. 1604-1612, 5// 2011.

- [25] L. Hart-Smith, *Adhesive-bonded double-lap joints*. National Aeronautics and Space Administration, 1973.
- [26] L. D. R. Grant, R. D. Adams, and L. F. M. da Silva, "Effect of the temperature on the strength of adhesively bonded single lap and T joints for the automotive industry," *International Journal of Adhesion and Adhesives*, vol. 29, no. 5, pp. 535-542, 7// 2009.
- [27] P. Hu, X. Han, W. D. Li, L. Li, and Q. Shao, "Research on the static strength performance of adhesive single lap joints subjected to extreme temperature environment for automotive industry," *International Journal of Adhesion and Adhesives*, vol. 41, pp. 119-126, 3// 2013.
- [28] J. F. P. Owens and P. Lee-Sullivan, "Stiffness behaviour due to fracture in adhesively bonded composite-to-aluminum joints II. Experimental," *International Journal of Adhesion and Adhesives*, vol. 20, no. 1, pp. 47-58, 2// 2000.
- [29] J. F. P. Owens and P. Lee-Sullivan, "Stiffness behaviour due to fracture in adhesively bonded composite-to-aluminum joints I. Theoretical model," *International Journal of Adhesion and Adhesives*, vol. 20, no. 1, pp. 39-45, 2// 2000.
- [30] M.-S. Seong, T.-H. Kim, K.-H. Nguyen, J.-H. Kweon, and J.-H. Choi, "A parametric study on the failure of bonded single-lap joints of carbon composite and aluminum," *Composite Structures*, vol. 86, no. 1-3, pp. 135-145, 11// 2008.
- [31] P. Colombi and G. Fava, "Fatigue behaviour of tensile steel/CFRP joints," *Composite Structures*, vol. 94, no. 8, pp. 2407-2417, 7// 2012.
- [32] R. Matsuzaki, M. Shibata, and A. Todoroki, "Improving performance of GFRP/aluminum single lap joints using bolted/co-cured hybrid method," *Composites Part A: Applied Science and Manufacturing*, vol. 39, no. 2, pp. 154-163, 2// 2008.
- [33] T.-C. Nguyen, Y. Bai, R. Al-Mahaidi, and X.-L. Zhao, "Time-dependent behaviour of steel/CFRP double strap joints subjected to combined thermal and mechanical loading," *Composite Structures*, vol. 94, no. 5, pp. 1826-1833, 4// 2012.
- [34] A. Agarwal, S. J. Foster, E. Hamed, and T. S. Ng, "Influence of freeze-thaw cycling on the bond strength of steel-FRP lap joints," *Composites Part B: Engineering*, vol. 60, pp. 178-185, 4// 2014.
- [35] A. Vassilopoulos and T. Keller, "Fatigue and fracture behavior of adhesively-bonded composite structural joints," in *Fatigue and Fracture of Adhesively-Bonded Composite Joints*: Woodhead Publishing, 2014, pp. 225-255.
- [36] Y. Zhang, A. P. Vassilopoulos, and T. Keller, "Stiffness degradation and fatigue life prediction of adhesively-bonded joints for fiber-reinforced polymer composites," *International Journal of Fatigue*, vol. 30, no. 10-11, pp. 1813-1820, 10// 2008.

- [37] T. P. Philippidis and A. P. Vassilopoulos, "Fatigue design allowables for GRP laminates based on stiffness degradation measurements," *Composites Science and Technology*, vol. 60, no. 15, pp. 2819-2828, 11// 2000.
- [38] S. I. Andersen, P. Brøndsted, and H. Lilholt, "Fatigue of polymeric composites for wingblades and the establishment of stiffness-controlled fatigue diagrams," in *1996 European Union wind energy conference. Proceedings*, ed: H.S. Stephens & Associates, 1996, pp. 950-953.
- [39] T. P. Philippidis and A. P. Vassilopoulos, "Fatigue of composite laminates under off-axis loading," *International Journal of Fatigue*, vol. 21, no. 3, pp. 253-262, 3// 1999.
- [40] S.-S. Pang, C. Yang, and Y. Zhao, "Joints and Adhesion Impact response of single-lap composite joints," *Composites Engineering*, vol. 5, no. 8, pp. 1011-1027, 1995/01/01 1995.
- [41] U. K. Vaidya, A. R. S. Gautam, M. Hosur, and P. Dutta, "Experimental–numerical studies of transverse impact response of adhesively bonded lap joints in composite structures," *International Journal of Adhesion and Adhesives*, vol. 26, no. 3, pp. 184-198, 6// 2006.
- [42] L. Liao, T. Sawa, and C. Huang, "Experimental and FEM studies on mechanical properties of single-lap adhesive joint with dissimilar adherends subjected to impact tensile loadings," *International Journal of Adhesion and Adhesives*, vol. 44, pp. 91-98, 7// 2013.
- [43] O. Sayman, V. Arıkan, A. Dogan, I. F. Soykok, and T. Dogan, "Failure analysis of adhesively bonded composite joints under transverse impact and different temperatures," *Composites Part B: Engineering*, vol. 54, pp. 409-414, 11// 2013.
- [44] W. Wu, Q. Liu, Z. Zong, G. Sun, and Q. Li, "Experimental investigation into transverse crashworthiness of CFRP adhesively bonded joints in vehicle structure," *Composite Structures*, vol. 106, pp. 581-589, 12// 2013.
- [45] "Aluminum, 5052, wrought, H11," in *CES EduPack 2015*, ed: Granta Design Limited, 2015.
- [46] "Carbon steel, AISI 1020, as rolled," in *CES EduPack 2015*, ed: Granta Design Limited, 2015.
- [47] "3M(TM) Scotch-Weld(TM) Urethane Adhesive DP620NS Black," in *Technical Data Sheet*, ed. St. Paul, MN: 3M Company, 2015.
- [48] *ASTM E1641-16 Standard Test Method for Decomposition Kinetics by Thermogravimetry Using the Ozawa/Flynn/Wall Method*, 2016.
- [49] *ASTM D5023-15 Standard Test Method for Plastics: Dynamic Mechanical Properties: In Flexure (Three-Point Bending)*, 2015.



- [50] Y. Bai and T. Keller, "Effects of thermal loading history on structural adhesive modulus across glass transition," *Construction and Building Materials*, vol. 25, no. 4, pp. 2162-2168, 4// 2011.
- [51] *ASTM D1002-10 Standard Test Method for Apparent Shear Strength of Single-Lap-Joint Adhesively Bonded Metal Specimens by Tension Loading (Metal-to-Metal)*, 2010.
- [52] *ASTM D3163-01 Standard Test Method for Determining Strength of Adhesively Bonded Rigid Plastic Lap-Shear Joints in Shear by Tension Loading*, 2014.
- [53] *ASTM D5868-01 Standard Test Method for Lap Shear Adhesion for Fiber Reinforced Plastic (FRP) Bonding*, 2014.
- [54] L. da Silva and R. Campilho, "Design of adhesively-bonded composite joints," *Fatigue and Fracture of Adhesively-Bonded Composite Joints*, vol. 52, p. 43, 2014.
- [55] M. D. Banea and L. F. M. da Silva, "Adhesively bonded joints in composite materials: An overview," *Proceedings of the Institution of Mechanical Engineers, Part L: Journal of Materials Design and Applications*, vol. 223, no. 1, pp. 1-18, January 1, 2009 2009.
- [56] W. C. de Goeij, M. J. L. van Tooren, and A. Beukers, "Composite adhesive joints under cyclic loading," *Materials & Design*, vol. 20, no. 5, pp. 213-221, 10/1/ 1999.
- [57] B. Broughton and M. Gower, *Measurement good practice guide No. 47 preparation and testing of adhesive joints*. NPL Materials Centre National Physical Laboratory, 2001.
- [58] *ASTM D3983-98 Standard Test Method for Measuring Strength and Shear Modulus of Nonrigid Adhesives by the Thick-Adherend Tensile-Lap Specimen*, 2011.
- [59] *ASTM D7136/D7136M - 15 Standard Test Method for Measuring the Damage Resistance of a Fiber-Reinforced Polymer Matrix Composite to a Drop-Weight Impact Event*, 2015.
- [60] H. F. Brinson and L. C. Brinson, *Polymer engineering science and viscoelasticity*. Springer, 2008.
- [61] R. D. Adams, J. Coppedale, V. Mallick, and H. Al-Hamdan, "The effect of temperature on the strength of adhesive joints," *International Journal of Adhesion and Adhesives*, vol. 12, no. 3, pp. 185-190, 1992/07/01 1992.
- [62] L. F. M. da Silva and R. D. Adams, "Adhesive joints at high and low temperatures using similar and dissimilar adherends and dual adhesives," *International Journal of Adhesion and Adhesives*, vol. 27, no. 3, pp. 216-226, 4// 2007.
- [63] L. F. M. da Silva and R. D. Adams, "Joint strength predictions for adhesive joints to be used over a wide temperature range," *International Journal of Adhesion and Adhesives*, vol. 27, no. 5, pp. 362-379, 7// 2007.

- [64] D. M. Brewis, J. Comyn, and R. J. A. Shalash, "The effect of moisture and temperature on the properties of an epoxide-polyamide adhesive in relation to its performance in single lap joints," *International Journal of Adhesion and Adhesives*, vol. 2, no. 4, pp. 215-222, 1982/10/01 1982.
- [65] L. J. Hart-Smith, *Adhesive-bonded single-lap joints*. Hampton, VA: Langley Research Center: National Aeronautics and Space Administration, 1973.
- [66] L. J. Hart-Smith, *Analysis and design of advanced composite bounded joints*. National Aeronautics and Space Administration, 1974.
- [67] D. R. Jones and M. F. Ashby, *Engineering materials 2: an introduction to microstructures, processing and design*. Butterworth-Heinemann, 2005.
- [68] M. T. Shaw and W. J. MacKnight, *Introduction to polymer viscoelasticity*. John Wiley & Sons, 2005.
- [69] L. F. M. da Silva, R. J. C. Carbas, G. W. Critchlow, M. A. V. Figueiredo, and K. Brown, "Effect of material, geometry, surface treatment and environment on the shear strength of single lap joints," *International Journal of Adhesion and Adhesives*, vol. 29, no. 6, pp. 621-632, 9// 2009.

## APPENDIX A. MATERIAL PROPERTIES AND INFORMATION

Table A1: Mechanical, physical, and thermal adherend properties

Property	Unit	Material		
		Composite	5052 Aluminum	A36 Steel
Tensile Modulus	GPa	51.81 (Long.) 9.991 (Trans.)	70.05	210.0
Tensile Strength	MPa	841.2 (Long.) 51.02 (Trans.)	191.5	447.5
Yield Strength	MPa	-	106.0	330
Flexural Modulus	GPa	55.30 (Long.) 11.72 (Trans.)	70.05	210.0
Flexural Strength	MPa	1441 (Long.) 107.6 (Trans.)	106.0	330.0
Compressive Strength	MPa	296.5 (Long.) 79.29 (Trans.)	106.0	330.0
Density	kg/m <sup>3</sup>	1938	2680	7850
Coeff. of Thermal Expansion	10 <sup>-6</sup> m/m·°C	6.120 (Long.) 27.72 (Trans.)	23.70	12.00
Thermal Conductivity	W/m·°C	0.2061	146.00	52.00

Long.= Longitudinal direction

Trans.= Transverse direction

Table A2: Adherend thickness measurement summary

Adherend	Thickness (mm)	St. Dev. (mm)
Composite	2.616	0.0120
5052 Aluminum	3.103	0.0261
A36 Steel	2.971	0.0189

**Certificate of Analysis**

The material covered by this certificate has been tested in accordance with Novum Glass LLC Quality Management System and complies with the applicable specification.

**Technical Series Solid Glass Microspheres**

Customer #	PO #	Novum #	Lot #
NA	SAMPLE	T-106-125	011314-04-MRG

Size: 120 to 140 Mesh

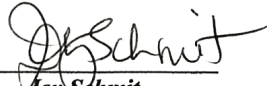
Quantity: 50 grams

Mfg Date: 08/20/15

**Specification:**

> 90 % within size range      Results: 99 %

> 90 % spherical                Results: 92 %

  
Joy Schmit  
 Quality Representative

03-01-16  
 Date

**Novum Glass LLC microspheres are made of Soda-Lime glass.  
 Size has been tested using ASTM D11 certified test sieves.  
 Sieves have been inspected optically with instrument calibration traceable to NIST.  
 Spherical quality has been evaluated using optical microscopy.**

Figure A1: Spacing bead certificate of analysis provided by Novum Glass, LLC

## APPENDIX B. TECHNICAL DRAWINGS

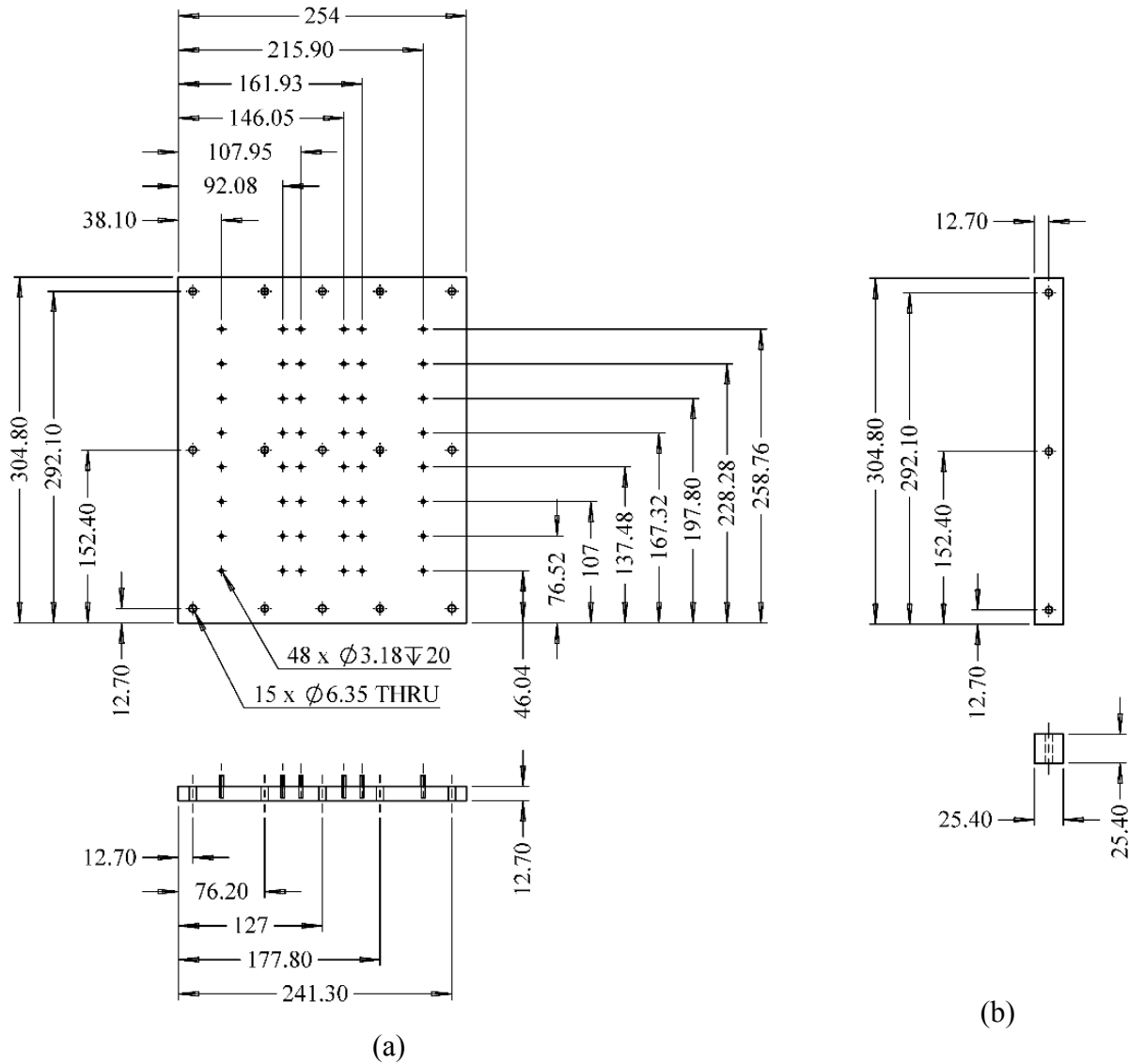


Figure B1: Technical drawing of the sample manufacturing jig components: (a) base and (b) clamp, dimensions in mm

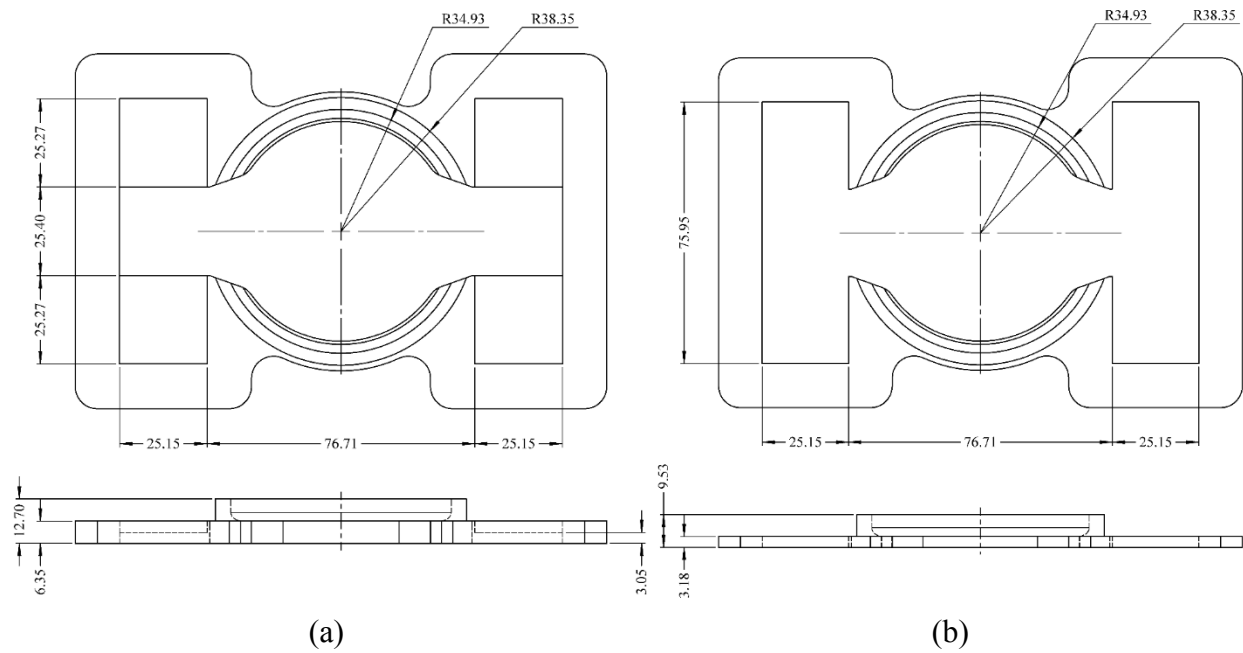


Figure B2: Technical drawing of the LVI jig components: (a) lower and (b) upper, dimensions in mm

## APPENDIX C. EXPERIMENTAL DATA

Table C1: Fatigue specimen spacing bead concentration summary

Sample	Adherend	Adhesive (mg)	Spacing Beads (mg)	wt%
1	Aluminum	5.3818	0.0552	1.026%
2	Aluminum	7.5380	0.0772	1.024%
3	Steel	7.6276	0.0794	1.041%
4	Aluminum	8.0054	0.0871	1.088%
5	Steel	8.7619	0.0893	1.019%
6	Aluminum	7.6414	0.0788	1.031%
7	Steel	8.0755	0.0834	1.033%
8	Aluminum	7.6745	0.0788	1.027%
9	Steel	8.3985	0.0886	1.055%
10	Aluminum	9.2048	0.0924	1.004%
11	Aluminum	7.8735	0.0814	1.034%
12	Steel	8.2659	0.0852	1.031%
13	Aluminum	7.9089	0.0801	1.013%
14	Steel	8.1715	0.0832	1.018%
15	Aluminum	7.8346	0.0791	1.010%
16	Steel	10.4162	0.1042	1.000%
17	Aluminum	7.8278	0.0783	1.000%
18	Steel	8.2991	0.0869	1.047%
19	Aluminum	7.6595	0.0869	1.135%

Table C2: LVI specimen spacing bead concentration summary

<b>Sample</b>	<b>Adherend</b>	<b>Adhesive (mg)</b>	<b>Spacing Beads (mg)</b>	<b>wt%</b>
1	Aluminum	7.4349	0.0739	0.994%
2	Aluminum	21.5209	0.2195	1.020%
3	Steel	15.2915	0.1566	1.024%
4	Aluminum	14.6748	0.1446	0.985%
5	Steel	15.2032	0.1550	1.020%
6	Steel	14.6991	0.1491	1.014%
7	Steel	13.9635	0.1429	1.023%
8	Steel	12.5281	0.1257	1.003%
9	Aluminum	12.5255	0.1259	1.005%
10	Aluminum	12.6573	0.1306	1.032%
11	Steel	12.5751	0.1268	1.008%
12	Steel	12.0917	0.1210	1.001%
13	Aluminum	12.9148	0.1294	1.002%
14	Composite	12.7419	0.1362	1.069%
15	Composite	11.9801	0.1198	1.000%
16	Composite	11.9463	0.1216	1.018%
17	Composite	12.6816	0.1275	1.005%
18	Composite	11.8855	0.1189	1.000%

Table C3: Bond line thickness summary

<b>Adherend</b>	<b>Bond Line Thickness (<math>\mu\text{m}</math>)</b>	<b>St. Dev. (<math>\mu\text{m}</math>)</b>
Composite	157	29.54
5052 Aluminum	138	41.98
A36 Steel	109	21.87

Table C4: Bond line thickness t test summary

<b>Parameter</b>	<b>Composite</b>	<b>5052 Aluminum</b>	<b>A36 Steel</b>
n	5	5	5
Mean	157.0	137.8	108.6
s	29.54	41.98	21.87
alpha	0.05	0.05	0.05
$\mu$	125	125	125
t (calculated)	2.420	0.680	-1.680
t (tabulated)	2.776	2.776	2.776



Table C5: Thermal degradation heating rate and temperature results

<b>Heating Rate (°C/min)</b>	<b>Degradation Temperature (°C)</b>
2.5	244.14
5	258.83
10	264.93
20	279.33

Table C6: Summary of DMA T<sub>g</sub> results

<b>Specimen</b>	<b>Width (mm)</b>	<b>Thickness (mm)</b>	<b>T<sub>g</sub> (°C)</b>
1	12.61	3.400	60.51
2	12.61	3.300	59.69
3	12.63	3.310	60.42

Table C7: Summary of monotonic results

<b>Adherend</b>	<b>Temperature (°C)</b>	<b>F<sub>ult</sub> (kN)</b>		<b>δ<sub>ult</sub> (mm)</b>		<b>Stiffness (kN/mm)</b>	
		Mean	St. Dev.	Mean	St. Dev.	Mean	St. Dev.
Aluminum	0	6.010	1.104	0.439	0.105	14.47	0.332
	25	8.738	0.439	0.582	0.029	16.491	0.207
	50	4.084	0.333	0.386	0.036	11.25	0.240
	75	1.383	0.184	0.158	0.017	9.315	0.423
Steel	0	8.398	0.683	0.575	0.083	16.37	1.135
	25	11.92	0.640	0.748	0.073	20.50	0.571
	50	5.438	0.445	0.447	0.023	12.45	0.457
	75	1.573	0.176	0.154	0.017	10.75	0.403

Table C8: Summary of steel SLJ fatigue results

Temp (°C)	LL	Specimen #	Nf	E1	Ef
0	0.5	1	151605	21.10	17.48
0	0.65	1	40516	23.03	19.79
0	0.65	2	36507	21.99	18.75
0	0.65	3	12226	21.88	19.46
0	0.8	1	5395	22.95	19.74
0	0.8	2	5439	23.02	19.86
0	0.8	3	10971	22.00	18.67
25	0.5	1	4531	23.71	20.33
25	0.5	2	6510	21.60	19.09
25	0.5	3	24880	22.70	19.97
25	0.65	1	9157	23.71	20.26
25	0.65	2	1264	23.32	21.44
25	0.65	3	6389	23.00	21.18
25	0.8	1	1677	23.62	22.25
25	0.8	2	1176	23.95	22.70
25	0.8	3	2030	23.80	22.08
50	0.5	1	374	19.38	18.97
50	0.5	2	1229	19.54	18.13
50	0.5	3	3216	19.99	15.24
50	0.65	1	984	19.38	18.52
50	0.65	2	754	19.17	17.80
50	0.65	3	183	19.91	18.51
50	0.8	1	195	20.77	18.75
50	0.8	2	245	19.95	19.68
50	0.8	3	192	20.78	18.92
75	0.5	1	871	13.51	4.24
75	0.5	2	1681	12.46	2.85
75	0.5	3	329	11.64	7.86
75	0.65	1	286	14.17	8.61
75	0.65	2	121	13.61	7.45
75	0.65	3	215	14.14	1.37
75	0.8	1	51	12.76	9.06
75	0.8	2	6	-	7.69
75	0.8	3	163	12.79	10.21

Nf= Final cycle

E1= Initial Stiffness

Ef= Final Stiffness

Table C9: Summary of aluminum SLJ fatigue results

<b>Temp (°C)</b>	<b>LL</b>	<b>Specimen #</b>	<b>Nf</b>	<b>E1</b>	<b>Ef</b>
0	0.50	1	344871	17.06	-
0	0.65	1	3534	17.55	14.39
0	0.65	2	31132	17.97	14.83
0	0.65	3	3758	17.83	14.94
0	0.8	1	17433	18.21	14.63
0	0.8	2	21039	17.97	15.79
0	0.8	3	17179	16.88	14.90
25	0.5	1	1413	18.06	15.82
25	0.5	2	6143	17.43	14.77
25	0.5	3	14454	17.64	15.57
25	0.65	1	1100	18.02	15.96
25	0.65	2	3477	17.66	15.81
25	0.65	3	4	14.10	-
25	0.8	1	293	-	-
25	0.8	2	1	-	-
25	0.8	3	162	-	-
50	0.5	1	3496	11.58	6.89
50	0.5	2	940	15.63	14.76
50	0.5	3	2737	16.37	14.38
50	0.65	1	198	15.82	14.92
50	0.65	2	1069	17.25	14.68
50	0.65	3	864	16.76	15.28
50	0.8	1	198	16.43	15.35
50	0.8	2	322	16.85	16.09
50	0.8	3	296	16.30	15.28
75	0.5	1	2859	11.00	5.36
75	0.5	2	4968	11.03	4.30
75	0.5	3	700	9.90	4.37
75	0.65	1	323	11.42	8.50
75	0.65	2	50	10.57	8.12
75	0.65	3	978	9.83	7.09
75	0.8	1	71	12.28	6.76
75	0.8	2	500	12.09	6.13
75	0.8	3	126	11.01	5.52

Table C10: Summary of composite SLJ LVI results

Temp (°C)	IV (m/s)	IFL (N)	IFD (mm)	Eif (J)	E1 (N/mm)	E2 (N/mm)	Fmax (N)	dmax (mm)	Eabs (J)
-20	1.001	209.2	0.100	0.012	2046	1377	1983	3.777	1.763
	0.998	210.0	0.095	0.011	2119	1368	1436	3.985	1.587
	1.016	201.2	0.092	0.010	2122	1286	1685	4.075	1.739
	0.998	201.1	0.093	0.010	2067	1232	1759	4.015	1.641
	1.019	202.8	0.092	0.010	2188	1468	1411	4.076	1.478
0	1.008	199.9	0.101	0.011	1951	1336	1391	4.038	1.809
	1.007	207.9	0.096	0.011	2004	1299	1971	3.910	1.968
	1.008	207.4	0.103	0.013	1923	1315	1816	3.887	1.918
	1.000	208.0	0.100	0.012	1975	1167	2063	3.856	2.182
	1.001	199.3	0.100	0.011	1941	1215	1835	4.026	2.029
25	1.000	187.7	0.100	0.011	1868	1150	1779	4.218	2.163
	1.006	196.2	0.101	0.011	1916	1172	2248	3.642	2.562
	1.006	187.8	0.086	0.008	2039	1186	2017	3.824	2.408
	1.009	179.8	0.099	0.010	1782	1097	1782	3.959	2.400
	1.009	196.2	0.101	0.011	1916	1204	1651	4.064	2.248
40	1.013	197.2	0.096	0.011	1896	1087	2465	2.750	1.871
	1.012	180.8	0.084	0.008	1895	1058	2251	3.481	2.814
	1.015	197.3	0.104	0.012	1861	1032	2458	2.776	1.910
	1.023	196.9	0.105	0.012	1815	990	2322	3.276	2.913
	1.021	196.7	0.105	0.011	1823	1048	1721	4.121	2.594
80	1.004	163.0	0.093	0.009	1591	662	1793	3.553	2.615
	1.016	161.9	0.094	0.009	1520	640	1700	3.704	2.998
	1.024	163.2	0.102	0.009	1519	663	1893	3.557	2.193
	1.021	170.4	0.102	0.010	1534	666	1769	3.606	2.746
	1.020	170.6	0.092	0.009	1644	672	1860	3.546	2.383
120	1.017	152.9	0.114	0.010	1218	521	1239	5.116	3.559
	1.022	152.3	0.115	0.010	1251	526	1210	5.106	3.598
	1.026	152.3	0.103	0.009	1296	522	1186	4.953	3.604
	1.024	152.2	0.105	0.009	1298	494	1257	5.178	3.666
	1.022	152.3	0.105	0.009	1290	504	1202	5.077	3.578

IV= Initial velocity  
 IFL= Initial failure load  
 IFD= Initial failure energy  
 Eif= Initial failure energy  
 E1= Stiffness prior to initial failure  
 E2= Stiffness post initial failure  
 Fmax= Maximum impact force  
 dmax= Maximum displacement  
 Eabs= Absorbed energy

Table C11: Summary of aluminum SLJ LVI results

<b>Temp (°C)</b>	<b>IV (m/s)</b>	<b>IFL (N)</b>	<b>IFD (mm)</b>	<b>Eif (J)</b>	<b>E1 (N/mm)</b>	<b>E2 (N/mm)</b>	<b>Fmax (N)</b>	<b>dmax (mm)</b>	<b>Eabs (J)</b>
-20	0.998	260.5	0.102	0.014	2611	2437	1244	3.975	2.654
	1.006	252.0	0.101	0.014	2472	2250	1285	4.147	2.655
	0.999	243.7	0.090	0.012	2604	1510	1370	3.768	2.575
	1.007	251.9	0.101	0.014	2496	2224	1326	3.825	2.640
	1.017	268.4	0.102	0.014	2581	2439	1258	4.093	2.866
0	1.002	242.4	0.100	0.014	2434	2560	1212	4.236	2.886
	0.997	242.0	0.112	0.015	2271	2222	1219	4.136	2.854
	0.997	249.9	0.112	0.016	2325	2580	1199	4.317	2.819
	0.999	249.3	0.095	0.013	2515	1939	1646	3.794	2.991
	1.000	249.9	0.112	0.015	2315	1649	1291	3.996	2.898
25	1.011	238.9	0.101	0.013	2373	2313	1112	4.428	3.159
	1.013	238.4	0.106	0.013	2272	2342	1348	4.103	3.080
	1.017	246.8	0.104	0.013	2364	2113	1267	4.371	3.199
	1.012	238.8	0.106	0.015	2209	2205	1161	4.307	3.086
	1.009	246.5	0.113	0.017	2223	1800	1348	3.934	3.132
40	1.016	255.0	0.117	0.016	2262	2134	1349	4.155	3.264
	1.016	238.2	0.104	0.013	2296	2115	1265	4.286	3.236
	1.021	246.1	0.107	0.014	2335	1658	1140	4.527	3.225
	1.015	238.3	0.104	0.014	2225	1655	1323	4.191	3.160
	1.015	238.3	0.104	0.013	2198	1632	1602	3.441	2.722
80	1.023	212.3	0.105	0.013	1967	914	1527	4.368	3.444
	1.020	202.7	0.102	0.012	1863	1091	1119	4.585	3.359
	1.030	210.6	0.103	0.012	1969	955	1077	4.940	3.443
	1.010	211.0	0.104	0.012	1981	975	1290	4.603	3.409
	1.008	201.7	0.103	0.012	1877	928	1541	3.858	3.500
120	1.014	183.7	0.116	0.011	1510	706	910	5.669	3.672
	1.019	183.5	0.104	0.011	1651	775	885	5.858	3.773
	1.016	183.8	0.114	0.012	1559	683	911	5.562	3.698
	1.016	183.6	0.114	0.011	1549	681	934	5.716	3.704
	0.996	184.6	0.105	0.011	1678	861	1003	5.309	3.508

Table C12: Summary of steel SLJ LVI results

<b>Temp (°C)</b>	<b>IV (m/s)</b>	<b>IFL (N)</b>	<b>IFD (mm)</b>	<b>Eif (J)</b>	<b>E1 (N/mm)</b>	<b>E2 (N/mm)</b>	<b>Fmax (N)</b>	<b>dmax (mm)</b>	<b>Eabs (J)</b>
-20	1.009	444.7	0.126	0.028	3912	4855	1871	2.959	2.038
	1.010	429.5	0.143	0.031	3314	3549	1903	2.948	1.973
	1.000	395.0	0.168	0.036	2588	3330	1840	2.996	1.749
	1.018	427.9	0.114	0.025	3948	4347	1947	2.898	2.051
	1.026	454.1	0.128	0.031	3850	4164	1867	3.170	2.000
0	1.003	450.2	0.127	0.031	3793	5121	1751	3.280	1.938
	1.008	434.7	0.128	0.028	3683	4574	1831	3.278	2.110
	1.003	432.7	0.120	0.026	3808	1969	1747	3.191	2.201
	1.001	440.7	0.124	0.029	3886	5087	1746	3.327	2.050
	1.001	439.4	0.120	0.027	3893	4339	1807	3.298	2.068
25	1.015	419.9	0.129	0.029	3564	5053	1754	3.118	2.569
	1.017	427.9	0.129	0.029	3629	5236	1745	3.156	2.612
	1.018	428.2	0.132	0.030	3537	4361	1721	3.281	2.540
	1.014	411.5	0.121	0.026	3633	4402	1695	3.251	2.613
	1.010	395.0	0.126	0.025	3422	3959	1769	3.151	2.435
40	1.021	434.6	0.140	0.031	3459	5046	1615	3.339	2.908
	1.019	409.8	0.129	0.027	3391	4339	1656	3.359	2.729
	1.021	408.7	0.130	0.029	3401	4472	1651	3.246	2.827
	1.011	410.4	0.126	0.027	3475	4301	1592	3.380	2.733
	1.015	410.2	0.139	0.030	3284	3946	1690	3.142	2.704
80	1.031	363.0	0.131	0.024	2907	4047	1347	3.839	3.297
	1.029	362.8	0.131	0.025	2956	3537	1427	3.522	3.304
	1.026	354.0	0.120	0.022	3024	3248	1577	3.603	3.368
	1.013	366.0	0.129	0.025	2986	3815	1635	3.414	3.137
	1.012	356.9	0.131	0.024	2843	1560	1282	3.781	3.165
120	1.012	312.7	0.141	0.024	2354	3455	1082	4.522	3.559
	1.012	304.5	0.138	0.021	2297	2992	1066	4.721	3.560
	1.014	296.1	0.139	0.021	2237	3460	1044	4.852	3.739
	1.018	311.6	0.139	0.023	2355	2824	1047	4.710	3.632
	1.015	311.6	0.126	0.022	2448	2846	1055	4.638	3.618